Bioinspired FGF-2 delivery for pharmaceutical application

Dissertation zur Erlangung des naturwissenschaftlichen Doktorgrades der Julius-Maximilians-Universität Würzburg

vorgelegt von

Gabriel Jones

aus Würzburg

Würzburg 2017

Eingereicht bei der Fakultät für Chemie und Pharmazie am

_____

Gutachter der schriftlichen Arbeit

1. Gutachter: _____

2. Gutachter: _____

Prüfer des öffentlichen Promotionskolloquiums

1. Prüfer: _____

2. Prüfer: _____

3. Prüfer: _____

Datum des öffentlichen Promotionskolloquiums

_____

Doktorurkunde ausgehändigt am

Die vorliegende Arbeit wurde in der Zeit von April 2011 bis Juni 2017

am Institut für Pharmazie und Lebensmittelchemie

der Bayerischen Julius-Maximilians-Universität Würzburg

unter Anleitung von

PD Dr. Tessa Lühmann

angefertigt.

TABLE OF CONTENTS

SUMMARY

In resent years the rate of biologics (proteins, cytokines and growth-factors) as newly registered drugs has steadily risen. The greatest challenge for pharmaceutical biologics poses its arrival at the desired target location due to e.g. proteolytic and pH dependent degradation, plasma protein binding, insolubility etc. Therefore, advanced drug delivery systems, where biologics are site directed immobilized to carriers mimicking endogenous storage sites such as the extra cellular matrix can enormously assist the application and consequently the release of exogenous administered pharmaceutical biologics. We have resorted to the fibroblast growth factor 2/ heparansulfate/ fibroblast growth factor bindingprotein 1 system as a model.

Phase I deals with the selection and subcloning of a wild type murine FGF-2 construct into the bacterial pHis-Trx vector system for high yields of expression and fast, feasible purification measurements. This first step enables the provision of mFGF-2, which plays a pivotal part as a growth factor in the wound healing process as well as the vascularization of tumors, for future investigations. Therefore, the correct expression of mFGF-2 was monitored via MALDI-MS and SDS-PAGE, whereas the proper folding of the tertiary beta-trefoil structure was assessed by fluorescence spectroscopy. The MTT assay allowed us to ensure that the bioactivity was comparable to sourced FGF-2. In the last step, the purity; a requirement for future binding- and protein-protein interaction assays was monitored chromatographically (RP-HPLC). In addition, a formulation for freeze-drying was developed to ensure protein stability and integrity over a period of 60 days. Altogether, the bacterial expression and purification proved to be suitable, leading to bioactive and stable production of mFGF-2.

In **Phase II** the expression, purification and characterization of FGFBP1, as the other key partner in the FGF-2/ HS/ FGFBP1 system is detailed. As FGFBP1 exhibits a complex tertiary structure, comprised of five highly conserved disulfide bonds and presumably multiple glycosylation sites, a eukaryotic expression was used. Human embryonic kidney cells (HEK 293F) as suspension cells were transiently transfected with DNA-PEI complexes, leading to expression of Fc-tagged murine FGFBP1. Different PEI to DNA ratios and expression durations were investigated for optimal expression yields, which were confirmed by western blot analysis and SDS-PAGE. LC-MS/MS analysis of trypsin and elastase digested FGFBP1 gave first insights of the three O-glycosylation sites. Furthermore, the

binding protein was modified by inserting a His_6-tag between the Fc-tag (for purification) and the binding protein itself to enable later complexation with radioactive ^{99m}Tc as radio ligand to track bio distribution of administered FGFBP1 in mice. Overall, expression, purification and characterization of mFGFBP1 variants were successful with a minor draw back of instability of the tag free binding protein.

Combining the insights and results of expressed FGF-2 as well as FGFBP1 directed us to the investigation of the interaction of each partner in the FGF-2/ HS/ FGFBP1 system as **Phase III**. Thermodynamic behavior of FGF-2 and low molecular weight heparin (enoxaparin), as a surrogate for HS, under physiological conditions (pH 7.4) and pathophysiological conditions, similar to hypoxic, tumorous conditions (acidic pH) were monitored by means of isothermal titration calorimetry. Buffer types, as well as the pH influences binding parameters such as stoichiometry (n), enthalpy (ΔH) and to some extent the dissociation constant (K_D). These findings paved the way for kinetic binding investigations, which were performed by surface plasmon resonance assays. For the first time the K_D of full length FGFBP1 and FGF-2 was measured. Furthermore the binding behavior of FGF-2 to FGFBP1 in the presence of various heparin concentrations suggest a kinetic driven release of bound FGF-2 by its chaperone FGFBP1.

Having gathered multiple data on the FGF-2 /HS /FGFBP1 system mainly in solution, our next step in **Phase IV** was the development of a test system for immobilized proteins. With the necessity to better understand and monitor the cellular effects of immobilized growth factors, we decorated glass slides in a site-specific manner with an RGD-peptide for adhesion of cells and via the copper(I)-catalyzed-azide-alkyne cycloaddition (CuAAC) a fluorescent dye (a precursor for modified proteins for click chemistry). Human osteosarcoma cells were able to grow an the slides and the fluorescence dye was immobilized in a biocompatible way allowing future thorough bioactivity assay such as MTT-assays and phospho-ERK-assays of immobilized growth factors.

ZUSAMMENFASSUNG

In den letzten Jahren ist der Anteil an Biologika (Proteine, Zytokine und Wachstumsfaktoren), die neu zugelassen wurden, kontinuierlich angestiegen. Die größte Herausforderung für Biopharmazeutika stellt das Erreichen des gewünschten Wirkortes dar, aufgrund von beispielsweise enzymatischen und pH abhängigem Abbau, Plasmaproteinbindung, und niedriger Löslichkeit. Daher können moderne Wirkstoffträgersysteme, in denen Biologika ortsspezifisch an Träger immobilisiert sind und endogene Aufbewahrungsorte nachahmen, wie zum Beispiel die extrazelluläre Matrix, die Anwendung enorm erleichtern und folglich auch die Freisetzung von Biopharmazeutika, die exogen verabreicht wurden ermöglichen. Wir haben uns auf das Fibroblasten-Wachstumsfaktor 2/ Heparansulfat/ Fibroblasten-Wachstumsfaktor Bindungsprotein 1 (FGF-2/ HS/ FGFBP1) System als Modell gestützt.

Abschnitt I handelt von der Auswahl und der Subklonierung von einem wildtypischen, murinen FGF-2 Konstrukt in ein bakterielles pHis-Trx Vektorsystem – für hohe Ausbeuten bei der Expression und für eine schnell durchführbare Aufreinigung. Dieser erste Schritt ermöglicht die Bereitstellung von mFGF-2 für zukünftige Untersuchungen, das eine zentrale Rolle als Wachstumsfaktor im Wundheilungsprozess spielt, genauso wie bei der Gefäßversorgung von Tumoren. Daher wurde die richtige Expression von mFGF-2 durch MALDI-MS und SDS-PAGE überwacht, wobei die korrekte Faltung der tertiären beta-Faltblatt-Struktur durch Fluoreszenzmikroskopie ausgewertet wurde. Mit dem MTT Test konnten wir gewährleisten, dass die Bioaktivität von mFGF-2 und dem käuflich erworbenen FGF-2 übereinstimmen. Im letzten Schritt wurde die Reinheit, die eine wichtige Voraussetzung für künftige Bindungs- und Protein-Protein-Wechselwirkung-Untersuchungen darstellt, chromatographisch (RP-HPLC) überwacht. Des Weiteren wurde eine Formulierung zur Gefriertrocknung entwickelt, um die Stabilität und Unversehrtheit des Proteins über 60 Tage sicherzustellen. Insgesamt erwiesen sich die bakterielle Expression und Aufreinigung als geeignet und führten zur Herstellung von bioaktivem und stabilem mFGF-2.

Im **Abschnitt II** wird die Expression, Aufreinigung und Charakterisierung von FGFBP1 genau beschrieben, ein ebenso wichtiger Partner im FGF-2/HS/FGFBP1-System. Da FGFBP1 eine komplexe tertiäre Struktur aufweist, die aus fünf hochkonservierten Disulfidbrücken und vermutlich einigen Glykosylierungsstellen besteht, wurde ein

eukaryotisches Expressionssystem angewendet. Menschliche embryonale Nierenzellen (HEK 293F) wurden als Suspensionszellen transient mit DNA-PEI Komplexen transfiziert und führten zur Expression von Fc markiertem mausartigem FGFBP1. Verschiedene PEI:DNA Verhältnisse wurden untersucht, sowie die Dauer der Expression variiert, um die Ausbeute der Expression zu optimieren. Die Ergebnisse wurden mittels Western Blot und SDS-PAGE bestätigt. Die LC-MS/MS Messung, des mit Trypsin und Elastase verdautem FGFBP1, ergaben erste Erkenntnisse über die drei O-Glykosylierungsstellen. Des Weiteren wurde das Fusionsprotein durch Einschub eines His_6-tags zwischen den Fc-tag und FGFBP1 erweitert, um dem Protein die Eigenschaft zu geben, mehrwertige Kationen zu komplexieren. ^{99m}Tc, als radioaktiver Ligand, kann in späteren Untersuchungen die Verteilung im Gewebe, anhand von Mäusen darstellen. Die Expression, Aufreinigung, sowie die Charakterisierung von den murinen FGFBP1 Varianten war erfolgreich, jedoch erwies sich das Bindungsprotein ohne Fc-Teil als weniger stabil.

Durch Zusammenfassung der Ergebnisse und Erkenntnisse der beiden exprimierten Proteine mFGF-2 und FGFBP1, konnten wir die Wechselwirkungen der Partner im FGF-2 /HS / FGFBP1 Systems untereinander im **Abschnitt III** untersuchen. Isotherme Titrationskalorimetrie wurde herangezogen, um das thermodynamische Verhalten von FGF-2 mit niedermolekularem Heparin (Enoxaparin), als Stellvertreter für HS, unter physiologischen Bedingungen (pH 7,4) und pathologischer Bedingungen (saurer pH, hervorgerufen durch Sauerstoffmangel im Tumorgewebe) aufzuklären. Sowohl die Art des Puffersystems als auch der pH Wert beeinflussen die Bindungsparameter: Enthalpie (ΔH), die Stöchiometrie (n) und zu einem gewissen Teil sogar die Dissoziationkonstante (K_D). Die thermodynamischen Untersuchungen ermöglichten im folgenden Schritt, mittels Oberflächen Plasmon Resonanz (SPR), kinetische Bindungsverhältnisse zu ermitteln. Zum ersten Mal wurde dank der SPR Dissoziationskonstanten von FGFBP1 und FGF-2 erfasst.

Da alle bisherigen Erkenntnisse des FGF-2/ HS/ FGFBP1 Systems hauptsächlich von in Lösung gebrachten Partnern gewonnen wurden, erfolgte im **Abschnitt IV** die Entwicklung eines Testsystems für immobilisierte Proteine. Durch die zwingende Notwendigkeit zelluläre Effekte von immobilisierten Wachstumsfaktoren zu verstehen und zu beobachten, haben wir Objektträger aus Glas, in einem ortsspezifischem Verfahren mit einem RGD-Peptid, für die Zellanhaftung und mittels 1,3-Dipolare Cycloaddition einen Fluoreszenzfarbstoff (ein Vorläufer für „clickbare“, modifizierte Proteine) dekoriert.

Menschliche Knochenkrebszellen waren in der Lage auf diesen Objektträgern zu wachsen und der Farbstoff konnte in einem nicht zytotoxischen Verfahren spezifisch an der Oberfläche immobilisiert werden. Dieses Testsystem erlaubt in Zukunft ausführliche Bioaktivitäts- und Proliferationsstudien von immobilisierten Proteinen durchzuführen.

INTRODUCTION

Fibroblast growth factor 2 (FGF-2)

FGF Family

Fibroblast growth factor 2 (FGF-2), also known as basic fibroblast growth factor (bFGF), fibroblast growth factor basic (FGFb) or heparin binding growth factor 2 (HBGF2) is a member of the fibroblast growth factor (FGF) superfamily. It was first isolated from bovine pituitary glands [1].

The fibroblast growth factor family comprises 22 mammalian fibroblast growth factors (FGF-1 – FGF-23), of which 18 (FGF-1 – FGF-10 and FGF-15 – FGF-23) signal through FGF-receptors (FGFRs). These are divided into seven subfamilies, dependent on variations in homology, sequence and phylogeny (**Table 1**).

Table 1. FGF subfamilies

Fgf1 subfamily	Fgf7 subfamily	Fgf4 subfamily	Fgf8 subfamily	Fgf9 subfamily	Fgf15/19 subfamily	Fgf11 subfamily
FGF-1	FGF-3	FGF-4	FGF-8	FGF-9	FGF-15/19	FGF-11
FGF-2	FGF-7	FGF-5	FGF-17	FGF-16	FGF-21	FGF-12
	FGF-10	FGF-6	FGF-18	FGF-20	FGF-23	FGF-13
	FGF-22					FGF-14

Most tissues show low trace amounts of FGF-2 (serum concentration ~16 ng/mL [2]), however it is highly expressed in the pituitary gland and in the brain. It plays an important role in a variety of mitogenic processes such as angiogenesis (growth and development of new blood vessels), wound healing, hematopoiesis such as megakaryocyptopoesis, granulopoiesis as well as stem cell survival and tissue homeostasis [3]. Furthermore FGF-2 supports survival of neural cells in the nervous system [4].

FGF-2 structure

Basic fibroblast growth factor was first identified as a 15 kDa peptide [1], which is a proteolytic product of the later discovered 18 kDa primary secreted form [5]. As many members of the FGF family, FGF-2 binds to proteoglycans (PG) e.g. heparin, hyaluronic acid, chondroitin sulfate and heparan sulfate PG (HSPGs). HPSGs are glycoproteins, containing a type of glycosaminglycan (GAG) and heparan sulphate (HS) chains that are covalently linked to the core protein. FGF-2 is stored in the extra cellular matrix (ECM) which consists of perlecan, syndecan, as well as betaglycan and is protected by this interaction with HS chains against denaturation, proteolysis, and thermal, and pH-dependent degradation [6]–[9].

Alternate downstream codons and in frame CUG codons of the conventional AUG codon result into multiple isoforms of FGF-2, ranging from 18-34 kDa. The larger 22, 22.5, 24 and 34 kDa isoforms are intracellular active and are transported into the nucleus, thereby modulating gene expression to stimulate cell growth [10], [11]. The 18 kDa FGF-2 isoform is distributed within the cytosol for secretion into the intracellular space [12]–[15]. 18 kDa FGF-2 is a globular protein comprising a single polypeptide of 155 amino acids as a precursor form, which is maturated into 146 amino acids after proteolytic cleavage [10]. It has an isoelectric point (p*I*) of 9.6 due to the high number of basic residues. The nucleotide and amino sequence comparison of human and bovine basic fibroblast growth factor shows a high degree of sequence conservation, with an overall sequence homology of over 98 % with only one amino acid being different [16]. Determination of the crystal structure of FGF-2 in absence and presence of heparan sulfate revealed that FGF-2 consists of 12 antiparallel β-sheets, known as a β-trefoil core, forming a trigonal pyramid structure (**Figure 1**) [17]–[19]. Each FGF-2 incorporates four cysteine residues without forming intramolecular disulfide bonds. Alkylation experiments revealed that the two outer cysteine (in the 155 aa hFGF-2 form: cysteine 34 and 101) are buried within the β-sheet core, whereas the other two cysteine residues are localized on the surface of FGF-2, susceptible for modification but also prone the molecule to chemical instability due to swift oxidation of the free thiol groups [17]–[25]. Phosphorylation via protein kinases A and C can occur on two sites (Ser 64 and Thr 12) [26].

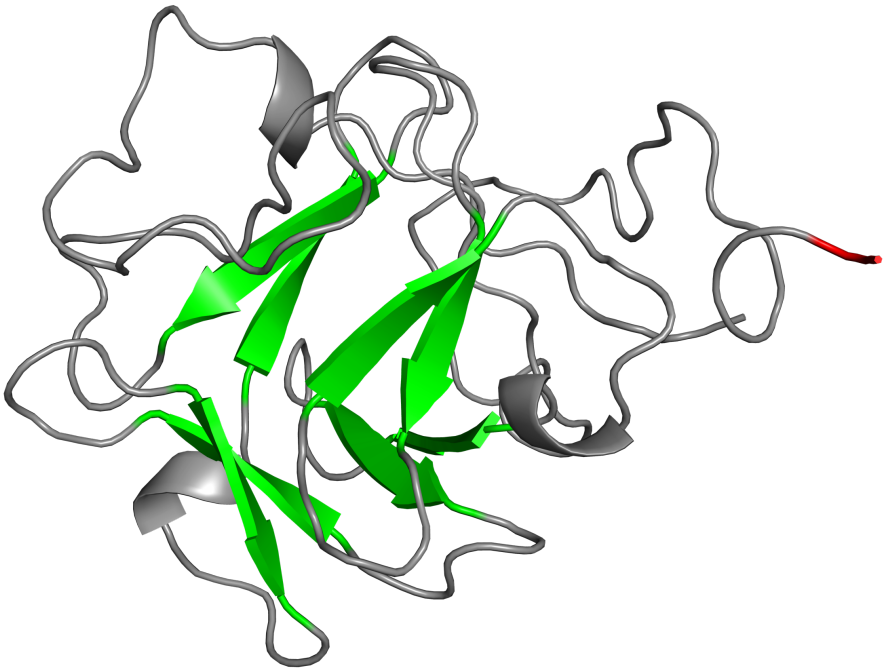

Figure 1. Structure of FGF-2: pdb file 1BLA: β-sheets (green), N-terminus (red).

FGF receptors

FGF-2 acts as an autocrine and paracrine growth factor through binding, dimerization and activation of specific cell surface receptors, known as fibroblast growth factor receptors (FGFRs) [27]–[29]. The four major receptor families of signaling receptor tyrosine kinases are FGFR1 (flg), FGFR2 (bek), FGFR3, and FGFR4 [30], [31]. FGFRs contain a conserved cytoplasmic tyrosine kinase domain, a single transmembrane domain and an extracellular domain, which defines the specificity of ligand binding. The extracellular ligand-binding domain is composed of two or three immunoglobulin (Ig)-like loops, labeled D1-D3 [32], [33]. A conserved positively charged region of D2 provides a low affinity binding site for heparan sulphates [34]–[36]. Alternative mRNA splicing generates several FGFR isoforms, an extracellular domain composed of either two or three Ig-like domains, soluble secreted FGFR forms and variations especially in the extracellular sequence of D3 thus altering the

ligand-binding specificity [37], [38]. On the FGFR2 gene exon 7 encodes for the N-terminal of D3 ("a" form), exon 8 and 9 encode for the C-terminal of D3 resulting into the FGFR forms "b" and "c", respectively. The FGFRs are found in various cells, however alternative splicing occurs in a tissue dependent manner, resulting into different isoforms as in epithelial "b" and mesenchymal "c" isoforms [39]–[43].

Table 2. FGF-2 binding of FGFR isoforms

Specificity	FGFR isoform				
FGF-2 specificity	FGFR1b	FGFR1c	FGFR2c	FGFR3c	FGFR4
no FGF-2 specificity	FGFR2b	FGFR3b			

Adapted from [44], [45].

FGF-Receptor signaling/ activation

An essential step in FGF signaling is the ligand induced dimerization of the FGFRs, which are classified as "high-affinity" receptors (K_D of ~20 pM) [46]. HSPGs are required for the signaling [34], [47]–[52] and bind FGFs directly as low affinity receptors (K_D of ~2 nM) [46]. Both crystal structure and biochemical experiments confirm a model, in which the FGF-dependent FGFR dimerization is induced by heparin. One molecule heparin binds one molecule FGF and one molecule FGFR resulting into a stable 1:1:1 FGF:FGFR:heparin ternary complex. A dimeric 2:2:2 FGF:FGFR:heparin complex is formed via the FGFR of each ternary complex, in which heparin plays a pivotal role to stabilize the dimerization [34]. Consequently, temporal and spatial expression of HSPG modulates signaling of FGF-2 on FGFRs. Because of the distinctive expression levels of FGFRs and HSPG in various cells and tissues, internalization of FGF-2 by its high - and low affinity receptors triggers pleiotropic effects [50], [52]–[58].

After FGFRs dimerization and autophosphorylation, a number of signal pathways are activated including ERK1/2 and p38 MAPK, P-I-3K/AKT, JNK and src. This activation results into different biological responses dependent on the downstream signaling cascade, including proliferation and differentiation.

FGF-2 Therapy

As FGF-2 acts on cells of mesenchymal origin, inducing differentiation and proliferation of multiple mammalian cells, classical systemic (intravenous) therapeutic administration is limited due its pleiotropic functions. Furthermore serum half-life of FGF-2 administered via intravenous (iv) and subcutaneous (sc) injections is approximately 50 min (mongrel dogs) [59]. Radioactive labeled ^{125}I-FGF-2 delivered intravenously into the Swan Ganz catheter and into the left atrium of dogs was primarily recovered from liver, kidneys spleen and lungs, illustrating the necessity of a local administration to reduce adverse effects and achieve therapeutically relevant concentrations in desired tissues [59], [60]. Therefore, local administration of FGF-2 is a viable option. Gelatin hydrogels were loaded with FGF-2 to enhance tendon-to-bone healing after rotator cuff injuries in rats. The rotator cuff injuries were improved biomechanically and histologically by increasing the growth of tenogenic progenitor cells, resulting into tendon and bone healing [61]. Another potential therapy-option of FGF-2 lies in cardiovascular diseases. Heparin beads for sustained-release of FGF-2 were administered in an open chest surgery to the ischemic myocardium and resulted in a prolonged revascularization, thus reduction of the ischemic region [62]. A different approach in regulating FGF-2 mediated FGFR signaling in therapy is the application of heparinoids, which mimic heparin, such as Suramin (polysulphated naphylurea) for prostate, kidney and bladder cancers [63], [64].

Fibroblast growth factor binding protein 1 (FGFBP1)

History

The fibroblast growth factor binding protein 1 (FGFBP1), also known as Mr 17 000 heparin-binding protein (HBp17) is a secreted protein that binds to various members of the FGF family such as FGF-1, FGF-2, FGF-7, FGF-10 and FGF-22 in a noncovalent, reversible manner [65]–[68]. It acts as a chaperone for its binding partners, protecting them from degradation and retaining their mitogenic activity [65], [67], [69]–[72].

FGFBP1 structure

The 17 kDa polypeptide with its primary structure consisting of 234 amino acids was first isolated from A431 human epidermoid carcinoma cells. It was found to bind FGF-1 and FGF-2 and interacts with heparan sulfates e.g. heparin [65]. It contains a signal sequence for secretion which is located N-terminally, rendering FGFBP1 with the feature of a canonical extracellular signal peptide [73]. FGFBP1 derives from a 26 kDA precursor protein after proteolytic cleavage of the C-terminal to a mature 23 kDa protein and processing to the 17 kDa product (p*I* = 8.3 at physiological pH) [65], [67]. Human FGFBP1 shares a high amino acid homology to the bovine, murine, rat and chicken sequence (**Figure 2A**) [69]. Furthermore, all 10 cysteine residues are highly conserved and share the same disulfide bond pattern, suggesting a strong conservation of the tertiary structure of FGFBP1 (**Figure 2B**) [65], [69], [70], [74], [75]. T7 phage display revealed the C-terminus (amino acids 193 – 234) as the main binding domain to FGF-2 [74] whereas the different binding site for heparan sulfates is located in the middle of the protein comprised of the basic amino acid cluster (amino acids 110 – 143 in bovine FGFBP1) [76].

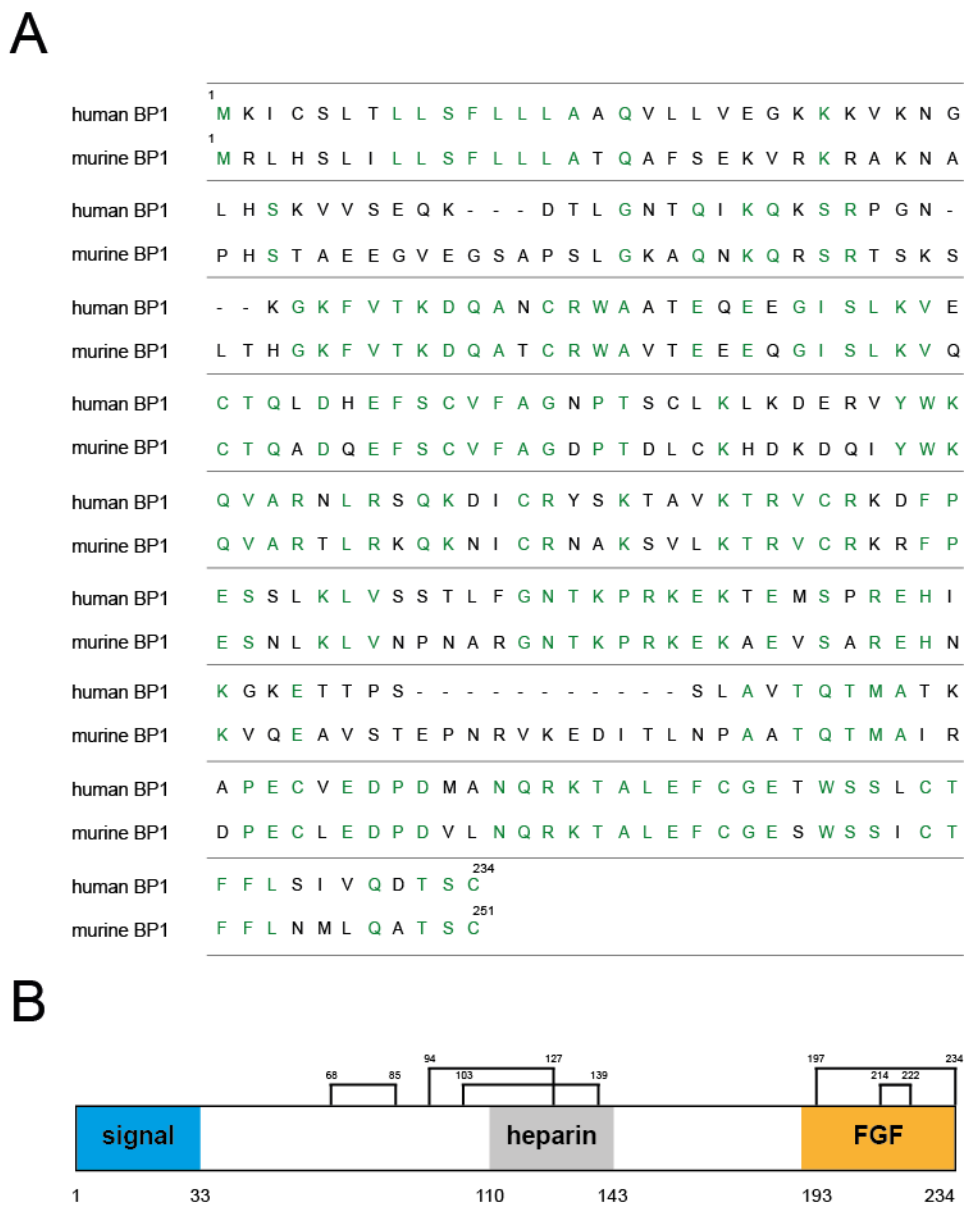

Figure 2. Structure of FGFBP1. (A) Amino acid alignment of human FGFBP1 (GeneBank ™ accession number NP_005121) and murine FGFBP1 (NP_032035). Identical amino acids are depicted in green. **(B)** Domain structure of the human FGFBP1 signal: signal sequence heparin: heparin binding site [76] FGF: FGF-2 binding site [74] brackets: disulfide bonds [69]. Adapted from [74].

Occurrence and release of FGFBP1

The expression rate of FGFBP1 in human adult tissues is very low and strictly regulated [70]. Expression is highly increased in squamous cell carcinoma cell lines (SCC) of lung, skin, cervix, head, neck and lung, colon adenocarcinoma cell lines and in SCC samples [67], [70], [72]. In mice, FGFBP1 expression is upregulated during the embryonic development,

particularly in epithelial cells such as in the lung, intestine and skin during developmental processes of these tissues [70]. Most FGFs are sequestered to and tightly bound by the HSPG of the ECM, quenching the biological activity [77], [78]. Both, FGF-1 and FGF-2, lack a signal peptide sequence and are thus not secreted through the endoplasmatic reticulum and Golgi apparatus [79]. Many FGFs, in particular FGF-2, need to be solubilized for full-activity [67]. Three mechanisms by which FGFs are released from the ECM are known (**Figure 3**): (i) heparanases cleaving the heparan sulfate chain of the HSPG, (ii) proteases degrading the core protein and (iii) FGFBP1 as a carrier protein actively shuttling its binding partner from the ECM to FGF-receptors [65], [67], [80]–[85].

.

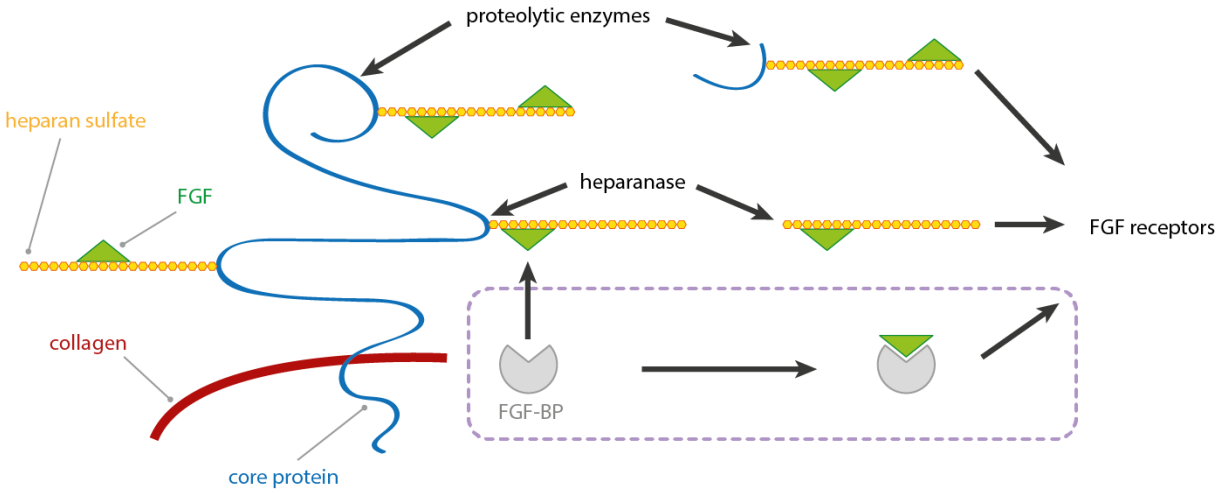

Figure 3. Release mechanism of FGFs from the ECM. Adapted from [86].

FGFBP1 as an angiogenic switch molecule plays a pivotal role by releasing various FGFs to exert their mitogenic and angiogenic activity during the early phase of tumor growth [87]. These findings were confirmed by decreasing the rate of blood vessel development and formation accompanied by reduced FGFBP1 by ribozyme targeting in human SCC and colon carcinoma cell lines and in xenografted tumors of mice [67], [72] as well as modulation of a non-tumorigenic cell line (SW-13) into tumoric phenotypes by addition of FGFBP1 [67]. Inhibition of angiogenesis was observed in presence of all-trans retinoic acids which reduce FGFBP1 expression in carcinoma xenografts, resulting into slower tumor growth [88], [89].

Besides tumor growth, angiogenesis plays a crucial part in wound healing [90]. Particularly FGF-2 but also FGF-7, 10 and 22, all binding partners of FGFBP1, are pivotal during multistep stages of wound healing [65]–[68], [91]–[95].

Surface decoration pharmaceutical proteins

A key strategy in tissue engineering is the presentation of growth factors that play a pivotal role in differentiation of cells and tissue regeneration [96]. However, chemical degradation, elimination and other means of inactivation of the presented therapeutic protein in the physiological environment may limit their therapeutic functions. Thus, high doses have to be applied/ administered (systemically or locally) to achieve desired therapeutic effects often resulting into unwanted side-effects, such as intolerances or toxicities [97], [98]. Local presentation of growth factors by means of immobilization strategies may allow circumventing these limitations. Covalent conjugation of therapeutic proteins to biomaterials as drug delivery systems allows spatial control, prolonged bioactivity (due to minimization of leaching) [99], [100] and reduced doses of the therapeutic factor. Not only therapeutic applications, as e.g. grafts benefit from these strategies but also diagnostic tools such as microarrays, biochips, imaging probes and biosensors [101], [102].

Immobilization strategies for pharmaceutical proteins

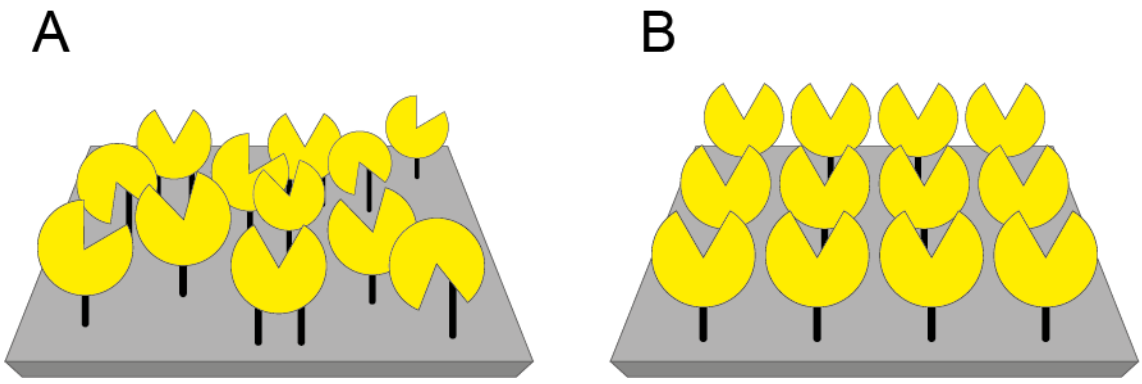

Figure 4. Difference between: (A) non-site specific and **(B)** site specific protein immobilization. Adapted from [103].

Non-site specific (random), covalent immobilization

Amine groups are strong and stable nucleophiles that easily react with activated carboxylic acids [104]–[106] and are abundantly present in proteins through the proteinogenic amino acid lysine, which composes up to 6-10 % of the overall amino acid sequence of proteins

[107], [108]. Carboxylic acids of the surface are activated into reactive N-hydroxysuccinimide (NHS) esters via classical 1-ethyl-3-(3-dimethylaminopropyl) carbodiimide (EDC)/ NHS chemistry which form stable amid bonds in aqueous buffers at neutral pH with the amine group of the protein [109]. Cysteines contain a nucleophilic thiol group that is very reactive at neutral pH values. The thiol group reacts readily with α,β-unsaturated carbonyls (e.g. maleimides) forming thioethers [110]. Free cysteines are scarcely present in most proteins, limiting the possible immobilization sites of the proteins. However, non-site specific immobilization of unmodified proteins unto surfaces results into a heterogeneous binding due to random orientation of the protein, consequently reducing or inactivating its biological activity [111]–[113].

Site-specific, covalent immobilization

Introduction of a chemically functionalized group into the protein structure permits selective modification e.g. by site-specifically coupling the protein to a corresponding reactive group presented onto a surface. Ideally, the introduced functionalized group allows bio-orthogonal chemistry, i.e., the immobilization reaction is unaffected by endogenous amino acids (their functional side groups) and unhindered by regular cellular biochemical reactions. The site, on which the functional chemical group is to be inserted, can be chosen strategically to regions not interfering with the receptor binding site, which is not crucial to the three dimensional conformational integrity and consequently not impairing biological activity. Implementing bio-orthogonal chemistries for surface decoration result into an oriented and covalent immobilization, therefore “click” reactions have recently gained growing popularity [114]–[118]. Characteristics of the “click” chemistry are mild reaction conditions, selectivity, and aqueous solution as reaction medium forming stable products under physiological conditions.

The modified Staudinger ligation is a bio-orthogonal method to form stable amid bonds via azides and triphenylphosphines [119] rather than the classical Staudinger ligation with hydrolysis susceptible amine bonds [120]. This method utilizes the bio-orthogonal reaction of azide groups with phosphines as demonstrated in protein immobilization of RNase S to microarray slides [121]. However, the drawback of this chemistry is the chemical instability of phosphine even under mild conditions.

Therefore the 1,3-dipolar cycloaddition, which was first performed in 1893 [122] gained a comeback as the archetypical “click” reaction. The copper(I)-catalyzed-azide-alkyne cycloaddition (CuAAC) results in a 1,2,3-triazole, a ligation process for azide functionalized

proteins [123]–[126]. Under physiological conditions and in an aqueous solution the catalysis to a disubstituted triazol as the sole product is highly specific [118], [121]. Cu(I) stabilizing agents such as THPTA or TBTA enhance the reaction kinetics [127], [128]. However the cytotoxicity of copper catalyst and possible protein precipitation limit the overall application of this method [129], [130]. Therefore copper free cycloadditions releasing ring strain energy of cyclooctyne groups allow a biocompatible Huisgen 1,3-dipolar azide-alkyne cycloaddition [131], [132].

The site selectivity is accomplished by predefining a site in the primary structure of the protein at which the following conjugation occurs. Manifold utilities in the synthetic chemistry facilitate the incorporation of diverse groups into the peptide during its synthesis [133]. A far greater challenge poses the insertion of non-natural amino acids into proteins, however it is succeeded by recombinant methods on the level of protein expression. Complex strategies such as intervening into the organism's native translational system by adding exogenous substrates for protein expression are required [130], [134]. Aminoacyl-tRNA synthetases control the incorporation of amino acids dependent to their corresponding codon. The "amber" codon (UAG) is assigned to a tRNA loaded via the aminoacyl-tRNA synthetase with non-canonical amino acids equipped with functional groups e.g., alkyne groups an pyrrolysine analogue [135]. These strategies enable a dual modification of biomaterials such as introducing RGD motifs, for cellular adhesion, and growth factors for cell assays.

Enzyme catalyzed immobilization.

Another immobilization strategy is the implementation of cross-linking enzymes such as microbial transglutaminase (MTG) from *Streptomyces mobaraensis*. The ε-amine of a lysine of one protein is transamidated to the amide of another glutamine [136], [137]. A suitable tag containing glutamine can be added C- or N-terminally to the therapeutic protein, whereas the biomaterial is decorated with a natural substrate of MTG such as casein. The immobilization is site-directed however the selectivity of the enzyme is low, leading to multiple random immobilizations.

AIM OF THESIS

The aim of this study was to investigate biomimetic concepts of nature and translate these to advanced drug delivery systems. We chose the FGF-2/ HS/ FGFBP1 system, as the current literature only poorly elucidates the interaction of either HS with FGF-2 and FGF-2 with FGFBP1 but not all three partners, thus leaving the questions unanswered how FGF-2, immobilized by the ECM, is released and if bound FGF-2 remains bioactive. Therefore, a wild type murine FGF-2 was expressed and characterized. Subsequently murine FGFBP1 with is complex tertiary structure was expressed in human cells and characterized. However, the initial goal was to investigate binding properties and mechanisms of FGF-2 with FGFBP1 in the presence of HS under various conditions (pH and buffer type). Finally, a test system to investigate site-specific immobilization of FGF-2 to planar surfaces was developed. Hence, the present work was subdivided into four phases (**Figure 5**).

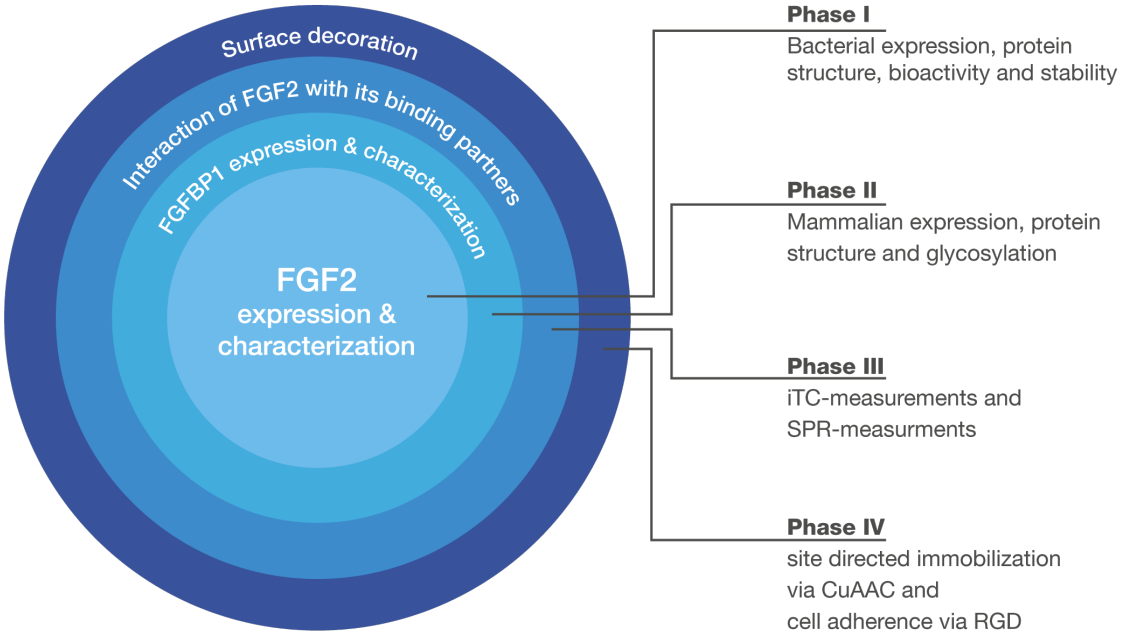

Figure 5. Study design for the development of advanced drug delivery system of FGF-2/ HS/ FGFBP1.

MATERIALS AND METHODS

Devices

Device	Type	Vendor
Incubator	TH15 + KS-15 Control	Edmund Bühler GmbH
	MIR 220 shaking incubator	Sanyo Gallenkamp
	HeraCell 150i	Thermo Scientific
Mixer	Thermomixer comfort	Eppendorf
Centrifuge	Allegra®X-15R Centrifuge + SX4750A rotor	Beckman Coulter
	Micro 2416 centrifuge	VWR
	Varifuge 3.ORS	Heraeus
	Centrifuge 5804 R + A-4-44 rotor	Eppendorf
	L8-60M Ultracentrifuge	Beckman-Coulter
UV/Vis spectrophotometer	Genesys 10S UV-Vis + Tray Cell (HellmaAnalytics)	Thermo Scientific
Microwave	NN-E209 W	Panasonic
Ultrasonic Homogenizer	Bandelin Sonoplus Homogenisatior HD3100 +UW 3100 + KE 76 Sonotrode	Bandelin
Rollermixer	Rollermixer SRT1	Stuart

Vortex Mixer	VV 3	VWR
Electrophoresis Power Supply	Model 3000Xi + Mini Protean II + Mini Sub Cell TG	Bio-Rad
Safety Cabinets	SAFE 2020	Thermo Scientific
Waterbath	ED thermostate	Julabo
Microscope		VWR
Hemocytometer	Neubauer	LO Laboroptik
Pipette controller	Accurpette	VWR
Geldocumentation	FluorChem FC2	Alpha Innotech
	Gene Flash	Bolabo Scientific Instruments
Thermalcycler	Personal Cycler	Biometra
Evaporator	TurboVap LV Evaporator	Zymark
Platereader	SpectraMax 250	Molecular Devices
UPLC	Elite La Chrome + DAD	VWR
FL Microscope	Z1 epi-fluorescence microscope	Zeiss
pH Meter	Phenomenal 221	VWR
Balances	Delta Range XR 105	Mettler Toledo
	AJ 100	Mettler
	Delta Range PB 3002	Mettler Toledo
Freeze-drier	Alpha 1-4 + LDC 1M	Christ
Protein Purification	ÄKTApurifier	GE

System		
SPR	ProteOn XPR 36	Bio-Rad
Shaker	KS 130 basic	IKA
Magnetic stirrer		
Dialysis Membrane	SpectraPor, MWCO 6000-8000	Spectrum Laboratories
Centrifugal Concentrator	Vivaspin 6 10000 MWCO	Sartorius stedim
Dialysis Devices	Slide-A-Lyzer MINI Dialysis Devices 10K MWCO	Thermo scientific

Solutions

Solution	Composition
Phosphate buffered saline pH 8.5	2.7 mM KCl 136.9 mM NaCl 4.3 mM Na_2HPO_4 1.5 mM KH_2PO_4
Transfer Buffer	25 mM tris 192 mM glycine 20 % (v/v) MeOH
SDS electrophoresis buffer	25 mM tris 192 mM glycine 1 % (w/v) SDS
Acrylamide/bisacrylamide solution 30 %/0.8 %	30 % (w/v) acrylamide 0.8 % N,N'-methylenebisacrylamide
Stacking gel buffer (4x) pH 6.8	500 mM tris 0.4 % (w/v) SDS
Seperating gel buffer (4x) pH 8.8	1.5 M tris 0.4 % (w/v) SDS
SDS sample buffer (6x)	7 mL (v/v) stacking gel buffer (4x) 3 mL glycerin 1 g SDS 1.2 mg bromphenol blue 0.6 M DTT
APS solution	10 % (w/v) ammonium persulfate
Coomassie stain solution	0.1 % (w/v) Coomassie Brilliant Blue 10 % (v/v) glacial acetic acid 50 % (v/v) MeOH
Coomassie destain solution	10 %(v/v) Glacial acetic acid 20 % (v/v) MeOH
Lysogeny broth (LB) medium pH 7.2	1 % tryptone 0.5 % NaCl 0.5 % yeast extract 0.5 % $MgSO_4$*7 H_2O 0.1 % glucose (w/v)
Low Salt LB medium pH 7.5	1 % tryptone 0.5 % NaCl 0.5 % yeast extract (w/v)
Glycerin stock solution	20 % (v/v) Glycerin in LB medium
SOC-medium	0.5 % (w/v) yeast extract 2 % (w/v) tryptone) 10 mM NaCl 2.5 mM KCl 10 mM $MgCl_2$ 10 mM $MgSO_4$ 20 mM glucose
Terrific broth (TB) medium	13.3 % (w/v) tryptone 26.7 % (w/v) yeast extract

	0.44 % (v/v) glycerine
10x phosphate buffer	170 mM $KHPO_4$ 720 mM K_2HPO_4
Trypan blue solution	0.5 % trypan blue 0.9 % NaCl
Agar medium pH 7.5	1.4 % agar 0.8 % NaCl 1 % tryptone 0.5 % yeast extract 0.5 % glucose (w/v)
Low salt agar medium pH 7.5	1.5 % (w/v) agar in low salt LB medium
Ampicillin solution	10 % (w/v) ampicillin-Na
Kanamycin solution	10 % (w/v) kanamycin sulfate
TAE buffer pH 8.5	40 mM tris 0.11 % (v/v) glacial acetic acid 2 mM EDTA
Blocking solution	5 % (w/v) skim milk powder in PBS (w/v)
Trypsin EDTA solution	0.25 % trypsin 0.02 % EDTA in PBS (w/v)
Binding buffer / solubilization buffer pH 7.5	10 mM tris 50 mM NaCl
MTT stain solution	0.5 % (v/w) MTT in PBS
Stain solubilization solution	3 % SDS 0.04 N HCl 81 % (v/v) 2-propanol
MG-63 assay medium	0.52 % (w/v) BSA 1.82 mM L-glutamine 91 U/ml penicillin G 91 µg/µL streptomycine 0.91 % (w/v) NEA in MEM-Medium
MG-63 growth medium	8.8 % FCS 1.77mM L-glutamine 88 U/ml penicillin G 88 µg/µL streptomycin 0.88 % NEA in MEM
NIH 3T3 growth medium	10 % FCS in DMEM (high glucose)
NIH 3T3 assay medium	0.5 % FCS 0.52 % (w/v) BSA 1.82 mM L-glutamine 91 U/ml Penicillin G 91 µg/µL Streptomycine 0.91 % (w/v) NEA in DMEM (high glucose)

PEI solution pH 7.5	0.1 % (w/v) PEI 25 mM HEPES 150 mM NaCl
Fixation solution	4 % (w/v) paraformaldehyde in PBS

All other chemicals were at least of analytical grade or from Sigma Aldrich.

Plasmids

pET11a (Novagen)
containing the pyrrolysin tRNA and the lipoprotein promoter lpp and the terminal RRN b/c as decribed by Eger et al.

Kindly provided by Dr. Marina Rubini

pRSF-Duet (Novagen)
containing the gene fort he pyrrolysine tRNA synthetase pylS in the MCS II as described by Eger et al.

Kindly provided by Dr. Marina Rubini

pHisTrx (derivative of pET-32a) (Novagen)
containing the gene for *E.coli* thioredoxin (trxA), an N-terminal 6-His tag, a thrombin cleavage site and a unique MCS.

Kindly provided by Dr. Richard a Kammerer

The plasmid containing the gene for *IgC_CH3 & CH4 and mFGFBP1 plasmid* was kindly provided by Novartis AG.

Methods

All experimental work described in the following was done by me, except for:

- Subcloning

  The strategy was discussed and planned by me in collaboration with Prof. Dr. Dr. Lorenz Meinel and Dr. Tessa Lühmann, and the technical work was performed by Cornelia Heindl (technical assistant).

- MALDI-MS

  The experiments were planned by me in collaboration with Prof. Dr. Dr. Lorenz Meinel and Dr. Tessa Lühmann. The preparation was undertaken by me, the technical work of the analytical part was performed by Dr. Jennifer Ritzer (peptide analysis) and Stephanie Lamer (protein analysis).
- Trypsin digestion and Nano LC-MS/MS analysis

  The strategy was discussed and planned by me in collaboration with Prof. Dr. Dr. Lorenz Meinel, Prof. Dr. Andreas Schlosser and Dr. Tessa Lühmann. The preparation was undertaken by me, the technical work , analysis of data and the method description was provided by Stephanie Lamer.
- Surface Plasmon Resonance

  The strategy was discussed and planned by me in collaboration with Prof. Dr. Dr. Lorenz Meinel, Prof. Dr. Thomas Müller, Dr. Joachim Nickel and Dr. Tessa Lühmann. The biotinylation was performed by me in collaboration with Dr. Joachim Nickel. The technical work of the SPR was performed by Prof. Dr. Thomas Müller, the analytical part by me in collaboration with Prof. Dr. Thomas Müller.

Cell culture

Cell counting

The hemocytometer was set up by covering the counting chamber with a cover slide until Newton's rings were observable, indicating proper contact of the two glass surfaces. Ten µL of the sample were pipetted to the edge of the cover slide and transferred into the hollowness due to the capillary forces. The average cell number was determined over 5 squares of 1 x 1

mm^2 and was divided by the volume of the chamber squares to calculate the cell concentration of the sample as following:

$$cell\ concentration\left[\frac{cells}{mL}\right] = \frac{number\ of\ cells}{volume\ of\ chamber\ [mL]}$$

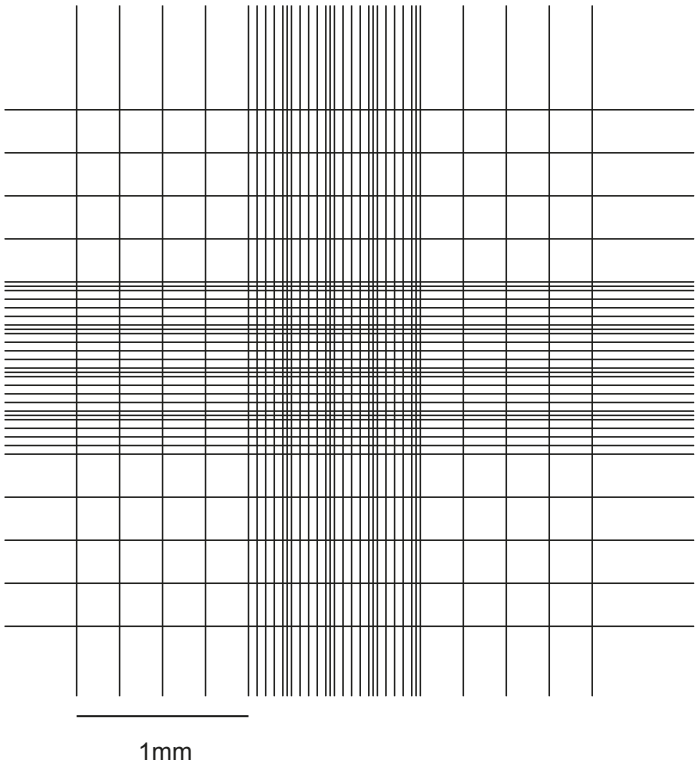

Figure 6. Hemocytometer grid

Cell viability

Cell viability was assessed by using the trypan blue staining procedure. Living cells have intact cell membranes and do not up take impermeable dyes (trypan blue), whereas dead cells are stained by trypan blue. One hundred microliter of cell suspension were mixed with 100 µL pre-warmed PBS. After adding 270 µL of pre warmed trypan blue solution, the cells were carefully mixed by pipetting up and down. The mixture was incubated for 4 minutes at 37 °C in the water bath. Five individual 1 mm^2 x1 mm^2 squares in the hemocytometer were analyzed by counting trypan blue positive and negative cells and viability was calculated as following:

$$\%\ of\ viable\ cells = \frac{number\ of\ viable\ cells}{total\ number\ of\ cells} \cdot 100$$

MG-63 cells

MG-63 cells were cultivated in MG-63 growth medium at 37 °C, 5 % CO_2 in a humid atmosphere. Cell passaging was performed at a confluency of approx. 80 % after 23 days in culture. The adherent cells were washed pre-warmed PBS to remove small remaining amounts of medium containing FCS. Detachment of cells was achieved with 3 mL of trypsin EDTA solution for 4 minutes at 37 °C. To inhibit the activity of trypsin 10 mL of growth medium was added to the cell suspension and centrifuged (250 g; room temperature; 5 min). After aspirating the supernatant, the cell pellet was resuspended in fresh growth medium. One tenth of the suspension was transferred to a new culture flask containing 15 mL growth medium.

HEK 293 F cells

Suspended HEK 293 Freestyle cells were cultivated in FreeStyle 293 expression medium in vented polycarbonate Erlenmeyer flasks in the incubator at 37 °C and 8 % CO_2 with humidified atmosphere and 130–180 rpm on an orbital shaker. The culture flasks were filled at a maximum volumetric degree of 20–40 % with cell suspension. HEK 293 Freestyle cells were maintained at a density range of 1–2 $*10^6$ cells / mL. Once cell density exceeded $2*10^6$ cells / mL cells were splitted by diluting the suspension 1:2 – 1:5 with fresh FreeStyle 293 expression medium. In order to avoid cell aggregation especially in the lower passages the diluted cell suspension was vortexed for 30 seconds in a 50 mL falcon tube and transferred afterwards to the Erlenmeyer flasks.

Transfection

HEK 293 F cells were splitted 24 hours prior to transfection to a concentration of $1*10^6$ cells / mL to ensure that the cells were in log-phase. The cells were counted in a hemocytometer and the viability was confirmed to be over 95 % in order to ensure an efficient transfection. The cell suspension was transferred to 50 mL tubes and centrifuged (5 minutes at room temperature, 250 g). The supernatant was removed by aspiration. Fresh pre-warmed HEK 293 Expression medium was added to the cell pellet to obtain a cell concentration of $2.5*10^6$ cells / mL. The suspension was transferred into vented Erlenmeyer flasks on the orbital shaker in the incubator of appropriate size so that the sample volume did not exceed 20 % of the total volume of the culture flask. The expression vector plasmid DNA of Fc-FGFBP1 resp. Fc-His-FGFBP1 and the PEI-solution was diluted with the expression medium to a concentration of 0.5 µg/µL. The corresponding volume of the DNA solution to achieve a final concentration of 1–6 µg/mL was added to the cell suspension and incubated for 5 minutes in the incubator. After 5 minutes of shaking, the PEI solution was pipetted to the suspension with a final

concentration of 9 µg/mL. After 24 h the same volume of HEK 293 Expression medium was added to dilute the suspension. After further 72 h the medium was harvested by spinning down the cells in falcon tubes (5000 g, 30 minutes, 4 °C). The clarified supernatant was filtered with a 0.22 µm membrane (Whatmanfilter) thereafter.

MTT Potency Assay

FGF-2 bioactivity was determined in human NIH-3T3 cells as previously described [138]. After trypsinization, NIH-3T3 cells were resuspended in growth medium at a concentration of $2*10^4$ cells / mL. One hundred µL (at a final concentration of $2*10^3$ cells) were pipetted into the wells of a 96-well tissue culture plate and incubated for 24 h at 37 °C and 5 % CO_2 in humidified atmosphere. After 24 h of incubation, the growth medium was exchanged against 100 µL per well of assay medium. After further 24 h, dilution series of mFGF-2 and purchased FGF-2 standard (R&D Systems) were prepared in assay medium at a concentration range from 50—0.02 ng/mL. One hundred microliter of each dilution was added to the wells and carefully mixed. 92 h post seeding, 50 µL of MTT staining solution was added to each well and incubated for 4 h at 37 °C and 5 % CO_2. The medium was carefully aspirated prior before adding 100 µL of stain solubilization solution to solubilize formed formazan crystals. The plate was sealed with parafilm and incubated in the dark at room temperature for 90 minutes. The absorbance was determined at a wavelength of 570 nm on a plate reader system.

WST-1 Assay

Bioactivity of FGF-2 was determined in human osteosarcoma MG-63 cells as previously described for insulin like growth factor 1 [139]. Briefly, $2*10^4$ MG-63 cells in 100 µL assay medium were seeded into the wells of a 96 wells tissue culture plate. 24 h after seeding, dilution series of 100 – 0.2 ng/mL mFGF-2 and a purchased FGF-2 standard (R&D Systems) were prepared in assay medium and 100 µL of each dilution was added to the cells in a 96-well plate and incubated for 48 h at 37 °C, 5 % CO_2. The pre-warmed WST-1 solution and the assay medium were mixed to equal parts and 20 µL of this mixture was gently added into the wells. After an incubation time of 4 h at 37 °C and 5 % CO_2, the well-plate was protected from light and 100 µL of the supernatant was transferred to a clear 96-well flat bottom microtiter plate. Water-soluble formazan was quantified at a wavelength of 450 nm using a plate reader system.

pERK / ERK signaling

$4*10^4$ MG-63 cells were seeded into the wells of the superstructure in assay medium in a final volume of 100 µL and incubated at 37 °C and 5 % CO_2 for 2 h, until the cells were adherent. Subsequently, the medium was removed and 75 µL of ice-cold M-PER Mammalian protein extraction reagent was added to each well. The Whatman Slideholder was placed on ice and was shaken for 10 minutes on an orbital shaker. The lysate was collected and centrifuged for 3 minutes at 12000 g. The supernatant was analyzed via Western Blot Analysis as described below.

Staining of actin cytoskeleton and cell nucleus

MG-63 cells were fixed with an aqueous formaldehyde solution (4 %, v/v) for 20 minutes and permeabilized with 0.3 % Triton X-100 and 1 % BSA in PBS (w/v) for 5 minutes. Staining of the actin cytoskeleton after permeabilization was performed with Alexa-488 phalloidin (1:1000 in PBS) (Invitrogen) for 20 minutes. Cell nuclei were stained with DAPI of a final concentration of 1 µg/mL in PBS for 15 minutes. The samples were washed 3 times with PBS and analyzed using a Zeiss Observer Z1 epi-fluorescence microscope (Zeiss, Oberkochen, Germany) at various magnifications.

Cell adhesion

The cell size of fixated and stained MG-63 cells (as mentioned above) was analyzed on the basis of microscopic images made with a Zeiss Observer Z1 epi-fluorescence microscope (Zeiss, Oberkochen, Germany). The captured images were analyzed using ImageJ.

Protein

SDS-PAGE

The SDS-PAGE was performed according to the standard protocol of [140]. 12–15 % separating gels and 3.9 % stacking gels for concentration of the sample were used. Therefore two 1.0 mm thick spacers at the sides between a 7.3 cm x10.2 cm glass plate and a 8.3 cm x 10.2 cm glass plate were assembled. The sandwich construct was tightly held by the clamps, which were cast into the casting stand sealing the lower edge of the sandwich. Acrylamide/bisacrylamide 30 %/0.8 % (v/v) in water and separating gel buffer were mixed in a 25 mL glass flask and degased at 18 mbar for 30 min. TEMED and APS solution were added under swirling. 5.5 mL of the separating gel solution was pipetted into the apparatus at the edges. 0.3 mL of 70 % 2-propanol (v/v) was overlaid to obtain an unbowed top of the separating gel. After allowing the gel to completely polymerize in approximately 30 min, the 70 % 2-propanol solution was poured off and thoroughly rinsed thrice with bidest. water and once washed with stacking gel buffer. The stacking gel was prepared in the same fashion as mentioned above. The solution likewise was pipetted carefully into the apparatus above the polymerized separating gel unto the top ledge of the smaller glass plate to avoid introducing air bubbles while squeezing the 1.0 mm thick Teflon comb between the to glass plates. After 30 min the condensation of the stacking gel was complete and the comb was carefully removed. The electrophoresis cell and lower buffer chamber were filled with SDS electrophoresis buffer. SDS sample buffer (6x) was diluted and mixed with the protein sample 1:6 and heated at 95 °C for 6 minutes. A maximum of 23 µL of each reduced and denatured protein sample and the size marker were applied to the pockets. The lid was closed and the cell was connected to the power supply and run at a constant potential of 80 V until the bromphenol blue tracking dye reached the separating gel. The voltage was augmented to 150 V until the tracking dye was 0.5 cm above the end of the separating gel. Theoretical masses and isoelectric point (p*I*) were all calculated using the ProtParam tool on the ExPASy portal (http://web.expasy.org/protparam).

Table 3. SDS-PAGE.

Solution	Separating gel		Stacking gel
	12 %	15 %	3.9 %
acrylamid/bisacrylamide solution 30 %/0.8 %	6.0 mL	7.5 mL	0.65 mL
Separating gel buffer (4x) pH 8.8	3.75 mL	3.75 mL	-
Stacking gel buffer (4x) pH 6.8	-	-	1.25 mL
Millipore water	5.25 mL	3.75 mL	3.05 mL
APS solution	0.05 mL	0.05 mL	25 µL

WB-Analysis

Subsequent to the protein separation by gel electrophoresis the gel was rinsed with water and placed briefly in the transfer buffer. Two 10 cm x 8 cm pads and two 9.5 cm x 7cm 0.22 µm filter paper were transferred in 4 °C transfer buffer. Meanwhile the gel was measured in size and a nitrocellulose blotting membrane with the same dimension as the gel was cut out and incubated in cold transfer buffer. A sandwich of the materials was built as depicted in **Figure 7**. Layer by layer air bubbles were removed by rolling gently a stirring rod over the upper layers. The sandwich was placed into the support grid in the transfer tank, filled with transfer buffer and an ice block for cooling. The proteins in the gel were transferred to the membrane at a constant voltage of 80 V until the pre-stained protein ladder was completely blotted to the membrane, leaving no traces on the gel.

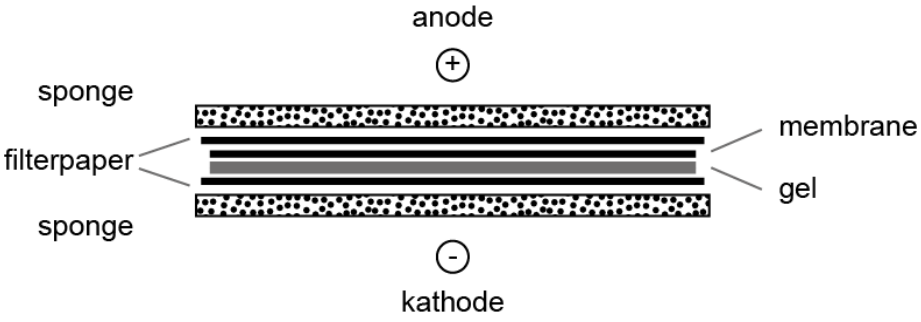

Figure 7. Assembly of the Western Blot cast

The washing and blocking steps (**Table 4**) of the blot were accomplished on an orbital shaker in an empty filter tip holder with approximately 50 mL of solution.

Table 4. Incubation and washing procedure of the western blot membrane.

	FGFBP	pErk	Erk
washing	-	3 times with TBST	
blocking	5 % skim milk in PBS (1h at RT)	5 % BSA in TBST (1h at RT)	
washing	-	3 times with TBST	
Incubation (1^{st} AB)	Over night at 4 °C 1:1000 anti-human FGFBP-Antibody (AB) in 5 % skim milk in PBS	Over night at 4 °C 1:1000 anti-human FGFBP-AB in 5 % skim milk in PBS	Over night at 4 °C 1:1000 anti-human FGFBP-AB in 5 % skim milk in PBS
washing	3 times with PBST	3 times with TBST	
washing	3 times with PBS	-	-
Incubation (2^{nd} AB)	1 h at RT 1:2000 rabbit anti-goat IgG		1.5 h at RT at 1:5000
washing	3x PBST	3x TBST	
washing	3x PBS	-	-

After the final washing step the membrane was freed of excess washing solution by holding the edge to a filter paper. According to the manufacturers instruction a total volume of 0.1 ml per mm^2 of the 1:1 mixture of the ECL solution mixture was overlaid and incubated for 5 minutes at room temperature. The excessive ECL solution was removed with a filter paper as mentioned before and immediately wrapped into a wrinkle free saran wrap to avoid dehydration. The chemiluminescent signals were captured using a CCD camera using a FluorChem FC2 imaging system (Protein Simple, Santa Clara, CA) with various exposure times depending on the intensity of the bands.

Protein purification

Frozen cell pellets were resuspended in binding buffer (10 mM tris, 100mM NaCl pH 7.5 1 mM PMSF) before being disintegrated by sonication with a sonifier (Sonoplus, Bandelin, Germany) with an amplitude of 75 % in 6 cycles of a one minute pulse (1.0 sec on; 0.8 sec off) under cooling. The lysate was centrifuged at 100.000 g for 1 h at 4°C and filtered (0.22 µM) the clarified lysate was pooled and collected. HiTrap Heparin HP columns connected to an ÄKTApurifier chromatography system (GE Healthcare) was used for protein purification. The columns were equilibrated with Eluent A (12 mM Na-Phosphate 300 mM NaCl) then the samples were loaded onto the column and washed with 15 column volumes of Eluent A. The HisTrx-FGF-2 fusion-protein was eluted with Eluent B (12 mM Na-Phosphate, 1.5 M NaCl). The fractions were collected due to their absorbance (A_{280}). The eluted fusion-protein was extensively dialyzed in the cold room against PBS supplemented with 0.5 mM DTT in Spectrapore dialysis membranes with a cut-off of 7 000 Da. The concentration of His-TrxFGF-2 was determined by UV-absorbance at λ= 280 nm, using an extinction coefficient of $E^{0.1\%} = 0.964$ [141]. The cleavage of the affinity-tag was performed at 4 °C for 24 h with 1 U of thrombin per mg of fusion-protein and an addition of 1 mM $CaCl_2$. The cleavage was stopped with 1 mM PMSF. Equilibrated columns were loaded with the sample then washed with 15 column volumes of Eluent A. FGF-2 protein was eluted with Eluent B (12 mM Na-phosphate, 1.5 M NaCl). The eluted samples were dialyzed extensively in the cold room against PBS with 1-3 mM DTT in Spectrapore dialysis membranes with a cut-off of 7 000 Da.

Protein Analysis was performed by SDS-PAGE. UV absorbance measurements were used to determine yields of fusion- and cleaved protein.

Protein Expression (mFGF-2)

An overnight culture of *E.coli JM109 (DE3)* (pHisTrx-mFGF-2) in LB_{Amp} were added to fresh TB_{Amp} Medium to an OD_{600} of 0.1 and grown in shake flasks at a temperature of 37 °C. At an OD_{600} of 0.6 the culture was induced by addition of 0.2 mM IPTG. After incubation at 30 °C for 5h, the cultures were harvested and the cell pellets were washed once with binding buffer (10 mM tris, 100 mM NaCl pH 7.5) and stored at -80 °C.

Fluorescence spectroscopy

Folding of plk-FGF-2 and wild-type FGF-2 was investigated on a LS 50 B fluorescence spectrophotometer (Perkin Elmer, Waltham, USA). Fluorescence emission spectra of FGF-2 and plk-FGF-2 samples were measured by excitation of tryptophan and tyrosine fluorescence at a wavelength of 280 nm and a scan speed of 240 nm/min in a 1 mm quartz cuvette. Unfolded samples 5 fold diluted compared to folded samples were prepared by heating at 90 °C for 10 min in the presence of 6 M guanidinium hydrochloride. Obtained spectra of emission fluorescence intensity values were baseline corrected by subtracting the spectrum of buffer.

Lyophilization

Lyophilization was carried out on a laboratory freezing dryer (Christ alpha 1-4). FGF-2 samples were formulated with a cryoprotectivum of 20 % sucrose (w/v) in PBS pH 7.4 supplemented with 1–3 mM DTT. Aliquots of 0.1–5 mL volume were frozen at -80 °C overnight. At a shelf temperature of -10 °C for 24 h with a vacuum level less than (0.16 mbar) and a condenser temperature of -65 °C the primary drying was undertaken. Secondary drying was conducted in three steps of shelf temperatures of -5 °C, 0 °C and 4 °C each for 12 h and a vacuum level below (0.16 mbar) and the condenser temperature at -65 °C. The lyophilized aliquots were stored at -80 °C.

HPLC analysis

Protein purity and stability were assessed on a RP-HPLC system using a VWR Hitachi LaChromUltra HPLC system equipped with a diode array detector. Twenty µL protein sample of approximately 1 mg/mL concentration was applied to a C4 column (4.0 mm x 125 mm, Macherey-Nagel, Düren, Germany), equilibrated by an ACN-water mixture (10:90) containing 0.1 % TFA. FGF-2 and derivates were eluted by a linear gradient of 10–50 % ACN containing 0.1 % TFA with a gradient of 1 % ACN/min and a flow rate of 1 mL/min. Oven temperature was kept at 42 °C and absorbance was monitored at 215 nm [142], [143].

MALDI-MS

According to manufacturer's instructions Zip Tip® pipette tips (C18 resin, Millipore, Billerica, MA) were used to desalt 20 µL of each sample. Five µL of the eluate was embedded in a matrix, consisting of equal parts of sinapinic acid and ACN/0.1 % TFA in water (1:4). An Autoflex II LRF instrument from Bruker Daltonics Inc. (Billerica, USA) fitted with a 337 nm wavelength nitrogen laser acquired the matrix-assisted laser desorption ionization spectra in the linear positive mode. Calibration of acquired mass spectra were undertaken with the external protein standard I from Bruker Daltonics Inc. (Billerica, USA), containing cytochrome C, myoglobin insuine and ubiquitin. Theoretical. Theoretical masses of wild-type proteins were calculated (http://web.expasy.org/peptide_mass).

NanoLC MS/MS after trypsin digest

Fc-FGFBP1 and FGFBP1 samples were digested with EndoH and PNGaseF by adding 1 U of the enzyme per µg sample for 30 minutes after heating the samples in 4x LDS sample buffer at 90 °C for 10 minutes. For in-gel digestion the excised gel bands were destained with 30 % ACN, shrunk with 100 % ACN, and dried in a Vacuum Concentrator (Concentrator 5301, Eppendorf, Hamburg, Germany). Digests with trypsin was performed overnight at 37 °C in 0.1 M NH_4HCO_3 (pH 8). About 0.1 µg of protease was used for one gel band. Peptides were extracted from the gel slices with 5 % formic acid.

NanoLC-MS/MS analyses were performed on an LTQ-Orbitrap Velos Pro (Thermo Scientific) equipped with an EASY-Spray Ion Source and coupled to an EASY-nLC 1000 (Thermo Scientific). Peptides were loaded on a trapping column (2 cm x 75 µm ID. PepMap C18 3 µm particles, 100 Å pore size) and separated on an EASY-Spray column (25 cm x 75 µm ID, PepMap C18 2 µm particles, 100 Å pore size) with a 30 minute linear gradient from 3% to 30% acetonitrile and 0.1% formic acid. MS scans were acquired in the Orbitrap analyzer with a resolution of 30000 at m/z 400, MS/MS scans were acquired in the Orbitrap analyzer with a resolution of 7500 at m/z 400 using HCD fragmentation with 30% normalized collision energy. A TOP5 data-dependent MS/MS method was used; dynamic exclusion was applied with a repeat count of 1 and an exclusion duration of 30 seconds; singly charged precursors were excluded from selection. Minimum signal threshold for precursor selection was set to 50000. Predictive AGC was used with AGC target a value of 5e5 for MS scans and 5e4 for MS/MS scans. The same options were used for ETD fragmentation except for the following settings: A TOP3 method was applied, ETD activation time was set to 90 ms,

minimum signal threshold for precursor selection was set to 75000, collision energy was set to 35%, AGC target was set to 300000 for fluoranthene. Lock mass option was applied for internal calibration in all runs using background ions from protonated decamethylcyclopentasiloxane (m/z 371.10124). Mascot Distiller 2.4 was used for raw data processing and for generating peak lists, essentially with standard settings for the Orbitrap Velos (high/high settings). Mascot Server 2.4 was used for database searching.

Purification of FGFBP1

Two HiTrap MabSelect SuRe (1 mL) columns (GE) connected in tandem to an ÄKTApurifier system were equilibrated with binding buffer (PBS pH 7.4). The samples were loaded onto the column and washed with binding buffer until the absorbance, measured at λ = 280 nm reached baseline. Fc-FGFBP1was eluted with 100 mM glycine buffer pH 3.3. The buffer exchange of the samples was also undertaken on the ÄKTApurifier chromatography system to which PBS equilibrated HiTrap Desalting columns were connected. The fractions were collected and stored at 2–8 °C. Protein analysis was performed by SDS-PAGE.

Isothermal titration calorimetry (iTC)

The energy values and thermodynamic parameters such as enthalpy-, entropy change, binding affinity and heat capacity of a given reaction can be measured by isothermal titration calorimetry.

A reference cell identical to the sample cell is held at a constant defined temperature. Temperature changes, in relation to the reference cell, of the sample cell due to reactions are maintained constant by a feedback circuit regulating the varied power input for the sample cell heater. The measurements consists firstly of the time, which depends on the amount of injected volume of the titrant into the sample cell and the number of injections and secondly the power input. In order to observe the energy changes and derive thermodynamic characteristics of the reaction the injection ensues incrementally. To determine the heat of reaction of the interaction between heparin and mFGF-2 the latter was dialyzed against the "measurement buffer" and the former was mixed with a 10-fold buffer then diluted with the one fold buffer to various concentrations. Due to the lower solubility of mFGF-2 (~ 90–120 μM) in physiological buffers compared to heparin a solution of FGF-2 was placed into the sample cell and heparin was incrementally added. Temperature (T), protein concentration, heparin concentration, buffers and injection programs of the measurements with Microcal iTC 200 are depicted in **Table 5**.

In order to measure the heat of ligand dilution into buffer a control experiment was conducted with the same concentration of HS and the according buffer in the sample cell with the same injection program. The curve was translated to 0 μcal/sec if constant heat values of the reference measurement occurred.

After the integration of the injection peaks their area (heat exchange per injection) are plotted against the molar ratio of heparin/ mFGF-2 and a regression is undertaken to determine the thermodynamic parameters. The sigmoidal fitted curve reveals the enthalpy change ΔH (difference of minimal and maximal y-value), stoichiometry n (x-value at the half of the maximal y-value) and the dissociation constant K_D (slope of the fitted curve). Binding of heparin to mFGF-2 leading to the free energy change (ΔG) was calculated from the relationship:

$$\Delta G = R \cdot T \cdot lnK_D$$

with R as the universal gas constant (1.99 cl/mol/K).

From the relationship:

$$T\Delta S = \Delta H - \Delta G$$

the entropic contribution (TΔS) to the free energy of binding was calculated [144].

Table 5. Compilation of the iTC measurements to determine the thermodynamic interaction of mFGF-2 with HS

Program	sample cell	syringe	buffer in sample cell	buffer in syringe	Temperature [K]
1[a]	30 μM mFGF-2	150 μM HS	$PBS_{0.5\ mM\ DTT}$ pH 7.4	$PBS_{0.5\ mM\ DTT}$ pH 7.4	293.15
2[a]	30 μM mFGF-2	150 μM HS	$PBS_{0.5\ mM\ DTT}$ pH 8.5	$PBS_{0.5\ mM\ DTT}$ pH 8.5	293.15
3[a]	30 μM mFGF-2	150 μM HS	$PBS_{0.5\ mM\ DTT}$ pH 5.5	$PBS_{0.5\ mM\ DTT}$ pH 5.5	293.15
4[a]	30 μM mFGF-2	150 μM HS	$Tris_{0.5\ mM\ DTT}$ pH 7.4	$Tris_{0.5\ mM\ DTT}$ pH 7.4	293.15
5[a]	30 μM mFGF-2	150 μM HS	$Tris_{0.5\ mM\ DTT}$ pH 8.5	$Tris_{0.5\ mM\ DTT}$ pH 8.5	293.15
6[a]	30 μM mFGF-2	150 μM HS	$Tris_{0.5\ mM\ DTT}$ pH 5.5	$Tris_{0.5\ mM\ DTT}$ pH 5.5	293.15

Program:

[a] 180 s initial delay, 0.2 μL in 0.4 s, 150 s spacing then 19 times 2.0 μL in 4.0 s, 400 rpm

Peptide Synthesis

Solid phase peptide synthesis on Wang resin of Fmoc protected amino acids was implemented to construct the glycine-arginine-alanine-aspartate-serine (GRGDS) peptide. The C-terminal amino acid was anchored to the Wang resin by pyridine / 2,6-dichlorobenzoyl in N'N-dimethyl formamide (DMF). The N terminal protecting group was cleaved with 20 % piperidine in DMF before the next amino acid was coupled. Coupling was carried on by activation with 1-hydroxybenzotriazol and diisopropylcarbodiimide. After coupling of the last

amino acid and cleaving of the protection group the DMF washed peptidyl resin was dried with diethyl ether. The side chain protecting groups and the peptide were cleaved from the resin with a 12.5 % scavenger mixture (ethanedithiol, m-cresol, thioanisol, water (1:2:2:2 v:v:v:v) in trifluoroacetic acid (v/v). Ice cold diethyl ether was added to the solution of cleaved peptide stored on ice. The precipitation was centrifuged and washed thrice with ice cold diethyl ether before drying the pellet over night. Preparative purification was carried out on an ÄKTApurifier and Fraction collector 900 with a Jupiter 15u C18 300A (21.2mm*250mm) column (Phenomenex Inc., Torrance, CA)). The column was equilibrated at 4° C with 6 % ACN 0.1 % TFA in water. Elution of the samples were performed with an linear gradient of 0.84 %/min up to a concentration of 60 % ACN 0.1 %TFA in water.

Fixed volumes of fractions were collected and the sample were frozen at -80 °C and lyophilized as mentioned above (FGF-2).

Printing

Fast frame slide holders and 16-well incubation chambers holding Nexterion® H slide were incubated for 15 h with 100 µL of protein print buffer (150 mM Na-Phosphate, pH 7.4 0.01 % w/v Tween 20) containing various peptides and carbohydrate analogues.

Table 6. Composition of printing solutions for surface decoration

	Component A	Component B
RGD + AzMan	GRGDS-Peptide 0.41 mM	AzidoMannose 0.06 mM
RGD	GRGDS-Peptide 0.41 mM	-
AzMan	-	AzidoMannose 0.06 mM
Man	-	Mannose 0.06 mM

To deactivate reactive groups of the surface with ethanolamine (primary amine) the excess solution was removed and the Nexterion® H slide was blocked with blocking solution (25 mM ethanolamine, 100 mM boric acid, 0.01 w/v Tween 20) for 1 h, washed three times with PBS 0.01 % w/v Tween 20 and three times with Millipore water. Water droplets on the coverslides were removed by centrifugation in a 50 mL Falcon tube at 200 g for 5 minutes. Storage of the slides was at 2-8 °C until further use.

Copper-catalyzed Azide-alkyne Huisgen cycloaddition (CuAAC)

A 5-fold molar excess of the fluorescence dye Acetylene flour F 488 (Jena Bioscience) was used. The CuAAC was performed in the presence of 2.5 mM L-ascorbic acid, 250 µM THPTA and 50µM $CuSO_4$ at room temperature. Copper(II)sulfate and THPTA were premixed and incubated with sodium ascorbate under air exclusion for 10 minutes to quench occurring reactive oxygen species. Adding 5mM EDTA stopped the CuAAC [115].

RP-HPLC analysis of peptides

The purity of lyophilized GRGDS-peptide samples were assessed by RP-HPLC using a VWR Hitachi LaChromUltra HPLC system equipped with a diode array detector. Separation was performed using a Source 15RPC ST 4.6/100 reversed-phase chromatography column (4.6 mm *100 mm, 15 µm) at 42 °C. The flow rate was set to 0.7 mL/min; the sample volume injected per run was 20 µL. Two eluents were used, eluent A consisted of water and 0.1% trifluoroacetic acid, and eluent B was 60 % acetonitrile and 0.1 % trifluoroacetic acid in water. Separation started with 90 % (v/v) eluent A and was changed over 45 min to 100 % Eluent B. Peptides were detected at 214 nm.

Subcloning

The cDNA of the gene encoding for full length murine fibroblast growth factor 2 (FGF-2, gene bank reference ID: NM_008006.2, amino acids 10-154) on the pMD18-T Simple Vector was purchased from Sino Biological Inc. and amplified by PCR using a forward primer 5′CCCGTCGACATGGCTGCCAGCGGCATC3′ introducing a SalI restriction site and a reverse primer 5′CCGAATTCTAATAATCAGCTCTTAGCAGACATTG3′ introducing a EcoRI restriction site. The amplified DNA sequence was cleaved by means of SalI and EcoRI restriction enzymes and then subcloned into the multiple cloning site of the pHisTrx plasmid after the N-terminally 6 x His tagged Escherichia coli thioredoxin followed by a thrombin cleavage site using the enzymes SalI and EcoRI, resulting plasmid mFGF-2 pHisTrx. After ligation the ligation product was transformed into the competent cells of *E.coli JM109 (DE3)* by heat shock. Recombinant colonies were selected by scoring for Ampicillin (100 µg/mL) resistance on agar plates.

Biotinylation

To biotinylate proteins unspecifically via primary amine groups, NHS-activated biotin (EZ-Link® Sulfo-NHS-LC-Biotin reagent) was used. To stochastically biotinylate each protein with one molecule of biotin (equimolar) the following calculations were used

$$(1)\ ml\ protein \cdot \frac{mg\ protein}{ml\ protein} \cdot \frac{mmol\ protein}{mg\ protein} \cdot \frac{1\ mmol\ biotin}{mmol\ protein} = mmol\ biotin$$

$$(2)\ mmol\ Biotin \cdot \frac{1000000\ \mu L}{L} \cdot \frac{L}{10\ mmol} = \mu L\ biotin$$

The calculated volume of biotin solution was added to the protein solved in PBS and incubated over night at 4°C. To remove excessive unreacted biotin the final reaction solution was dialyzed using Vivaspin 6 centrifugal filters with a minimum of a 1 000 000 fold buffer exchange.

Surface plasmon resonance (SPR)

Surface plasmon resonance serves as a qualitative analysis for *in vitro* protein-protein-interaction, which can track the interaction in real time and reveals their binding kinetic. While one protein (ligand) is immobilized on the matrix of a gold plated glass prism (biosensor), the other protein (analyte), dissolved in the measurement buffer at various concentration flows over the other. Due to changes of the refractive index during the association phase the binding of the interaction partners that leads to a mass increase on the surface of the biosensor can be detected and these changes are represented in resonance units (RU). 1 RU equals a mass increase of 1 pg/mm^2. The dissociation phase commences via perfusion of pure measurement buffer, the refractive index changes due to the detachment of the analyte from the immobilized protein. Out of this sensogram the kinetic parameters *ka* (association-) and *kd* (dissociation rate) can be determined, which leads to the computation of the dissociation constant K_D. The analysis of interactions between FGF-2 and FGFBP1 was conducted with an SPR ProteOn^{TM} XPR 36 system (Bio-Rad).

The alginate matrix of the biosensor was coated with neutravidin, which is immobilized via the amino coupling with the ε-amino-groups of lysine. As a consequence the immobilization occurs non-covalently through the biotinylated ligands.

The activation of the matrix of a ProteOn^{TM} GLC Biosensor (Bio-Rad) takes place by perfusion of an EDC/sulfo-NHS- solution (100 mM 1 ethyl-3-(3-dimethylaminopropyl) carbodiimide, 25 mM N-hydroxysulfosuccininimide) for 120 s and a flow rate of 100 µL /min. Subsequent neutravidin was diluted 100 fold in a 10 mM acetic buffer pH 4.0 and flows over the activated biosensor until the desired surface density was achieved (100 µL/min). Still active carboxyl groups were inactivated by ethanolamine (300 s, 100 µL/min). With a flow

rate of 100 µL/min the biotinylated ligand diluted in measurement buffer was loaded until the desired loading density was achieved.

Various concentrations of the analyte were diluted in measurement buffer and flows over the biosensor (300 s, 100 µL/min). The evaluation of the kinetic was done by forming a mean during the association phase at equilibrium and plotted via a Michaelis Menten growth model implementing OriginPro 8. In order to regenerate the ligand for further measurements the chip was washed with 4 M $MgCl_2$ (18 s, 100 µL/min) and subsequent 10 mM glycine buffer, pH 1.5 (18 s, 100 µL/min).

Statistical analysis

All data are reported as mean ± standard deviation of at least three independent experiments unless specified otherwise. Statistical significance was calculated by one-way ANOVA with an overall significance level of 0.05 (Minitab).

RESULTS

FGF-2 (Phase I)

Bacterial expression and extraction of mFGF-2

Expression of mFGF-2

In order to express adequate amounts of bioactive mFGF-2, we chose a pHisTrx vector [145] encoding for a thrombin cleavable N-terminal fusion-protein of His_6-tagged thioredoxin and of murine FGF-2, which was transformed in *JM109 (DE3)* bacteria. Thioredoxin supports folding during bacterial expression to form soluble thioredoxin fusion-proteins of the subcloned mammalian gene [146]. Cultivation was performed in shaker flasks at 37 °C in TB medium following standard protocols. Before induction with IPTG no detectable bands with the expected electrophoretical mobility of the fusion-protein (31.379 kDa) (http://web.expasy.org/protparam) were observed as analyzed by reduced SDS-PAGE **(Figure 8)**. T7 promoter based expression of the fusion-protein HisTrx-FGF-2 was induced with 0.2 mM IPTG at an OD_{600} of 0.6 at a temperature of 30 °C. To monitor expression of the fusion-protein, bacterial lysates were qualitatively analyzed after different time points after IPTG induction (1, 2, 3, 4, 5 hours, respectively; **Figure 8**). The intensity of the fusion-protein HisTrx-FGF-2 band in the bacterial lysate increased over time and showed highest levels of HisTrx-FGF-2 after 4 hours of bacterial expression. After harvest, bacterial extracts were produced by ultra-sonification. As shown in **Figure 8**, bacterial cells were lysed with three cycles of sonication and the fusion-protein HisTrx-FGF-2 was found to remain soluble in the supernatant after ultracentrifugation, a prerequisite for further chromatographic purification.

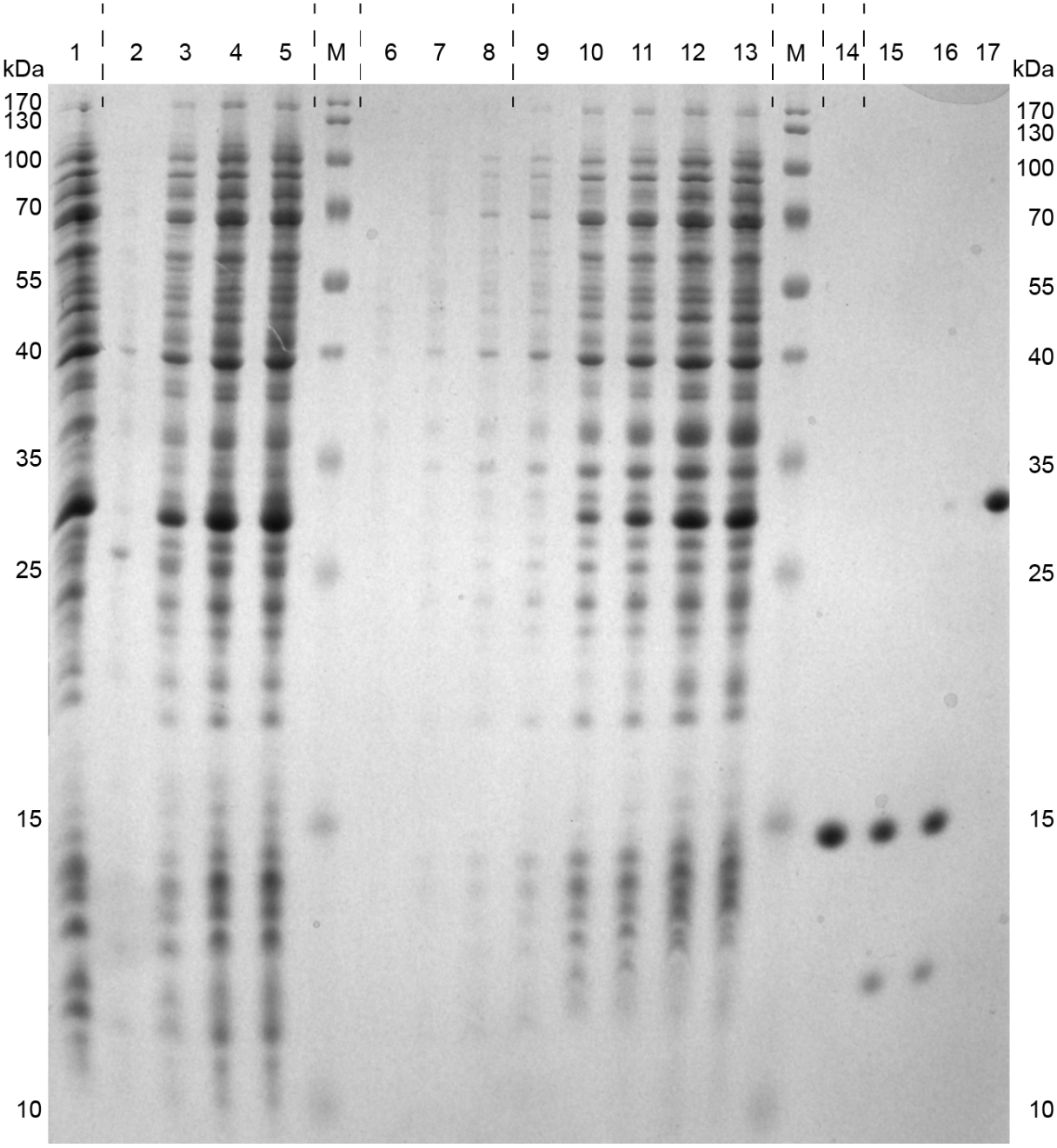

Figure 8. SDS-PAGE analysis of mFGF-2 expression and of purification after Coomassie Brilliant Blue staining. Lane 1: supernatant after ultracentrifugation, lanes 2-5: supernatant after cycles of sonication, lane 2, before sonication, lane 3, after first cycle, lane 4, after third cycle, lane 5, after fourth cycle, M: marker, lanes 6-8 cell growth after 0 h (OD_{600} of 0.1), 1 h (OD_{600} of 0.3) resp. 2 h (OD_{600} of 0.6), lanes 9-13 supernatant after 0 h, 1 h, 2 h, 4 h, resp. 5 h of induction with IPTG, lane 14: purified mFGF-2, lanes 15-17 after 24 h, 5 h resp. 0 h of digestion with thrombin.

Purification and thrombin cleavage

The purification of the fusion-protein HisTrx-FGF-2 was achieved by heparin affinity chromatography using two equilibrated HiTrap Heparin HP columns connected on an ÄKTApurifier system.

The supernatant, collected after the ultracentrifugation of the bacterial extract, was loaded on the column with a flow rate of approximately 0.8 mL/min and was subsequently washed with 15 column volumes before initiation of the gradient elution. A linear gradient was implemented over 12 column volumes. To ensure complete elution of bound HisTrx-FGF-2 a 15 column volume step of Eluent B was used. As depicted in **Figure 9A** bacterial proteins, not interacting with heparin, were in the flow-through. The major peak observable at λ=280 nm was eluted with a concentration of Eluent B at 100 % and collected for the subsequent digestion with thrombin after extensive dialysis at 4 °C against PBS supplemented with 0.5 mM DTT as anti-oxidative agent to prevent intermolecular disulphide-bond formation [141]. The HisTrx-FGF-2 fusion-protein was digested with 1 U of thrombin per 1 µg of protein at 4 °C for 24 h and for 5 h, respectively and the efficiency of the thrombin digest was qualitatively analyzed by SDS-PAGE (**Figure 8**). Incubation-time was found to affect thrombin digest efficiency: 24 hours of incubation time resulted in a complete cleavage of the fusion-protein into two defined bands of His tagged-thioredoxin (13.698 kDa) and of mFGF-2 (17.667 kDa) (http://web.expasy.org/protparam) in contrast to shorter incubation times (5 hours) (**Figure 8**).

Fractions of the main peak (**Figure 9B**), containing mFGF-2 were pooled and dialyzed against PBS supplemented with 0.5 mM DTT. SDS-PAGE and Coomassie staining confirmed a high purity and presence of a protein with a size of ~ 15 kDa (**Figure 8**) in line with the calculated molecular weight of FGF-2 (17.667 kDa).

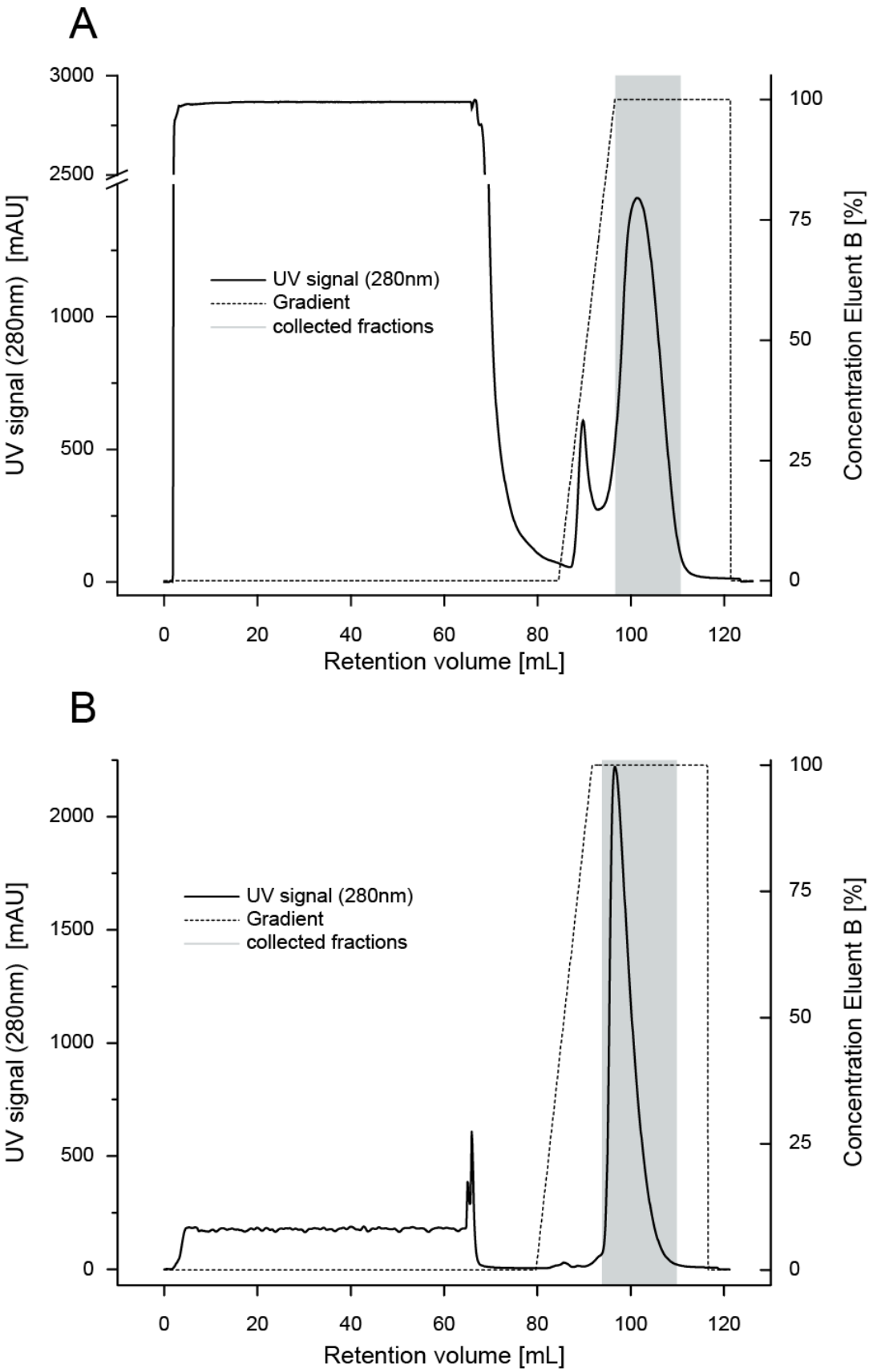

Figure 9. ÄKTA chromatogram. (A) Purification of HisTrx-FGF-2 fusion-protein from bacterial extract. **(B)** Purification of mFGF-2 after thrombin cleavage.

Characterization of mFGF-2

Folding of mFGF-2

In order to analyze the structural integrity of mFGF-2, fluorescence emission spectra of folded and unfolded mFGF-2 after excitation of tyrosine and tryptophan residues at 280 nm samples were monitored. Protein fluorescence is usually dominated by the fluorescence emitted by aromatic amino acids such as tryptophan in the protein structure (lambda max ~ 350 nm in polar solvents [22], [147]. Sluzky et al. described a total fluorescence quenching of the single tryptophan (Trp-122 in mFGF-2 and Trp-123 in hFGF-2) buried within the folded FGF-2 structure. The fluorescence emission spectrum of folded FGF-2 is therefore dominated by tyrosine fluorescence (λ_{max} ~ 306 nm) [148].

Figure 10 displays the fluorescence emission spectra of folded FGF-2 (1 mg/ mL in PBS) and as control unfolded FGF-2 (0.2 mg/mL) after treatment with 6 M guanidinium hydrochloride as denaturing agent and heating to 90 °C for 10 minutes. We observed a dominant fluorescence of the untreated sample of FGF-2 with a maximum peak at λ = 308 nm, indicating a proper folding of the recombinant expressed mFGF-2 due to the complete fluorescence quenching of the single tryptophan residue at λ = 360 nm. After denaturation, the main fluorescence emission was shifted from λ = 308 nm to λ = 355 nm (**Figure 10**, light grey line) as consequence of the emerging tryptophan residue fluorescence. As tryptophan fluorescence emission is strongest, the fluorescence emission spectrum of unfolded mFGF-2 is dominated by a peak at λ = 360 nm (tryptophan fluorescence) and shows a shoulder with 3-times reduced intensity at λ = 308 nm, displaying tyrosine fluorescence.

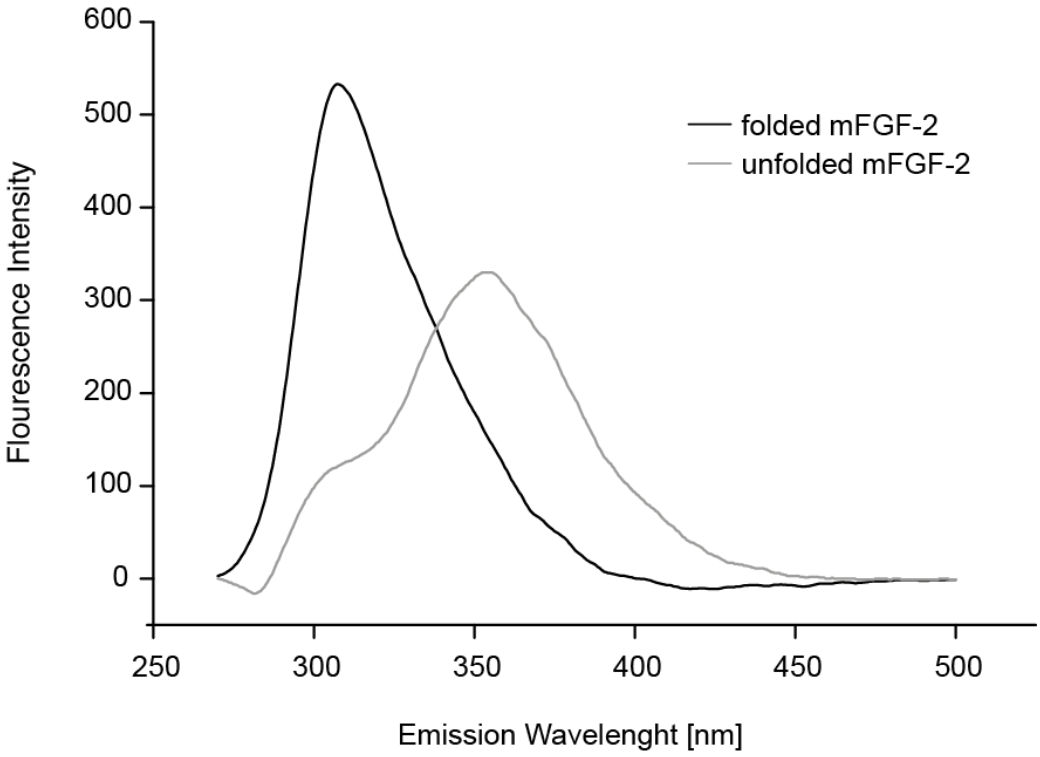

Figure 10. Base-line corrected fluorescence emission spectra of unfolded and folded mFGF-2. Folded mFGF-2: 1 mg/mL mFGF-2 in PBS at 25 °C, unfolded mFGF-2: 0.2 mg/mL mFGF-2 in PBS additionally containing 6.4 M GdmCL heated 10 minutes at 90 °C prior to measurement at 25 °C.

Mass spectrometry

Mass spectrometry analysis (MALDI-TOF) of mFGF-2 revealed that mFGF-2 protein was fully expressed due to the found mass [M+H^+] of 17 667 Da (**Figure 11**), which is in line to the calculated molecular weight of 17 667 Da. Other observable peaks in the mass spectra of mFGF-2 were pseudomoleculions [M+$2H^+$] (m/z of 8 833.11) and [M+$3H^+$] (m/z of 5 888.52) of mFGF-2.

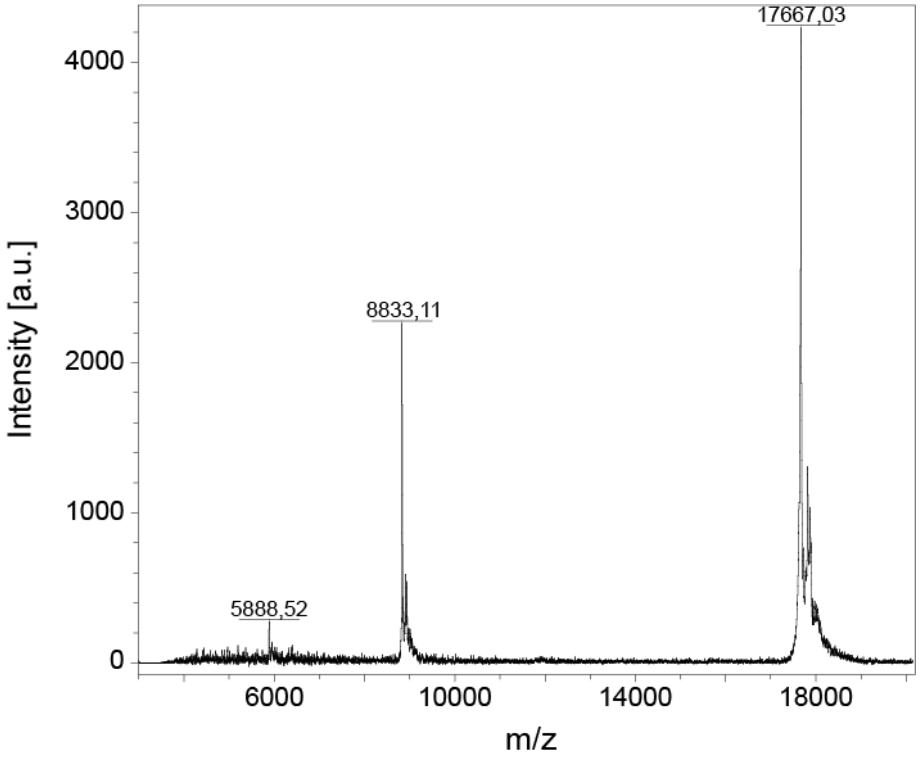

Figure 11. Mass spectrometry analysis of mFGF-2.

Purity

To assess the purity of recombinant expressed mFGF-2 after purification via heparin affinity chromatography, reverse-phase HPLC analysis was performed. The chromatogram revealed a single, nearly symmetrical peak (96 % peak area) (**Figure 12)**. Furthermore, the single eluted peak with a retention time of 28.5 min corresponding to 38.5 % of ACN in H_2O which is characteristic for mFGF-2 as described previously by Chen et al. for a C 4 column (4.6 mm, 250 mm, Macherey-Nagel, Düren, Germany) [143].

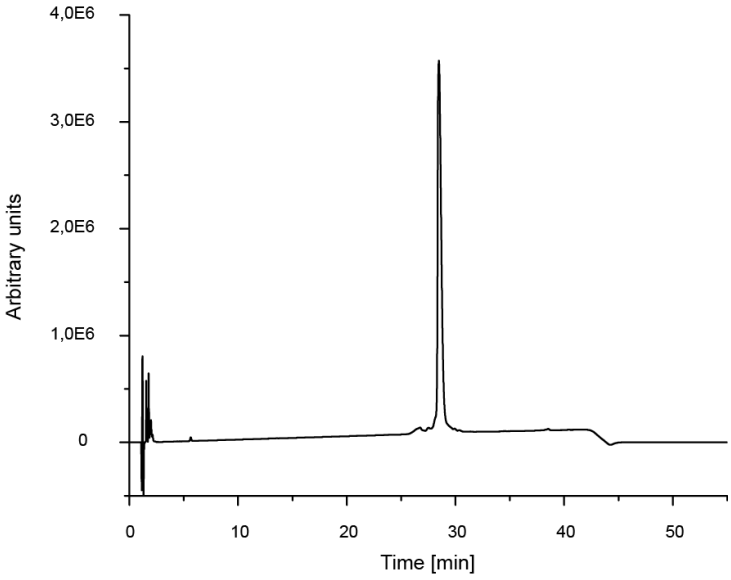

Figure 12. Reverse-phase HPLC analysis of purified mFGF-2 sample.

Bioactivity

Via MTT-Assay and WST-1 assay the bioactivity of FGF-2 was assessed using NIH 3T3 cells resp. MG-63 cells, which were serum depleted before incubation with FGF-2. The potency of FGF-2 was demonstrated for the recombinant expressed mFGF-2 and was compared to sourced mFGF-2 (R&D Systems, Minneapolis USA) (**Figure 13**). With EC_{50} values of mFGF-2 and FGF-2 (sourced) of 0.31 ng/mL (17.547 pM) resp. 1.96 ng/mL proved to have the potency to stimulate NIH 3T3 cell growth, showing us that the expressed mFGF-2 is bioactive, comparable to the sourced growth factor. With EC_{50} values of mFGF-2 and FGF-2 (sourced) of 2.41 ng/mL (0.14 nM) resp. 2.01 ng/mL proved also to have the potency to stimulate MG-63 cell growth, showing us that the expressed mFGF-2 is bioactive, comparable to the sourced growth factor.

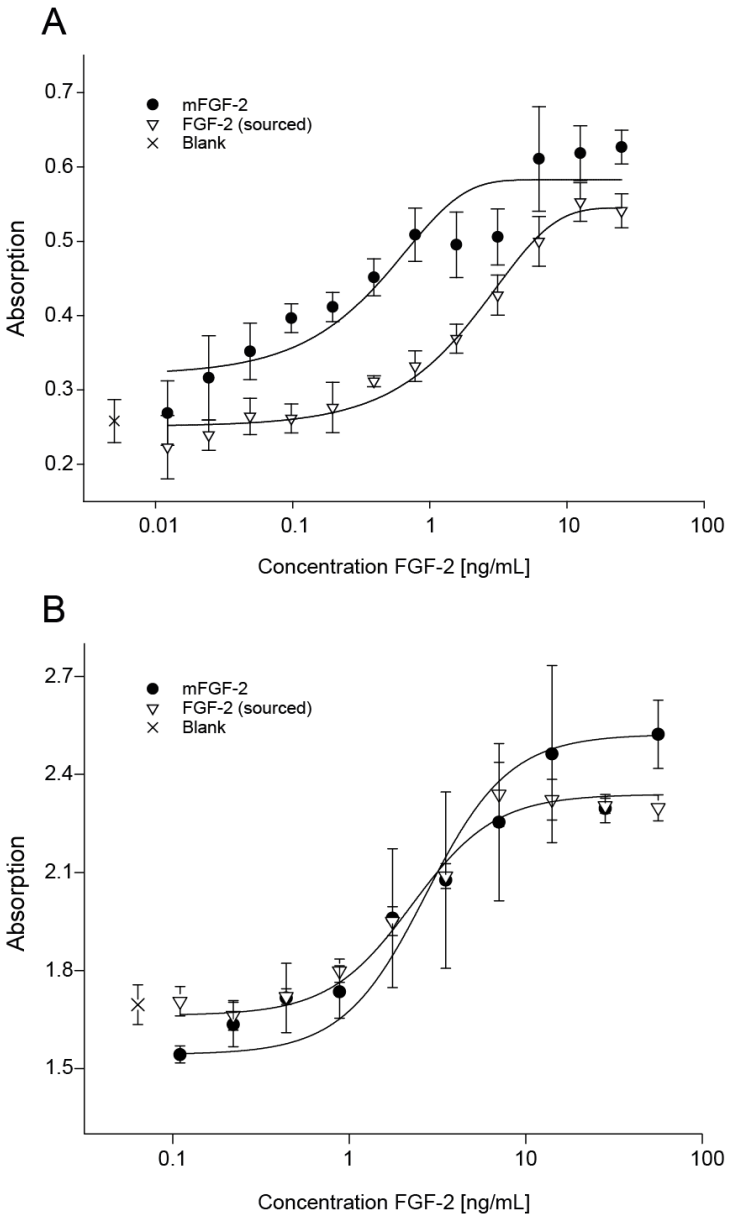

Figure 13. Proliferation assay of mFGF-2 and sourced FGF-2 in respect to concentration. **(A)** NIH 3T3 cells – MTT assay. **(B)** MG-63 cell – WST1 assay. Sourced mFGF-2 (R&D Systems) were used as reference and the blank value is highlighted separately.

Stability

To assess the stability during long-term storage of FGF-2, samples were lyophilized and stored at -80 °C. At various time points up to 2 months (60 days) samples were reconstituted and analyzed chromatographically with the afore mentioned HPLC method. The chromatogram of each time point showed a similar retention time of ~ 28.5 min (**Figure 14B**), whereas no additional peaks appeared during the time course, showing the integrity of stored

FGF-2. (**Figure 14A**) Integration of the peaks revealed a purity of least 88.86 ± 0.79 % (n = 3) main peak area of each time point (**Figure 15**). Statistical data analysis was performed by a one-way analysis of variance (ANOVA). All samples showed no statistical significance with $p < 0.05$. Stability of freeze dried samples for long-term storage was ensured over a course of 60 days.

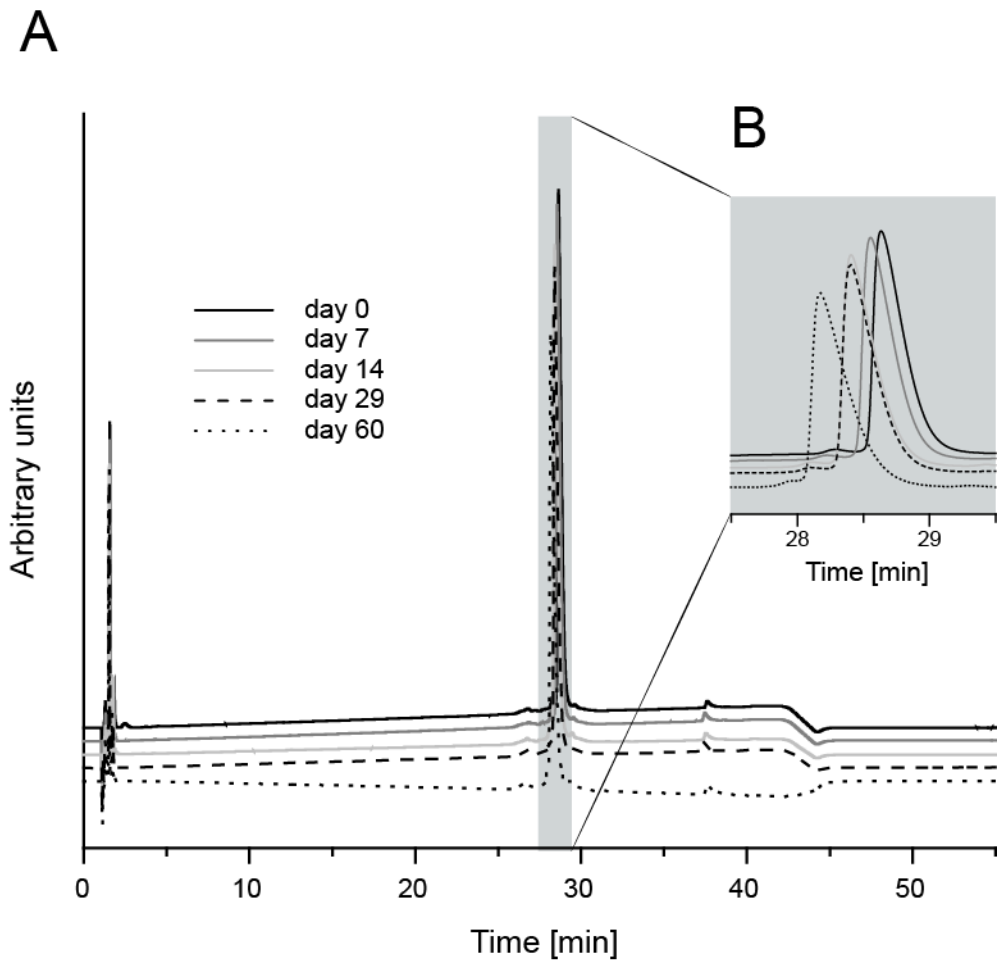

Figure 14. Stability of mFGF-2 after lyophilization. HPLC chromatograms of lyophilized mFGF-2 samples stored at -80 °C after different time points.

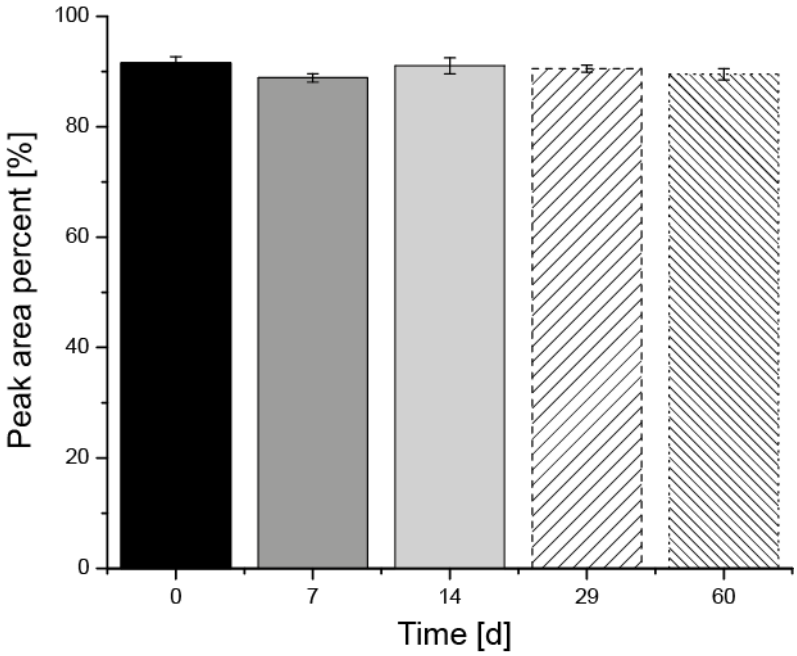

Figure 15. Stability of mFGF-2 after lyophilization. Main peak-area in percent after integration of the main peak of the HPLC chromatograms of lyophilized mFGF-2 samples stored at -80 °C after different time points (n=3). No significant differences ($p < 0.05$) were found.

FGFBP1 (Phase II)

Expression and purification of FGFBP1

Transient transfection of HEK 293F cells

To express adequate amounts of murine Fc-FGFBP1 the suspension cell-line HEK 293 Freestyle was chosen. Cells were transiently transfected following established protocols [149]. We chose a pFuse vector encoding for a tobacco etch virus protease cleavable N-terminal fusion-protein of Fc-tagged murine FGFBP1. The Fc-tag facilitates future purification steps due to its binding properties to protein A, which is also commonly used during recombinant antibody purification [150]–[152]. Cultivation of suspension type HEK 293 Freestyle cells was performed in vented shaker flasks in Freestyle 293 expression medium following the manufacturer's procedure.

Protein expression of HEK 293F cells

At first the period of Fc-FGFBP1 expression was determined in HEK 293 Freestyle cells by monitoring the cell viability by trypan blue staining after PEI transfection [153]. On day 4 after the transient transfection cell viability dropped significantly to 79.9 ± 2.8 % compared to earlier time points (day 0 = 88.5 ± 2.3 % and day 1 = 89.4 ± 3.0 %) (**Figure 16**). Harvesting of the mammalian cell supernatant was therefore performed after 3 days of transfection (day 3) to avoid potential degradation of Fc-FGFBP1 through released proteases of dead cells.

Western blot analysis resulted in no detectable levels of expression of Fc-FGFBP1 before transfection (**Figure 17**). Expression and secretion of Fc-FGFBP1 into the cell supernatant was detected 24 h after transfection with the Fc-FGFBP1 plasmid. A single band of approximately 80 kDa was observable (molecular weight and theoretical isoelectric point of Fc-FGFBP1: 56.6 kDa resp. 9.02 | http://web.expasy.org/protparam). Expression levels of Fc-FGFBP1 remained constant throughout all further investigated time points. Electrophoretic mobility of the basic protein Fc-FGFBP1 was slower than predicted due to their basicity as observed by Lametsch et al. and due to the glycosylation [69]. Western Blot analysis revealed no perceptible growth of Fc-FGFBP1 band intensity or degradation production after three days of transfection. Therefore, the cell supernatant was harvested after three days for all tested conditions.

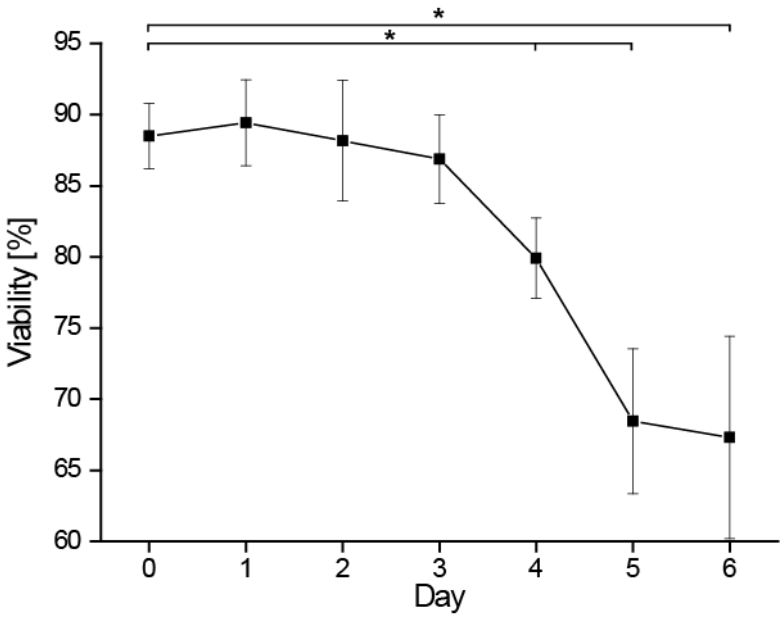

Figure 16. Viability of HEK 293 F cells during expression of Fc-FGFBP1 assessed by trypan blue staining (n=6). The asterisk highlights significant differences exclusively of day 0 ($p < 0.05$).

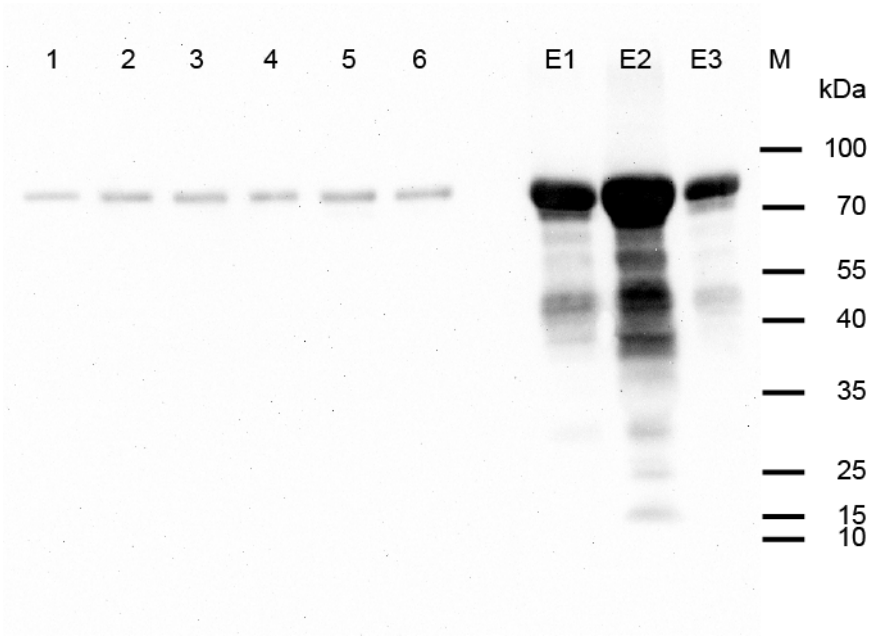

Figure 17. Western blot analysis of Fc-FGFBP1. (1)-(6) Supernatant of transfected HEK 293F cells with Fc-FGFBP1 after 1 resp. 6 days. (E1)-(E3) eluted fractions of Fc-FGFBP1 after affinity purification with MabSelect SuRe columns via ÄKTApurifier.

Purification of FGFBP1

Purification of Fc- tagged FGFBP1 was performed with the cleared supernatant after 3 days of expression using protein A based affinity chromatography. One distinct peak during the elution phase of the chromatography was observed and λ = 280 nm positive fractions were collected (**Figure 18**). Western blot analysis resulted in a higher concentrated protein band in the eluate with identical electrophoretic mobility as observed in the cell supernatant. Due to the higher concentration, degradation products with higher electrophoretic i.e. lower molecular mass were also detected (**Figure 17**).

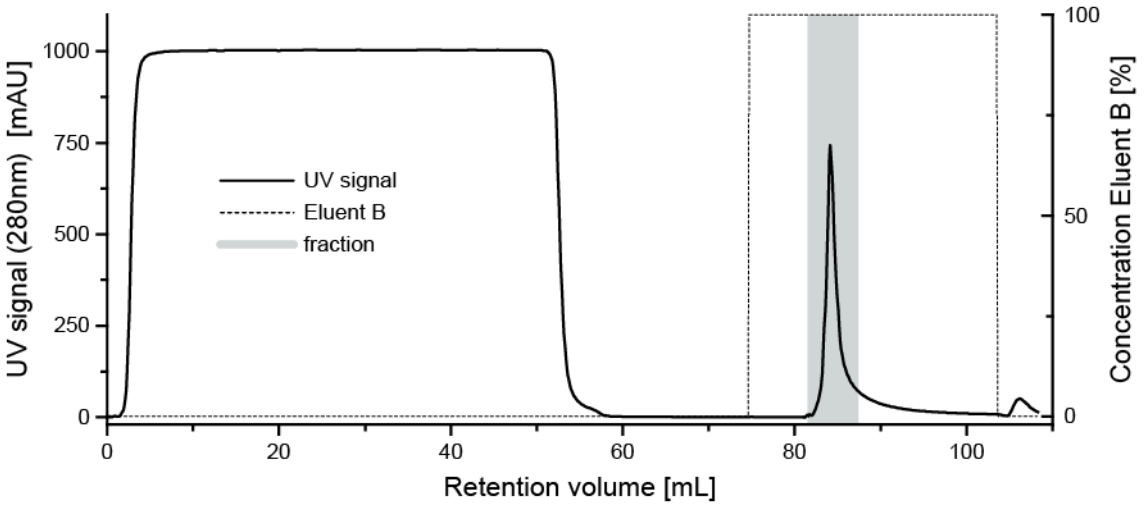

Figure 18. Protein A Affinity chromatography of Fc-FGFBP1. Binding and washing phase with PBS, elution phase commencing with 0.1 M glycine buffer pH 3.3.

To ensure a fast buffer exchange to physiological values of eluted fractions (0.1 M glycine pH 3.3 neutralized with 1 M tris pH 9) a size exclusion chromatography was subsequently performed. The peak of the UV signal was collected and pooled before the minima of the conductivity i.e. the elution of the glycine buffer occurred (**Figure 19**).

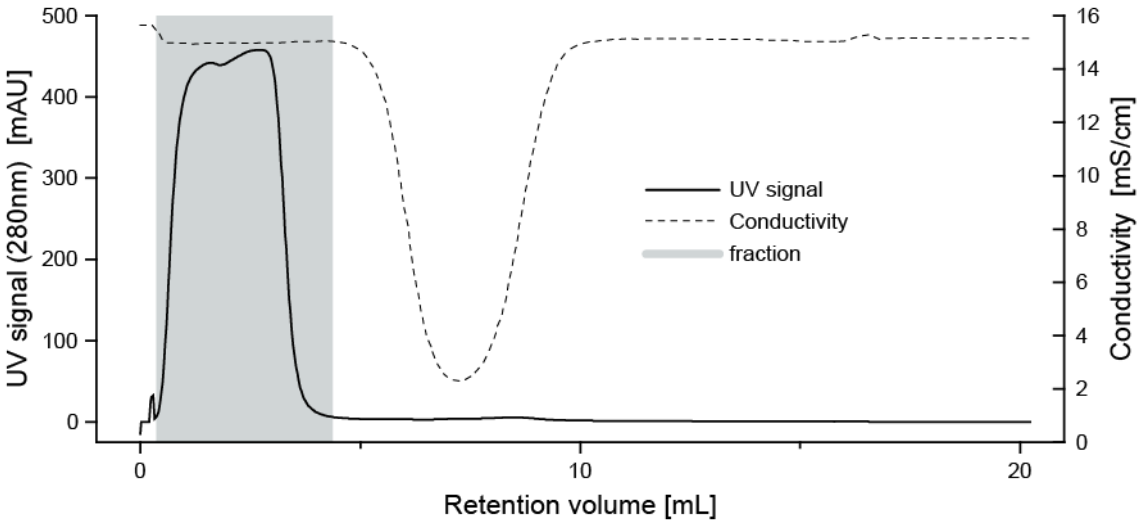

Figure 19. Elution profile of size exclusion chromatography of Fc-FGFBP. Exchange of buffer is visualized.

To quantitatively analyze the purity of the Fc-FGFBP1 in the eluted samples, a SDS-PAGE followed by Coomassie staining was performed (**Figure 20**). In line with the positive band detected by immunoblotting a distinct main band with highest intensity with a size of approximately 80 kDa was detected. Moreover, a protein band with lower intensity with a size of ~ 35 kDa was observed, which was not further investigated.

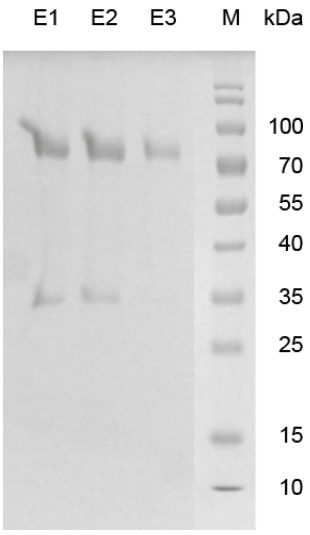

Figure 20. SDS-PAGE analysis of Fc-FGFBP1 purification after Coomassie Brilliant Blue staining. (E1)-(E3) eluted fractions of Fc-FGFBP1 after affinity purification with MabSelect SuRe columns via ÄKTApurifier, (M) marker.

Next, the Fc-FGFBP1 fusion-protein was exposed to AcTEV® protease in order to liberate the binding protein from its Fc-tag. Cleavage of the fusion-protein Fc-FGFBP1 was monitored by SDS-PAGE to determine the optimal cleavage time (**Figure 21**). The Fc-FGFBP1 band, running at ~ 80 kDa was observed to diminish from 2 h (lane 2) to 48 h (lane 5), and two new bands of ~ 37 kDa and ~ 35 kDa (lanes 2 – 5) were simultaneously detected revealing a successful cleavage of the Fc-FGFBP1 fusion-protein.

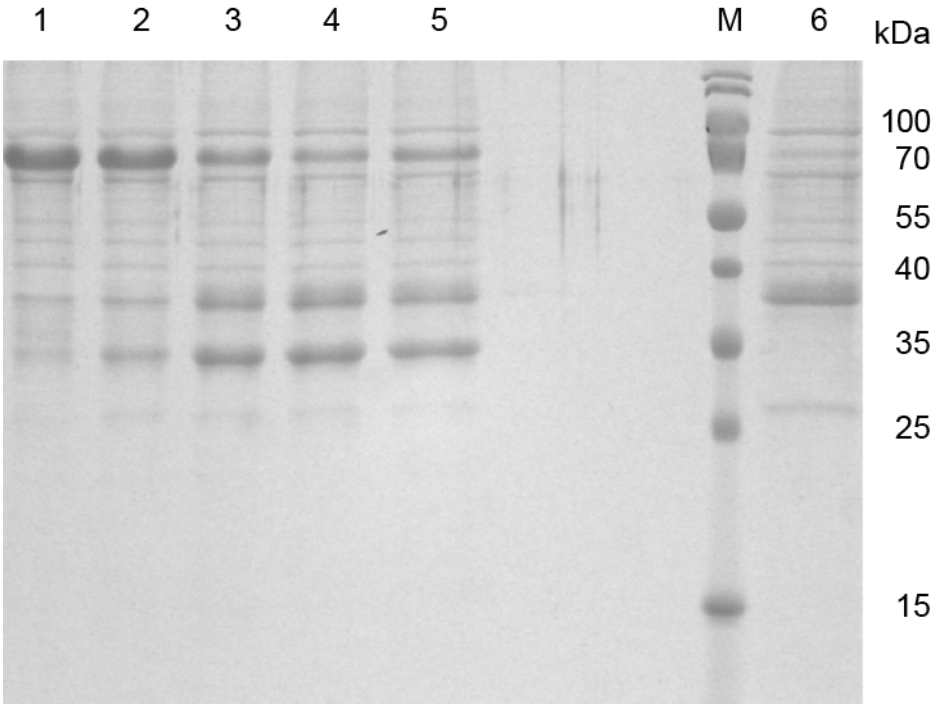

Figure 21. SDS-PAGE analysis of Fc-FGFBP1 digestion with AcTEV® protease after Coomassie Brilliant Blue staining. (1) sample at 0 h of digestion; (2) after 2 h of digestion; (3) after 16 h of digestion; (4) after 38 h of digestion; (5) after 48 h of digestion; (6) digested sample after Fc-tag removal with MabSelect SuRe column via ÄKTApurifier; (M) marker

To remove uncleaved Fc-FGFBP1 and the Fc-tag from the cleavage solution, the identical purification protocol for the fused Fc-FGFBP1 from the cell supernatant was used. The affinity chromatogram revealed a broad peak during the loading and washing phase (**Figure 22**) and was subsequently collected and further analyzed. The second peak was eluted during the elution phase with 0.1 M glycine buffer pH 3.3. In lane 6 (**Figure 21**) the band with the highest intensity revealed the same electrophoretic mobility as the ~37 kDa protein as

observed during AcTEV protease cleavage (lane 3 – lane 5), indicating the successful isolation of the FGFBP1.

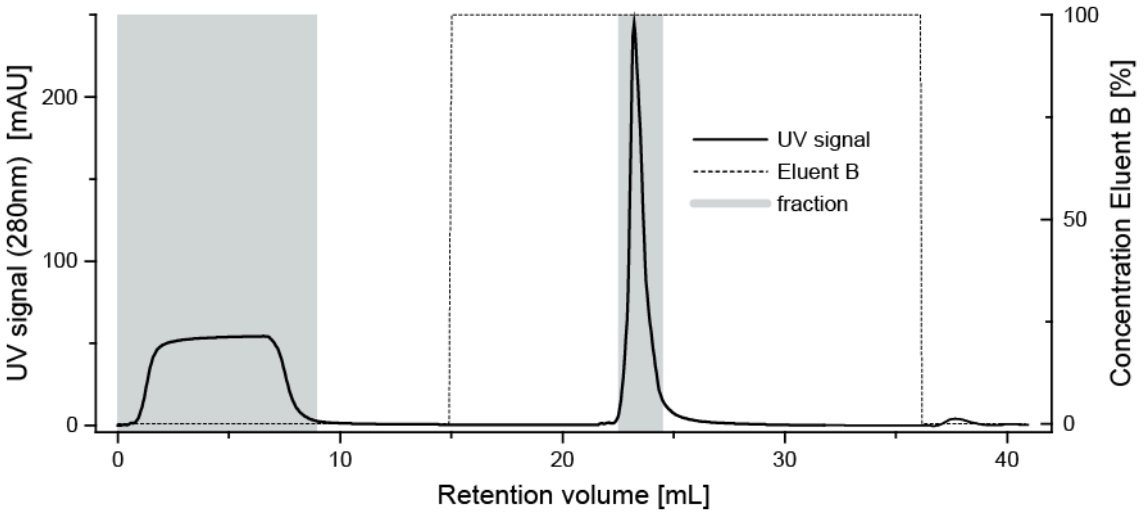

Figure 22. Protein A affinity chromatography of digested Fc-FGFBP1 with AcTEV Protease after 24 h.

FGFBP1 characterization

Glycosylation

Migration of Fc-FGFBP1 (calculated to 56 kDa) as a ~80 kDa protein in SDS-polyacrylamide gels suggest posttranslational modifications such as glycosylation [69]. Therefore, O-Glycosylation sites of FGFBP1 were further investigated by mass spectrometry (MS). PNGase F and Endo H were used to deglycosylate the glycoprotein and facilitate subsequent LC-MS/MS analysis. Deglycosylated and acetylated FGFBP1 was cleaved from its fusion-protein via AcTEV protease and was separated by SDS–PAGE. The Coomassie-stained protein band was excised and digested either with trypsin or elastase to broaden peptide sequence coverage. Evolving peptide fragments were analyzed by nanoLC-MS/MS using electron-transfer dissociation (ETD), and higher-energy C-trap dissociation (HCD). Peptide fragments with confirmed O-glycosylation sites were examined via ETD fragmentation. Two O-glycosylation sites were found in the NAPH**S**TAEEGVEGSAP**S**LGK fragment at S-34 (bold) and S#-7 (bold) with multiple glycan residues (**Figure 24**). A further O-glycosylation site at T-60 (bold) in the fragment FV**T**KDQATCR with one glycan residue (Hex) was identified (**Figure 25**). The overall sequence coverage by nanoLC-MS/MS was 76.4 % (**Figure 23**).

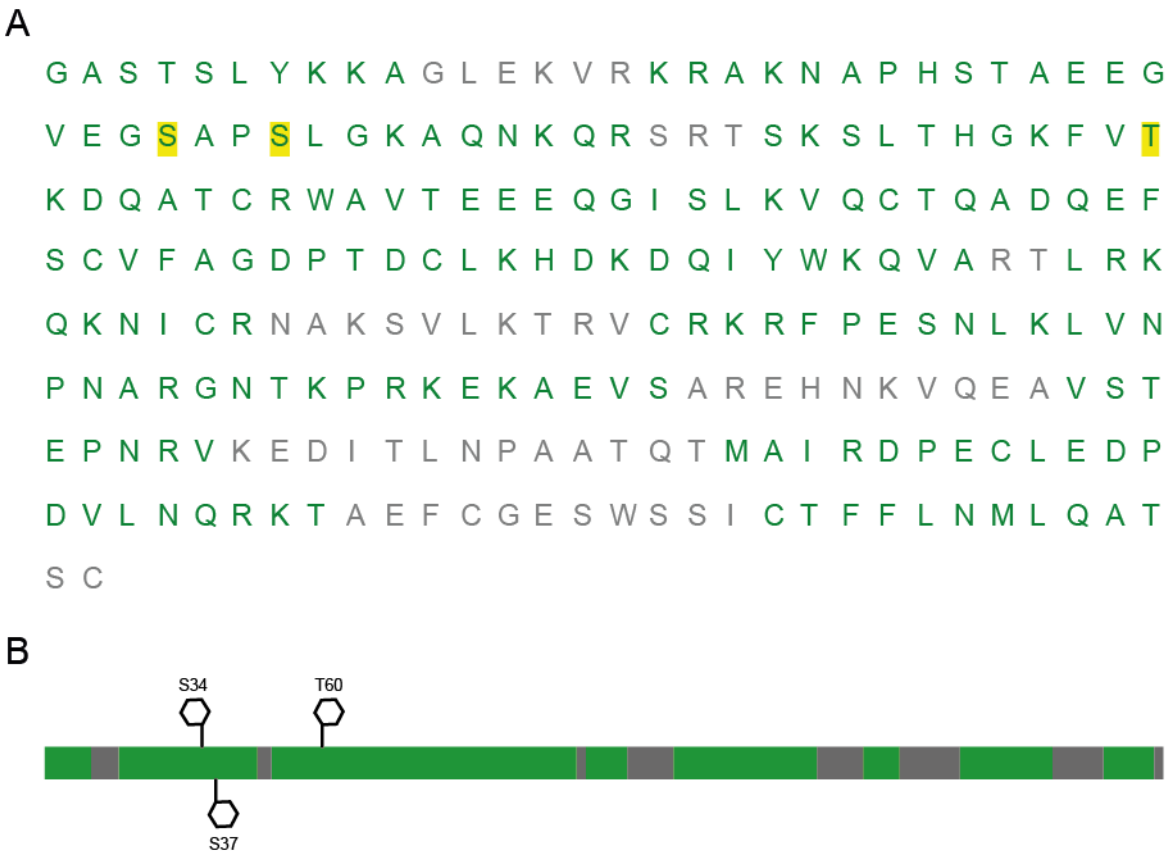

Figure 23. Amino acid sequence coverage for FGFBP1 determined by a combination of trypsin and elastase digestion with subsequent MALDI-ECD and HCD analysis. **(A)** **(Green)** recovered segments, **(gray)** not recovered segments, O-glycosylation sites are highlighted in yellow. **(B)** Sketch of FGFBP1 **(green)** recovered segments, **(gray)** not recovered segments, **(hexagon)** O-glycosylation sites.

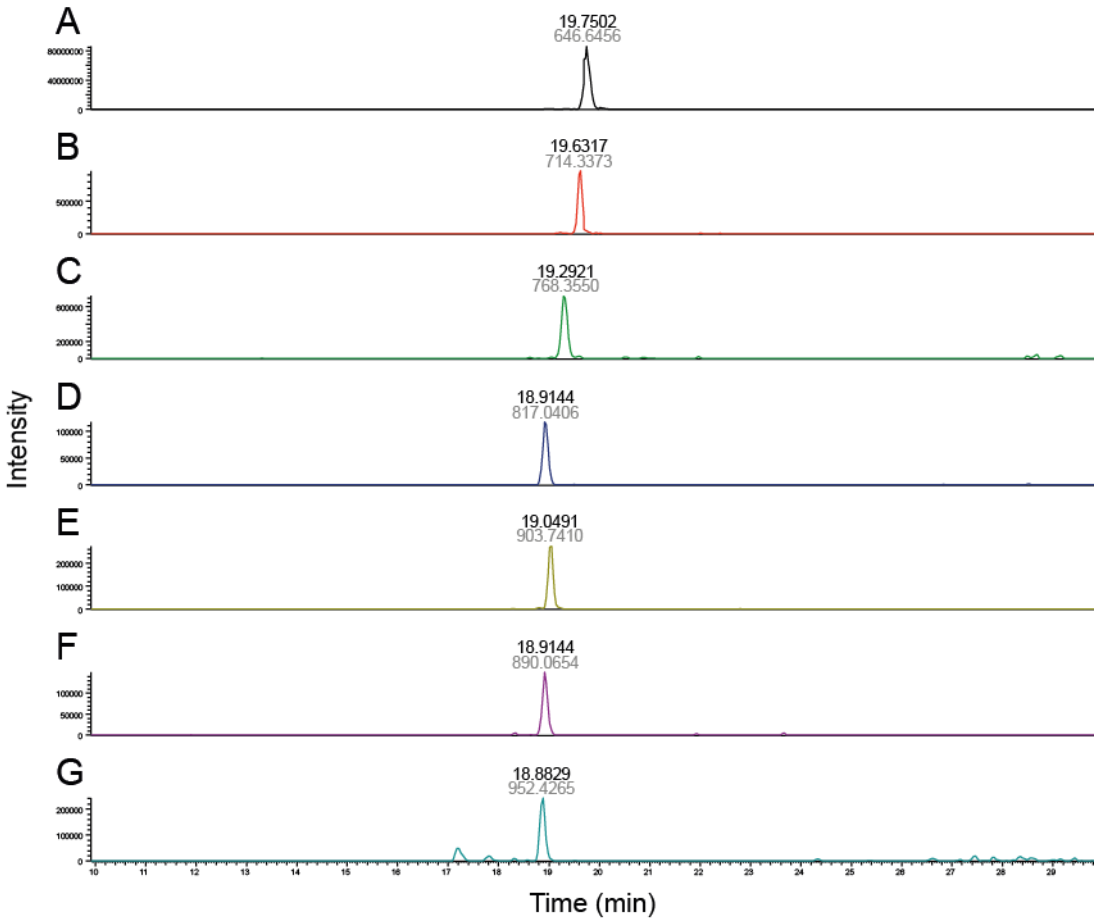

Figure 24. MALDI-ETD spectrum of the NAPHSTAEEGVEGSAPSLGK fragment of FGFBP1 after trypsin digestion with various saccharide residues. (A) NAPHSTAEEGVEGSAPSLGK peptide. **(B)** NAPHSTAEEGVEGSAPSLGK + 1x HexNac. **(C)** NAPHSTAEEGVEGSAPSLGK + 1x HexNac + 1x Hex. **(D)** NAPHSTAEEGVEGSAPSLGK + 1x HexNac(1)Fuc(1) + 1x Hex. **(E)** NAPHSTAEEGVEGSAPSLGK + 3x HexNac + 1x Hex. **(F)** NAPHSTAEEGVEGSAPSLGK 2x HexNac + 2x Hex. **(G)** NAPHSTAEEGVEGSAPSLGK + 1x HexNac(1)Fuc(1) + 2x HexNac + 1x Hex. The retention time is in bold (**black**) and the mass of the precursor ion is in bold (gray).

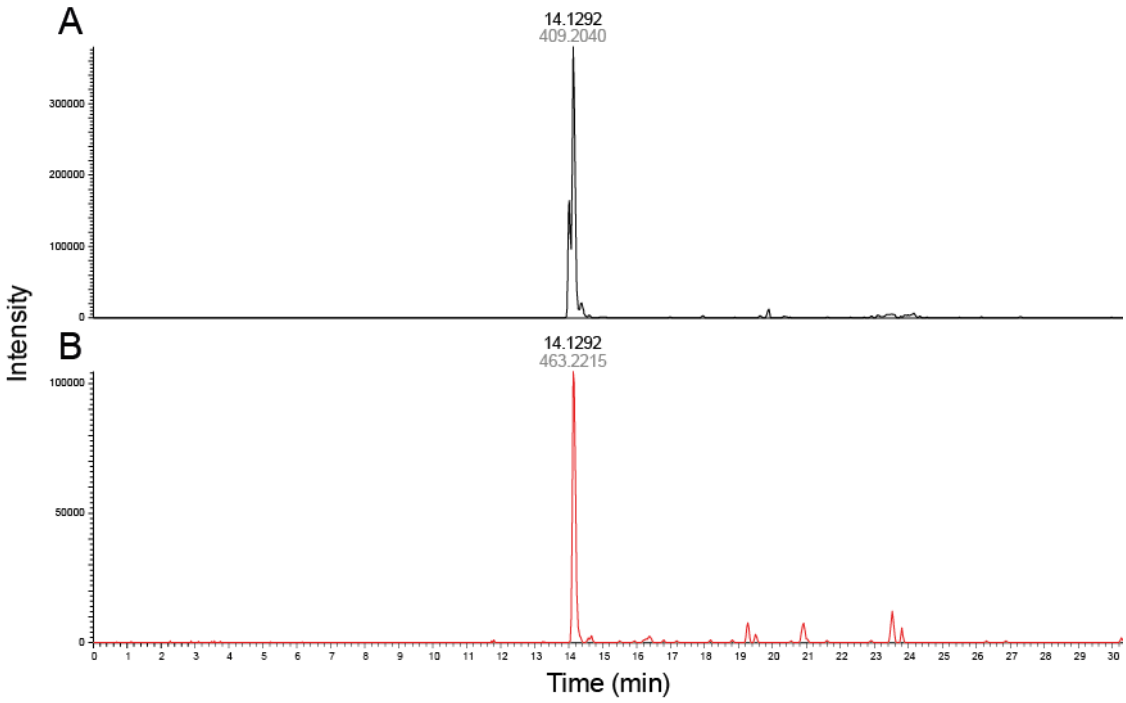

Figure 25. MALDI-ETD spectrum of the FVTKDQATCR fragment of FGFBP1 after trypsin digestion with various saccharide residues. (A) FVTKDQATCR peptide. **(B)** FVTKDQATCR + 1x Hex. The retention time is in bold **black** and the mass of the precursor ion is in bold gray.

Transfection and Expression of His-FGFBP1

To lay the groundwork in establishing an in vivo imaging assay of FGFBP1, we subcloned a His_6-tagged FGFPB1 protein. The His_6-tag was introduced to give the FGFBP1 a N-terminal chelator (after cleavage of the Fc-tag) to complex ^{99m}Tc, which is a radioactive tracer.

At first, various ratios between PEI and plasmid DNA (w/w: 9/1 – 9/6) were used to test for transfection efficiency in HEK 293 F cells. Western Blot analysis revealed that each ratio resulted in successful expression of the Fc-His-FGFBP1 protein with an increase of band intensity from lane 1 (w/w ratio: 9/1) to lane 4 (w/w ratio: 9/4), whereas no further increase in signal intensity was observed in lane 5 and lane 6 compared to lane 4, respectively (**Figure 26**). Thus a suitable PEI to DNA w/w ratio of 9/4 was chosen for further transfection.

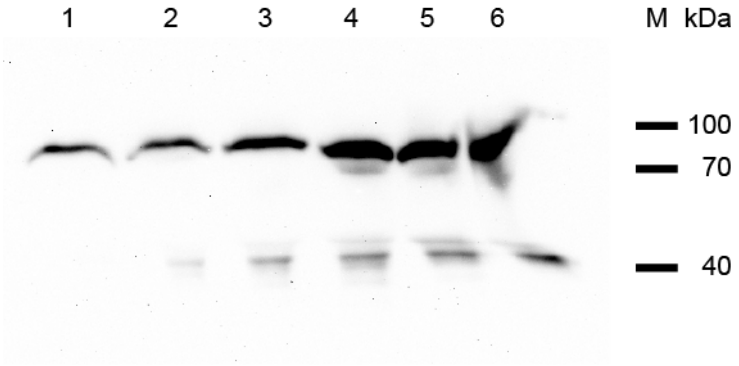

Figure 26. Western blot analysis of Fc-His-FGFBP1 on day 2 of expression with various PEI: DNA (w/w) ratios (lane 1) PEI / DNA: 9/1, (lane 2) PEI / DNA: 9/2, (lane 3) PEI / DNA: 9/3, (lane 4) PEI / DNA: 9/4, (lane 5) PEI / DNA: 9/5, (lane 6) PEI / DNA: 9/6.

Purification of His-FGFBP1

Purification of Fc- tagged His-FGFBP1 was performed with the cleared supernatant after 3 days of expression using affinity chromatography of protein A as described above. The elution phase of the chromatogram revealed One distinct peak and the λ= 280 nm positive fractions were collected and analyzed (**Figure 27**).

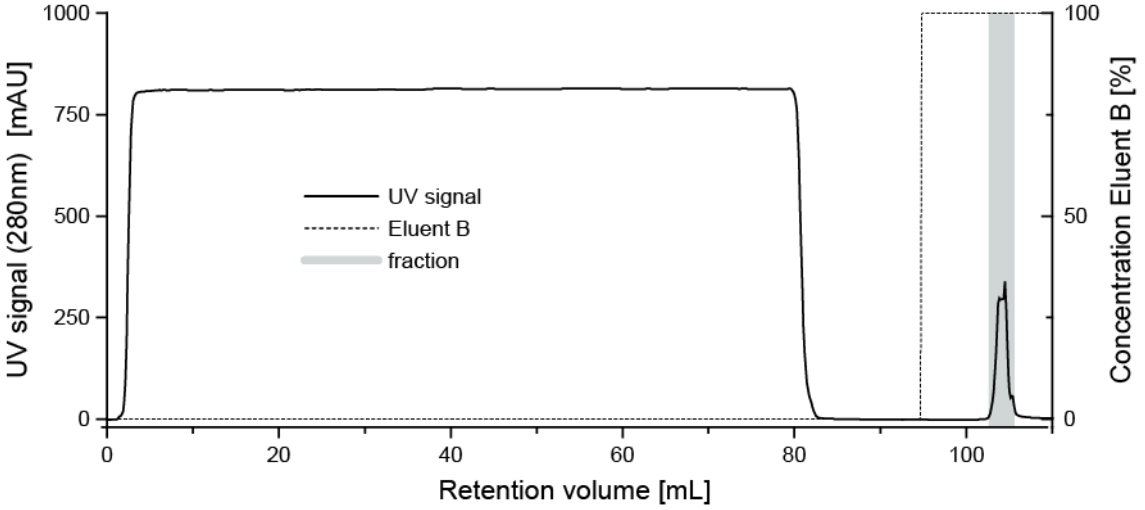

Figure 27. Protein A-Affinity chromatography of Fc-His-FGFBP1.

To check for purity, the eluted and desalted samples were analyzed by SDS-PAGE followed by Coomassie staining. As shown for the Fc-FGFBP1 (**Figure 20**), a distinct main band with

highest intensity of approximately 80 kDa was detected by SDS-PAGE after Coomassie staining (**Figure 28**).

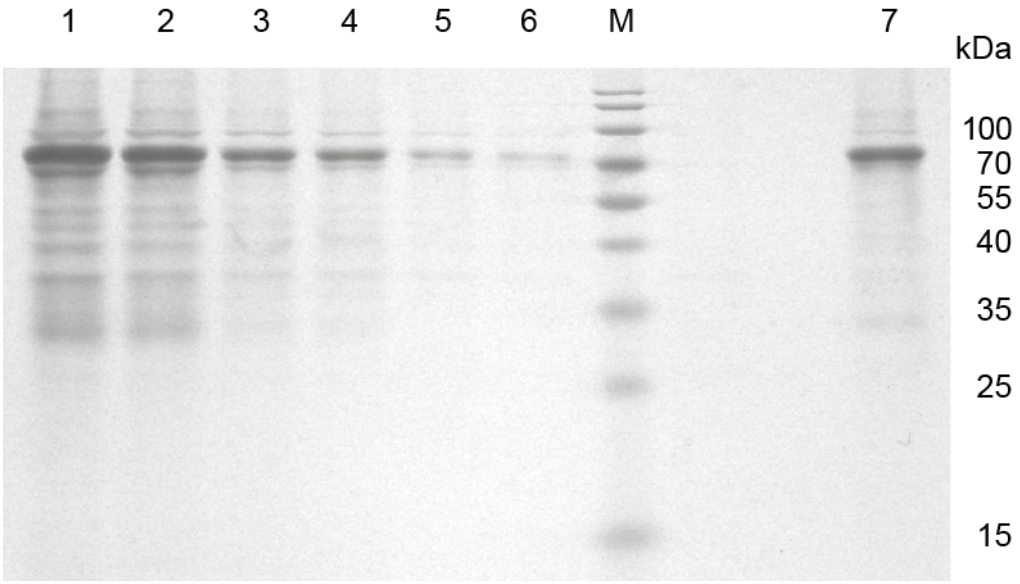

Figure 28. SDS-PAGE analysis of Fc-His-FGFBP1 purification after Coomassie Brilliant Blue staining. (Lane 1)-(lane 6) eluted fractions of Fc-FGFBP1 after buffer exchange implementing size exclusion chromatography with Desalt HP columns via ÄKTApurifier, (lane 7) Fc-FGFBP1 stored at 4 °C and 7 days after purification, (M) marker.

Next the Fc-His-FGFBP1 fusion-protein was exposed to AcTEV® protease to liberate the binding protein from its Fc-tag. Cleavage of the fusion-protein Fc-His-FGFBP1 was monitored by SDS-PAGE (**Figure 29**). The Fc-His-FGFBP1 band, running at ~ 80 kDa (lane 1) was observed to diminish from 2 h (lane 2) to 16 h (lane 3), and two new bands of ~ 37 kDa and ~ 35 kDa (lanes 2 and 3) were simultaneously detected revealing a successful cleavage of the Fc-His-FGFBP1 fusion-protein.

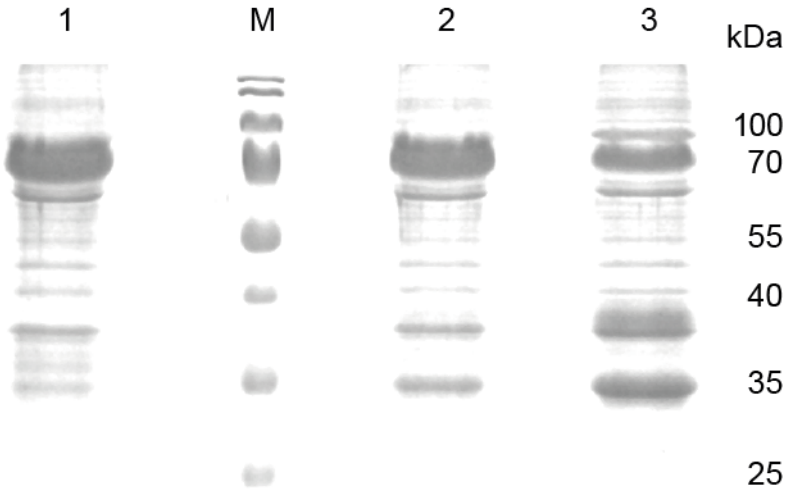

Figure 29. SDS-PAGE analysis of Fc-FGFBP1 digestion with AcTEV® protease after Coomassie Brilliant Blue staining. (Lane 1) sample at 0 h of digestion, (lane 2) after 2 h of digestion, (lane 3) after 16 h of digestion, (M) marker.

Interaction of FGF-2 with its binding partners (Phase III)

Isothermal titration calorimetry (iTC)

Heparin – mFGF-2 in PBS

The binding of low MW heparin (enoxaparin, ~ 4 500 Da, Clexane® Sanofi Aventis) to murine FGF-2 was determined by isothermal titration calorimetry. The influence of the pH value as well as the buffer type on the mFGF-2-heparin interaction, in particular the binding parameters dissociation constant (K_D), stoichiometry (n), enthalpy (ΔH), free energy change (ΔG) and the entropic contribution to the free energy of binding ($T\Delta S$) were investigated.

Representative titrations at pH values from 5.5 over 7.4 to 8.5 of mFGF-2 with heparin in PBS are presented in **Figure 30**. All binding isotherms showed a sigmoidal slope after fitting and were of exothermic nature with defined plateaus at the start and end of each titration (**Figure 20**). An overview of all calculated and observed binding parameters for all three pH values in PBS is presented in **Table 7**. The stoichiometry (n) ranged from 2.97±0.11 to 3.41±0.29, indicating that approximately three molecules of mFGF-2 are bound to one molecule of low MW heparin. Moreover, single binding constants were fitted resulting in K_D values of 221±20 nM, 232±5 nM and 293±32 nM for pH 5.5, 7.4 and 8.5 respectively. With declining acidity of the PBS buffers the enthalpic contribution to the interaction (ΔH) increased from -12.7±0.5 to 20.2±1.1 kcal/mol.

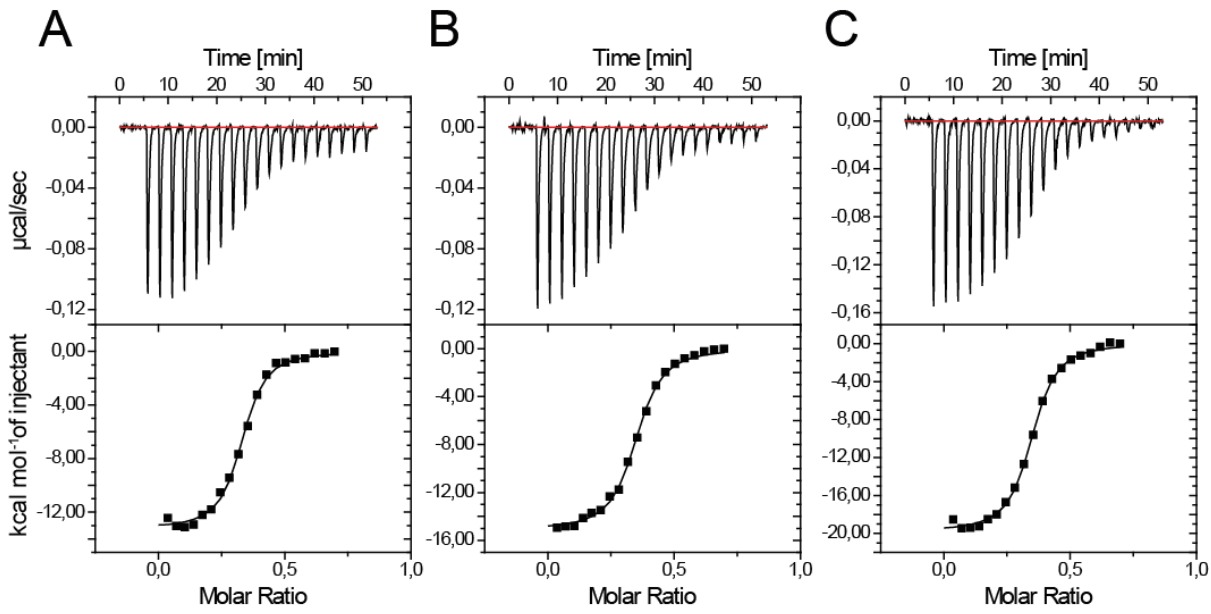

Figure 30. iTC-Analysis of mFGF-2-Heparin interaction at 20 °C in PBS. Depiction of the generated heat (µcal/sec) of the complexation after checking the generated heat of a blank titration. The lower diagram represents the measured points after integration of the peak area of the upper diagram. (**A)** PBS buffer at pH 5.5, **(B)** PBS buffer at pH 7.4, **(C)** PBS buffer at pH 8.5.

Table 7. Results of iTC titrations of mFGF-2 and Heparin in PBS.

Titration	T [K]	Repetitions	n	K_D [nM]	ΔH [kcal/mol]	ΔG [kcal/mol]	TΔS [kcal/mol
pH 5.5	293.15	3	3.41±0.29	221±20	-12.7±0.5	-8.9±0.1	-3.8±0.5
pH 7.4	293.15	4	2.97±0.11	232±5	-15.4±0.5	-8.9±0.0	-6.5±0.5
pH 8.5	293.15	5	3.29±0.42	293±32	-20.2±1.1	-8.8±0.1	-11.4±0.1

Heparin – mFGF-2 in tris buffer

To better understand binding properties of mFGF-2 with heparin as surrogate for heparansulfates, additionally to pH changes a tris buffer was selected to understand the influence of buffer types on the interaction. Representative titrations at pH values from 7.4 to 8.5 of mFGF-2 with heparin in tris buffer are presented in **Figure 21**. Both binding isotherms displayed a sigmoidal slope and were exothermic with plateaus at the start and end of each

titration (**Figure 31**). An overview of the calculated and observed binding parameters, after fitting for each pH value in tris buffer is presented in **Table 8**. At pH 7.4 three to four molecules of mFGF-2 are bound by one molecule of heparin (n= 3.49±0.31) whereas at a higher pH value of 8.5 the binding stoichiometry shifts to five molecules of protein to one molecule of heparin (n= 4.94±0.42). The single binding constant K_D of 235±67 nM at pH 7.4 decreased to 318±67 nM at pH 8.5. The exothermic enthalpy change ΔH in tris buffer at pH 7.4 and 8.5 was undistinguishable (-15.9±0.5 kcal/mol resp. -14.2±0.5 kcal/mol).

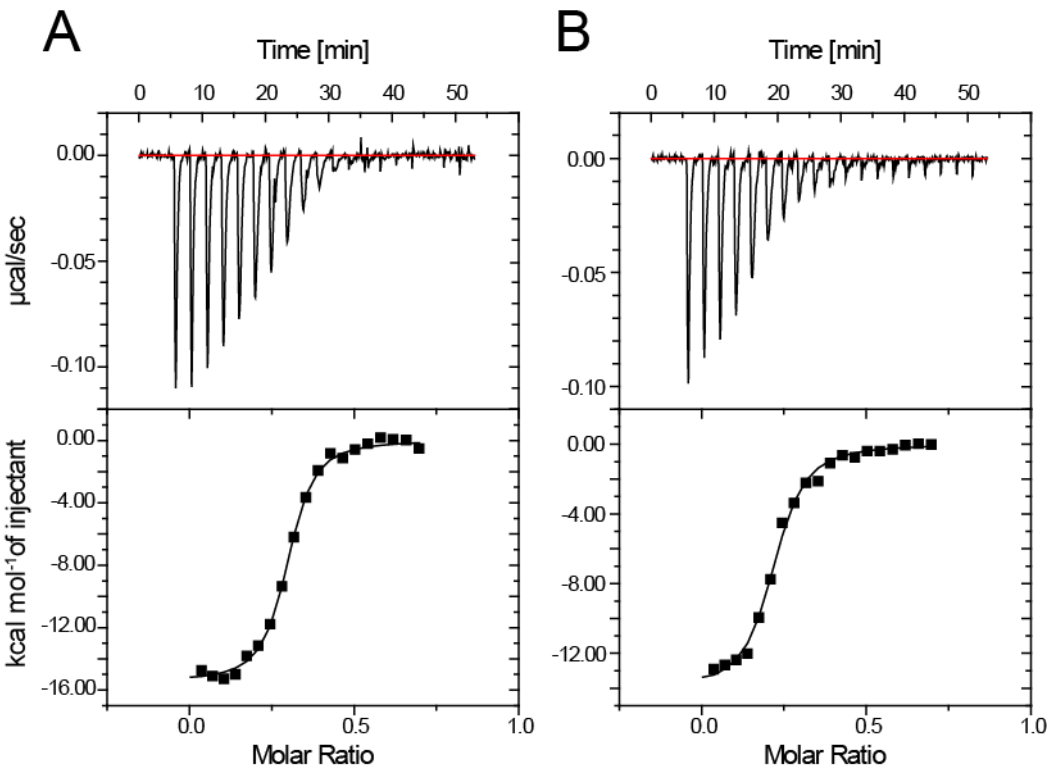

Figure 31. iTC-Analysis of mFGF-2-Heparin interaction at 20 °C in tris buffer. Depiction of the generated heat (µcal/sec) of the complexation, after checking the generated heat of a blank titration. The lower diagram represents the measured points after integration of the peak area of the upper diagram. **(A)** Tris buffer at pH 7.4, **(B)** tris buffer at pH 8.5.

Table 8. Results of iTC titrations of mFGF-2 and Heparin in tris buffer

Titration	T [K]	Repetitions	n	K_D [nM]	ΔH [kcal/mol]	ΔG [kcal/mol]	TΔS [kcal/mol
pH 7.4	293.15	4	3.49±0.31	235±67	-15.9±0.5	-11.3±0.1	-4.5±0.3
pH 8.5	293.15	4	4.94±0.42	318±67	-14.2±0.5	-11.1±0.1	-3.0±065

Surface Plasmon Resonance (SPR)

Binding properties of sourced hFGFBP1 (R&D Systems) and recombinant expressed mFGF-2 of *E.coli* were investigated by surface plasmon resonance spectroscopy (SPR). The interaction of these two partners, especially in presence of heparin as surrogate of heparin sulfates will provide a better understanding of the binding properties and the modulation of the FGF-2 release via FGFBP1 from the ECM.

After activating the surface of the biosensor with an EDC/sulfo-NHS-solution (100 mM / 25 mM) loading of saturated neutravidin (0.1 mg/mL, 10 mM Na-Acetate buffer pH 4.0) to approximately 300 RU was mediated by primary amine coupling. The remaining free activated carboxylic groups on the surface were saturated with ethanolamine. As ligand the biotinylated hFGFBP1 was immobilized on the neutravidin of the biosensor surface by avidin-biotin interaction. Neutravidin binds virtually irreversible to biotin and thus can be used for covalent ligand immobilization [154], [155]. Descending concentrations of mFGF-2 ranging from 200 nM to 6.25 nM were perfused through the hFGFBP1 decorated biosensor surface in order to measure association and dissociation kinetics (**Figure 32A**). To diminish possible influences caused by different densities of immobilized hFGFBP1 on the biosensor, the analyte mFGF-2 was used to perfuse through the same sensor in ascending concentrations from 6.25 nM up to 200 nM (**Figure 32B**).

Short association and dissociation phases of the interaction of mFGF-2 and hFGFBP1 were plotted (**Figure 33**). The analysis of the sensograms based on Michaelis-Menten kinetics is summarized in **Table 9**. A dissociation constant K_D of 69±12 nM was calculated between the ligand (hFGFBP1) and the analyte (mFGF-2).

Table 9. Summary of dissociation constant and maximally binding capacity of hFGFBP1 and mFGF-2 in the presence or absence of heparin by using a Michaelis-Menten based fitting algorithm.

Run	Ligand	Analyte A (A_A)	Analyte B (A_B)	Molar ratio A_A / A_B	K_D [nM]	R_{max} [RU]
1	hFGFBP1	mFGF-2	-	-	69±12	105
2	hFGFBP1	mFGF-2	low MW HS	10 / 1	52±16	68
3	hFGFBP1	mFGF-2	low MW HS	1 / 1	18±4	50
4	hFGFBP1	mFGF-2	low MW HS	1 / 10	no binding	-
5	hFGFBP1	-	low MW HS	-	no binding	-
6	hFGFBP1	mFGF-2	-	-	17±1	61

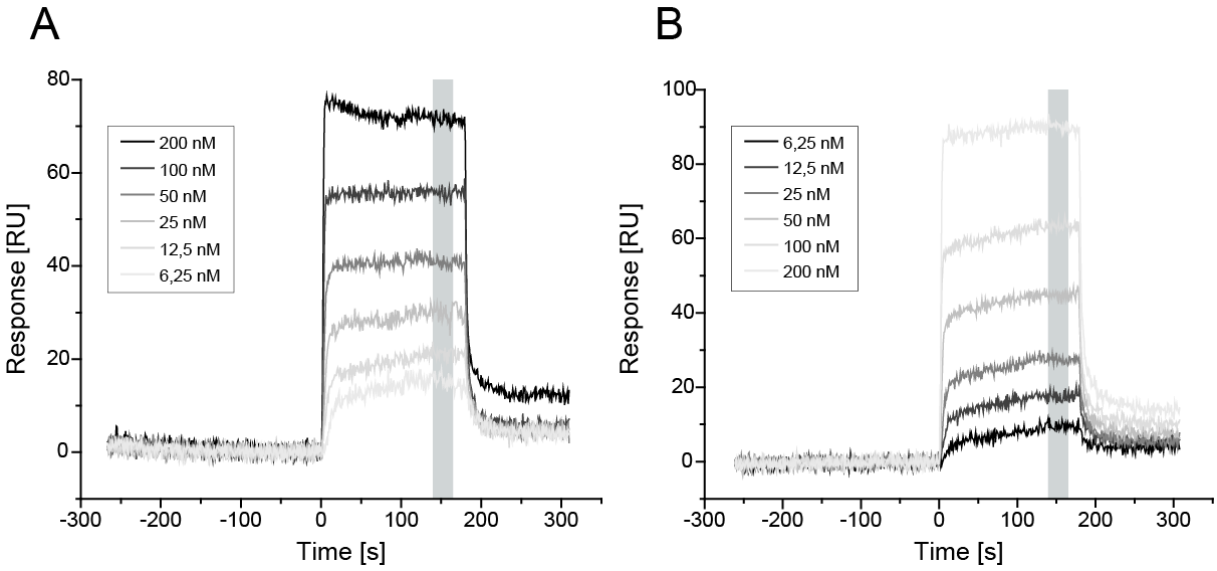

Figure 32. Sensogram for the determination of activity of hFGFBP1 (ligand). (A) Descending mFGF-2 (analyte) concentration of the lanes. **(B)** Ascending mFGF-2 (analyte) concentration of the lanes. At the point of time 0 s the association phase begins and lasts for 180 s, after which the dissociation phase commences with a duration of 150 s. The flow rate was 100 µL/min. The gray area during the equilibration stages indicates the datapoints which were used to measure the activity of the ligand and the analyte.

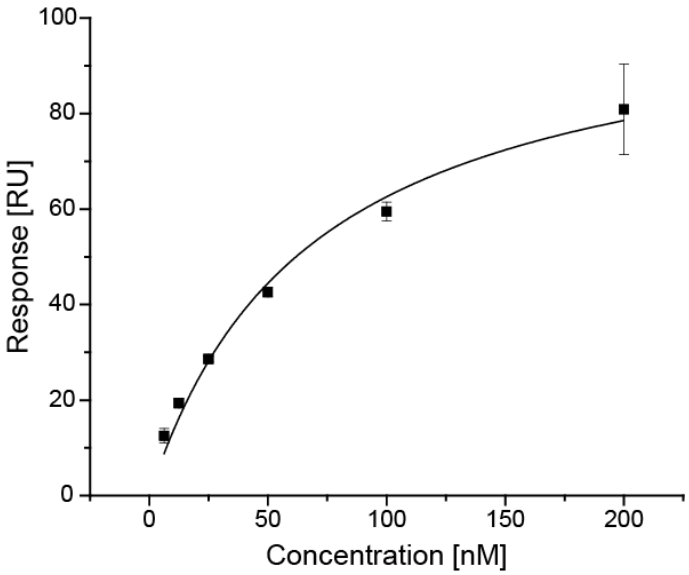

Figure 33. Diagram of response in dependence of the mFGF-2 (analyte) concentration in equilibrated phase. The mean Response [RU] of each ligand concentration is plotted against its respective ligand concentration and was analyzed by Michaelis-Menten based model algorithm.

As FGF-2 has two binding sites – one with high affinity to FGF receptors and another one with low affinity for heparan sulfates such as found in the ECM and on the cellular surface – we added low MW heparin to the mFGF-2 solution as analyte to trigger FGF-2 binding to heparin before SPR analysis [46], [47], [55]. Our aim was to investigate the influence of heparin on the binding interaction between FGFBP1 and FGF-2 complexed with heparin. In the first attempt low MW heparin was added so that a 10-fold molecular FGF-2 excess was generated. The obtained sensograms (**Figure 34A**) had extremely short dissociation and association phases comparable to the sensograms without the presence of heparin. **Figure 34B** shows however that a lower maximal binding capacity R_{max} was reached, whereas the dissociation constant of 52±16 nM remained unaltered in respect to conditions without addition of heparin as displayed in **Table 9**.

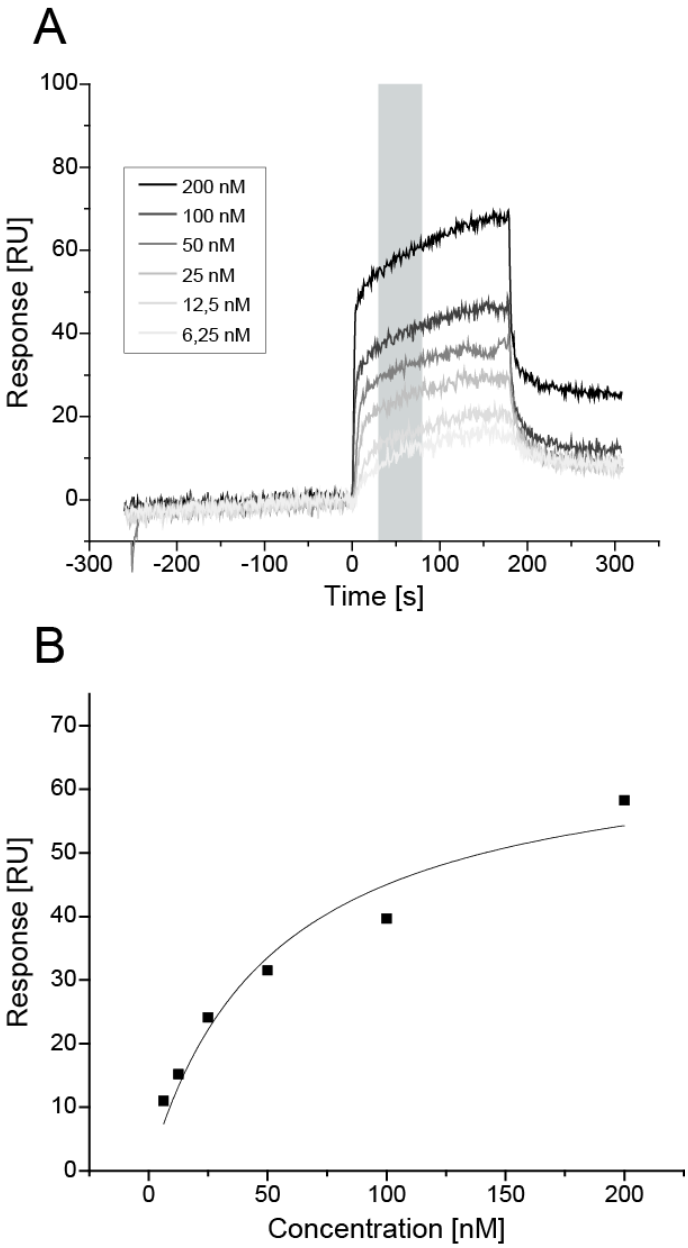

Figure 34. **Sensogram for the determination of activity of hFGFBP1 (ligand). (A)** mFGF-2 (analyte) in presence of heparin (10:1). At the point of time 0 s the association phase begins and lasts180 s, after which the dissociation phase commences with a duration of 150 s. The flow rate was 100 μL/min. The gray area in equlibrium indicates the datapoints, which were used to measure the activity of ligand and analyte**. (B)** Diagram of response in dependence of the mFGF-2 (analyte) concentration in the presence of heparin in equilibrium.

We then used the same setup as before but increased the concentration of low MW heparin to an equimolar ratio with mFGF-2 (ratio 1/1). Notably, an even lesser maximal binding capacity (R_{max}) of 50 RU was observed compared to the FGF-2/heparin ratio before (10/1). The

binding of the hFGFBP1/ mFGF-2/ heparin complex had a dissociation constant of 18±4 nM **Figure 35B** and **Table 9** with an extremely fast association and dissociation (**Figure 35A**).

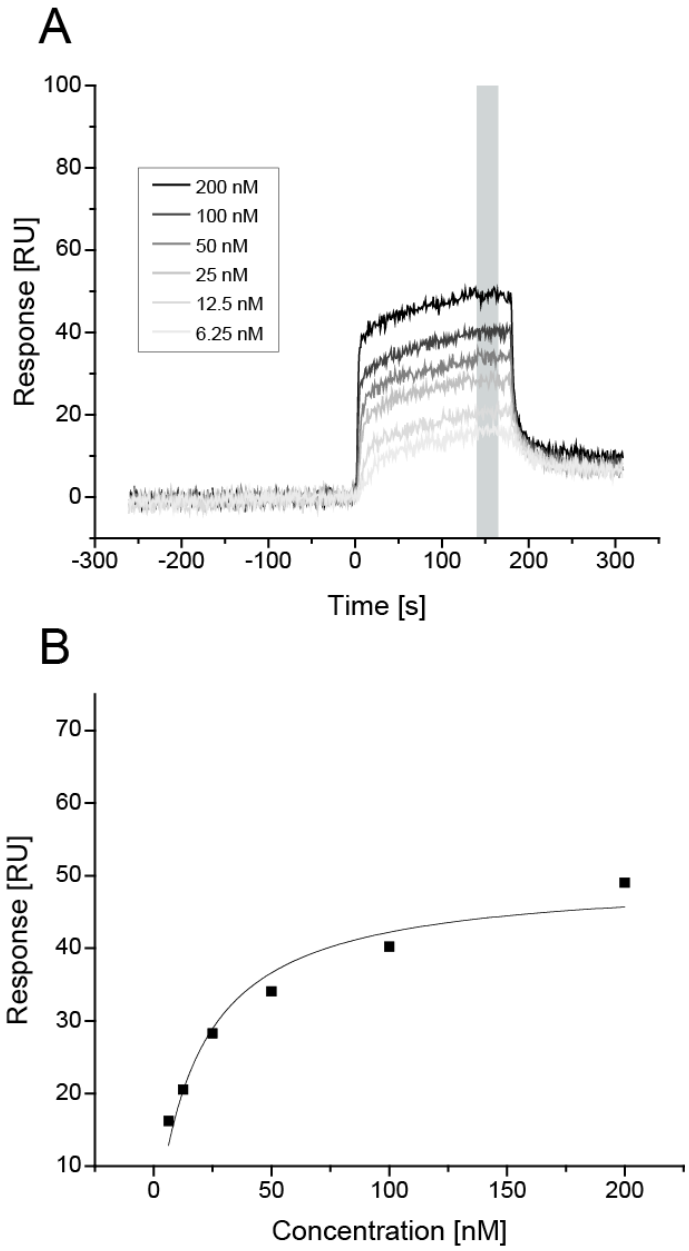

Figure 35. Sensogram for the determination of activity of hFGFBP1 (ligand). (A) mFGF-2 (analyte) in presence of heparin (1:1) At the point of time 0 s the association phase started and lasted for180 s, after which the dissociation phase commenced with a duration of 150 s. The flow rate was 100 µL/min. The gray area in equilibrium indicates the datapoints, which were used to measure the activity of ligand and analyte**. (B)** Diagram of response in dependence of the mFGF-2 (analyte) concentration in presence of Heparin in equilibrium.

The mFGF-2/ heparin ratio was modified to a 10-fold excess of low MW heparin. Sensograms are presented in (**Figure 36A**) and showed no specific interaction of mFGF-2 to hFGFBP1 in excess of heparin.

To guarantee that the lack of binding in the previous analysis was not due to competitive binding of both analytes (mFGF-2 and low MW heparin) to the ligand hFGFBP1, exclusively heparin in descending concentrations (200 nM, 100 nM, 50 nM, 25 nM, 12.5 nM and 6.25 nM) was allowed to perfuse on the hFGFBP1 decorated biosensor surface as control experiment. No specific binding of enoxaparin to the immobilized hFGFBP1 on the surface could be detected (**Figure 36B**).

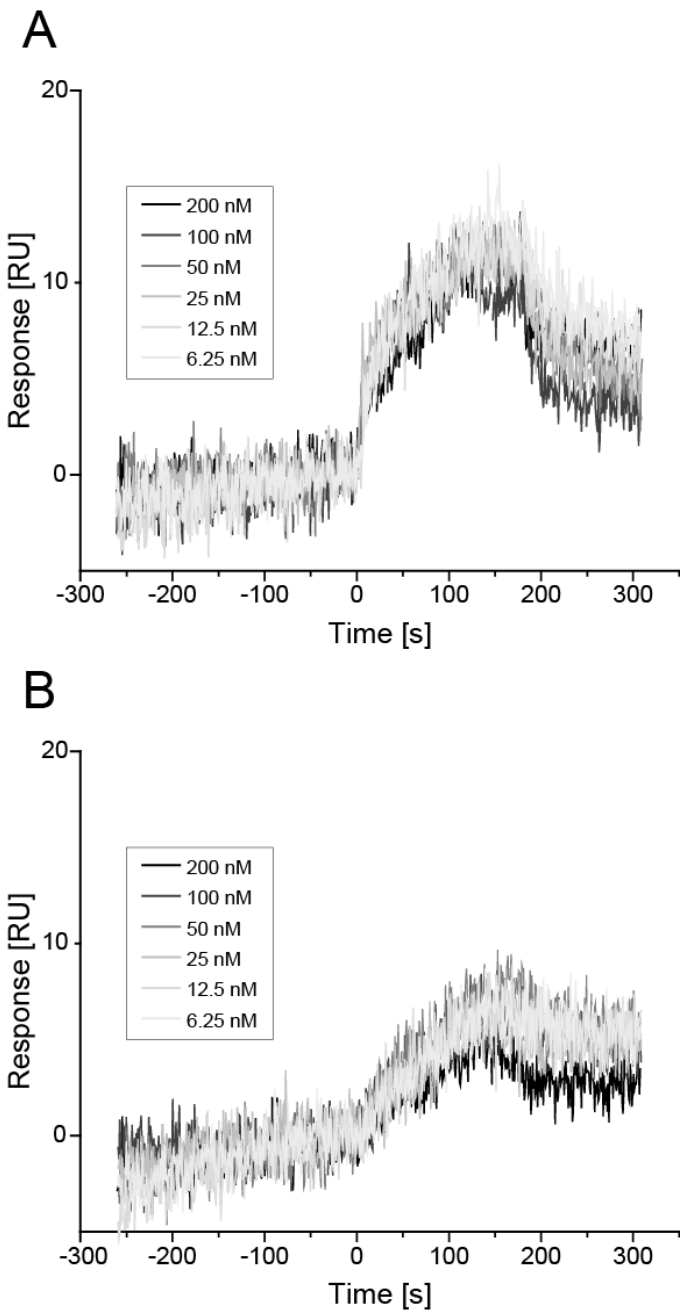

Figure 36. Sensogram for the determination of activity of hFGFBP1 (ligand). (A) mFGF-2 (analyte) in presence of heparin (1:10). At the point of time 0 s the association phase begins and lasts 180 s, after which the dissociation phase commences with a duration of 150 s. The flow rate was 100 µL/min. **(B)** Enoxaparin (analyte). At the point of time 0 s the association phase begins and lasts180 s, after which the dissociation phase commences with a duration of 150 s. The flow rate was 100 µL/min.

After multiple perfusions of low MW heparin over the hFGFBP1 loaded biosensor surface the first experiment (Run 1, **Table 9**) with an ascending analyte concentration was repeated with the identical chip and immobilized hFGFBP1 as control experiment. We asked if the pre-

treatment with low MW heparin had any influence on the interaction between hFGFBP1 with mFGF-2. The obtained sensograms (**Figure 37A**) were found to be identical to the previous ones (**Figure 32A**) with an exception of the signal of 200 nM mFGF-2 as analyte. This finding results to decreased dissociation constant K_D of 17±1 nM and a decreased binding capacity (R_{max}) of 61 RU.

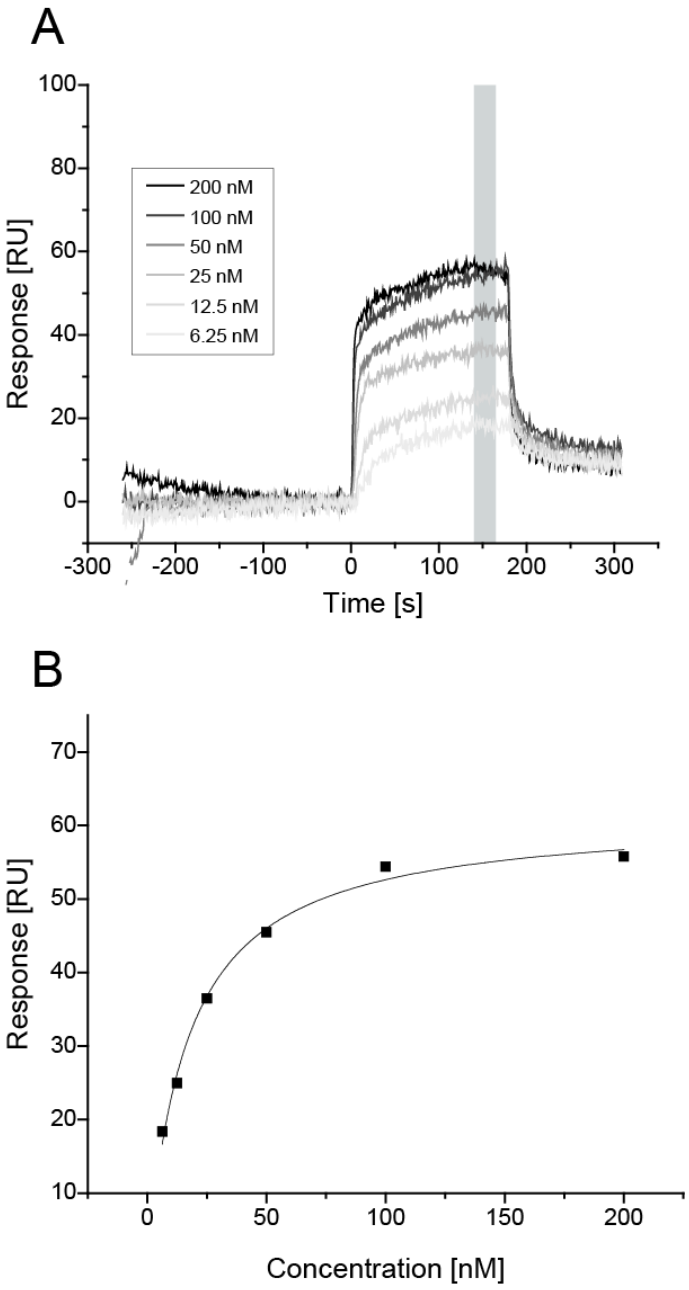

Figure 37. Sensogram for the determination of activity of hFGFBP1 (ligand) and the influence of chip-heparin interaction. (A) Descending mFGF-2 (analyte) concentration of the lanes, after the chip had contact with heparin. At the point of time 0 s the association phase begins and lasts 180 s, after which the dissociation phase commences with a duration of 150 s. The flow rate was 100 µL/min. The gray area in equilibrium indicates the datapoints, which were used to measure the activity of ligand and analyte**. (B)** Diagram of response in dependence of the mFGF-2 (analyte) concentration after chip contact with heparin.

Surface decoration (Phase IV)

To establish a set up for investigating surface decoration on planar non-adhesive surfaces (Nexterion® H slides) osteosarcoma cells (MG-63) were used because of their dose dependent response to growth factors such as IGF-I [139], [156] and FGF-2 (**Figure 13**). Furthermore previous experiments showed superior cell adhesion of MG-63 cells to glass surfaces compared to NIH 3T3 cells (data not shown). To ensure enhanced cell adhesion on the polar surface due to the polymers as spacers for the glass surface and carboxylic groups an adhesive ligand and integrin recognition molecule (RGD-motif) [157] was synthesized by solid phase peptide synthesis (SPPS). The sequence of the peptide was GRGDS as it has been previously shown to enhance cell adhesion on silk scaffolds after EDC/NHS based immobilization [158]. The MALDI-TOF spectrum of the GRGDS peptide after removing the protecting groups showed a predominant peak of 491.05 Da (**Figure 38A**), which corroborates with the estimated molecular weight of 490.4 Da (http://web.expasy.org/protparam). To evaluate the purity, the GRGDS sample was subjected to an RP-HPLC system. Due to the polarity of the peptide it showed a short retention time with a distinct peak at approximately 3 min, whereas the impurities eluted later and at higher ACN concentrations (**Figure 39A**). To remove volatile impurities, such as trifluoroacetic acid and other components of the scavenger solution the peptide was freeze dried and reconstituted in 3 % ACN 0.1 % TFA.

An RP-FPLC was implemented to mainly remove and separate other peptides, which were also synthesized as byproducts other than GRGDS. As in the RP-HPLC a broad distinctive peak was eluted early in the elution phase at a concentration of approximately 15 % of eluent B (0.1 % TFA in ACN) (**Figure 40**). Fractions were collected and lyophilized to remove the volatile TFA, which is cytotoxic and could hinder subsequent analysis with human cell lines [159]. The freeze-dried cake was reconstituted in 3% ACN to a concentration of ~ 10 mg/mL and analyzed as previously mentioned by RP-HPLC and MALDI-TOF. **Figure 33B** shows a mass spectrum with a distinct peak of 491.07 Da, which still corroborates with the estimated molecular weight of 490.4 Da. The chromatogram of the HPLC analysis reveals a single predominant peak with a retention time of 2 min (**Figure 39B**) and no further impurities.

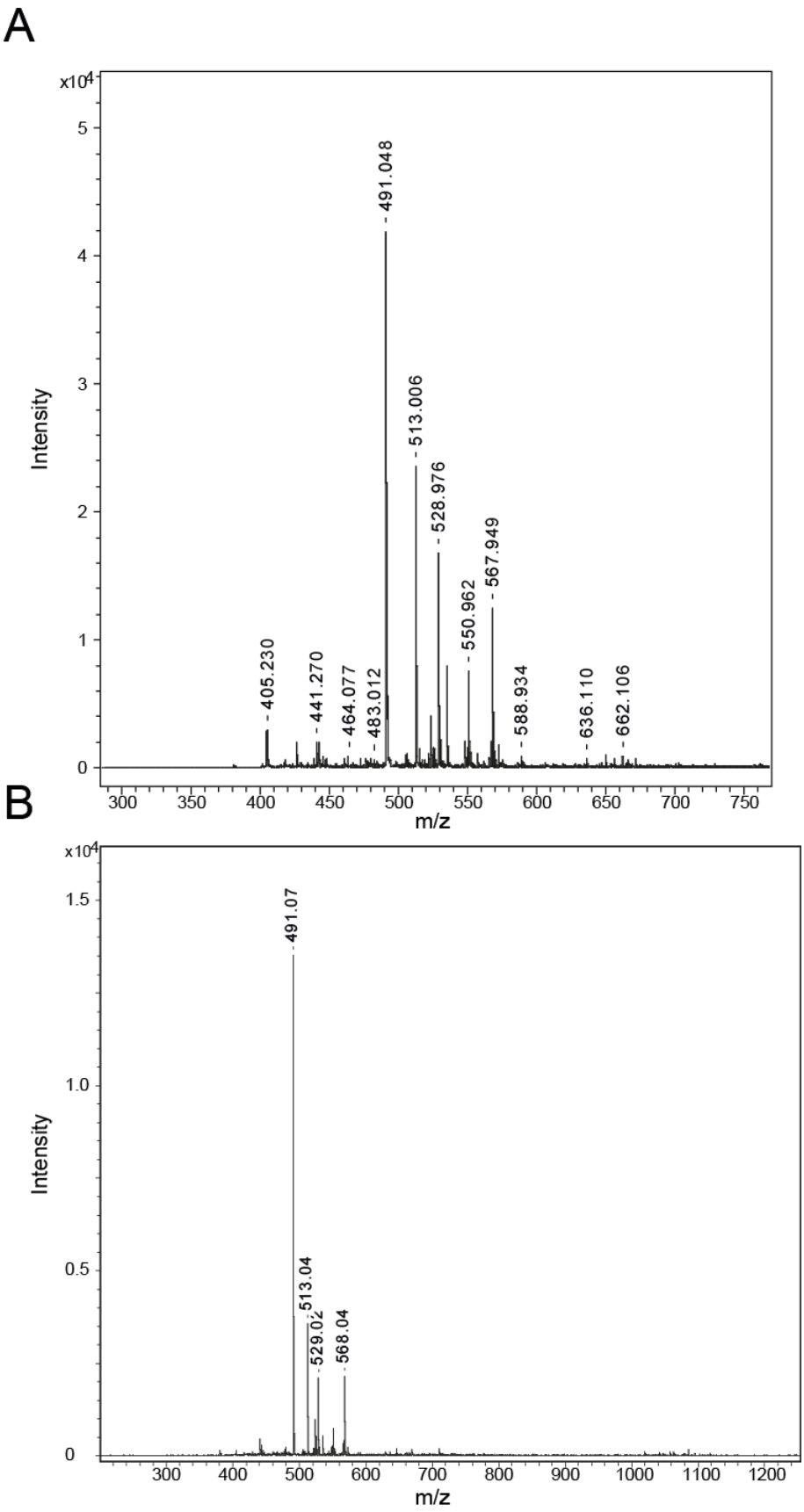

Figure 38. MALDI-TOF Mass spectrum (A) Sample of GRGDS-Peptide after solid phase peptide synthesis. **(B)** Collected Fractions of GRGDS-Peptide after FPLC purification and lyophilization.

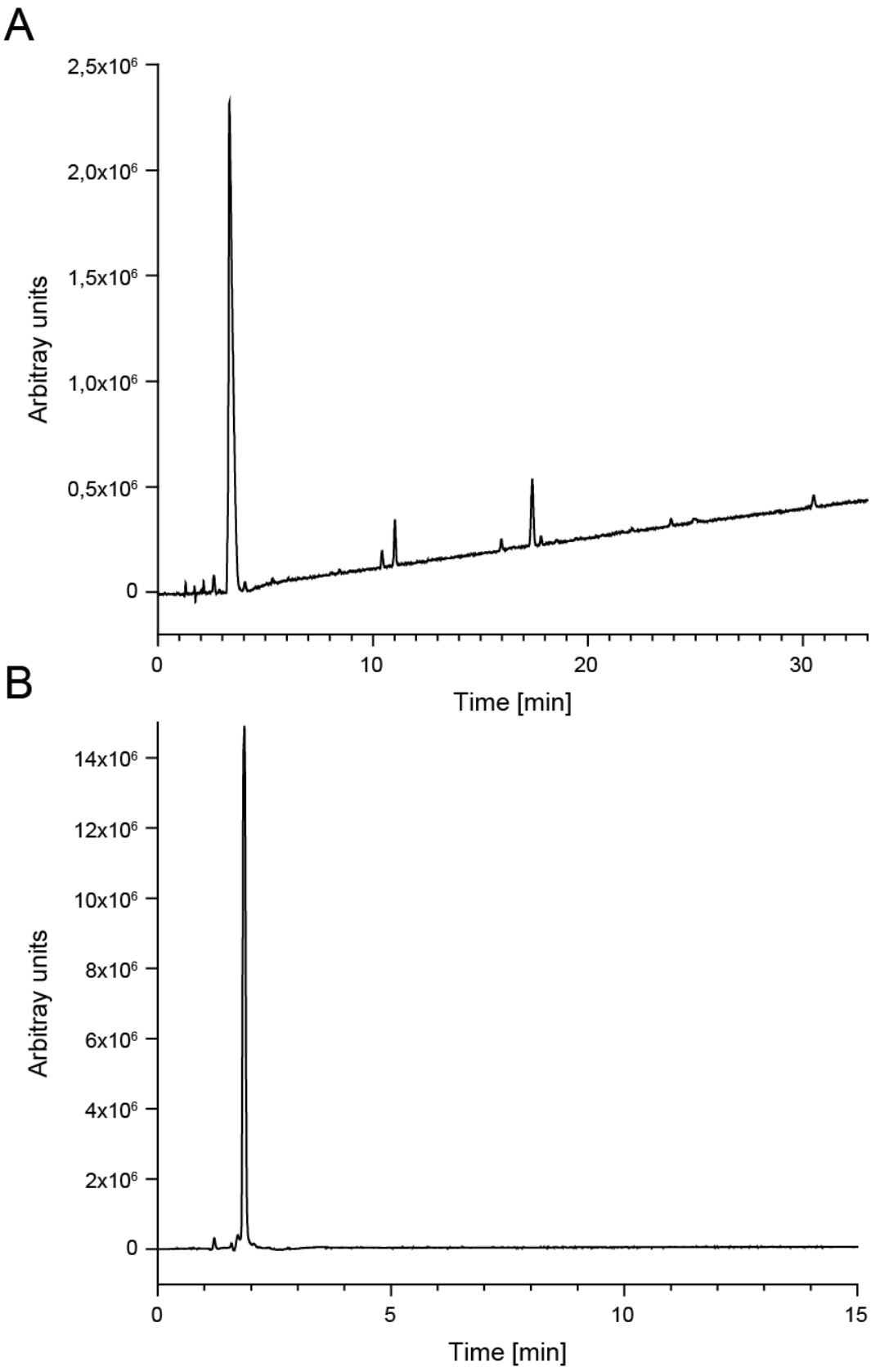

Figure 39. RP-HPLC chromatogram of GRGDS-Peptide (A) Sample of GRGDS-Peptide after solid phase peptide synthesis and first cycle of lyophilization. **(B)** Collected Fractions of GRGDS-Peptide after FPLC Purification and second cycle of lyophilization (~10 mg/mL in ACN).

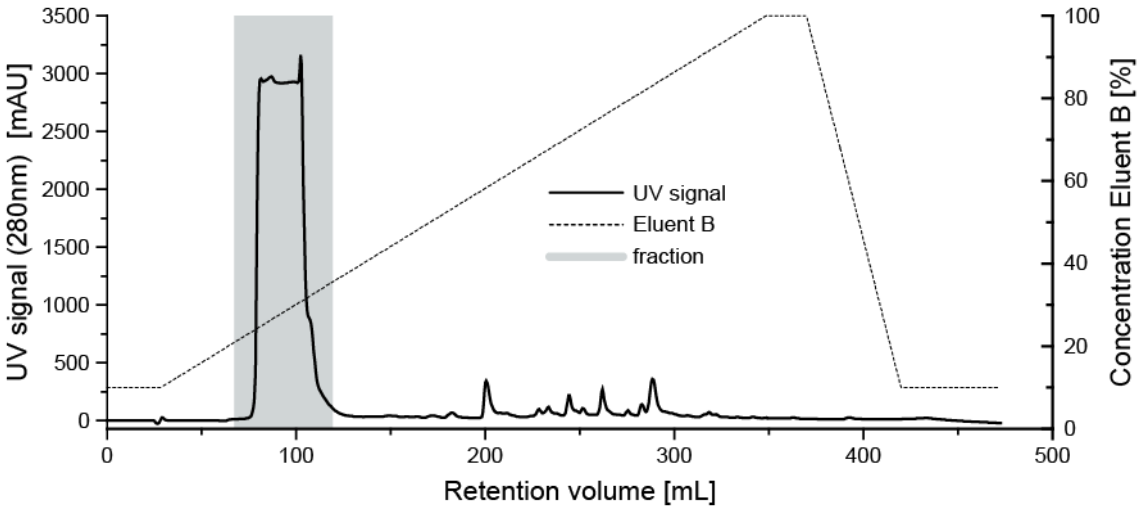

Figure 40. RP-FPLC chromatogram of GRGDS-Peptide after solidphase peptide synthesis and first cycle of lyophilization.

Nexterion® H slides were decorated by EDC/NHS chemistry mainly with an azido sugar, Azido Mannose (AzMan) to introduce an azido group to the surface of the glass slides as a partner for subsequent bio-orthogonal copper(I)-catalyzed azide alkyne cycloaddition (CuAAC) (**Figure 41**). The azido mannose and the GRGDS peptide were simultaneously coupled via EDC/NHS chemistry to investigate if and to which extent the immobilized RGD-peptide influenced the click reaction rate and yield. Thus a fluorophor with an acetylene function, Acetylene flour F 488 (Jena Bioscience) was added to the click reaction mixture. As expected, surfaces exclusively decorated with azido mannose sugar and supplemented with the catalyst Cu(I) in the click reaction mixture showed an extensive immobilization of the fluorophor Acetylene flour F 488 (**Figure 42A,B**). Surfaces remained non-fluorescent with either lacking the decoration with AzMan (**Figure 42C**) or lacking the catalyst Cu(I) in the click reaction mixture (**Figure 42D,E**).

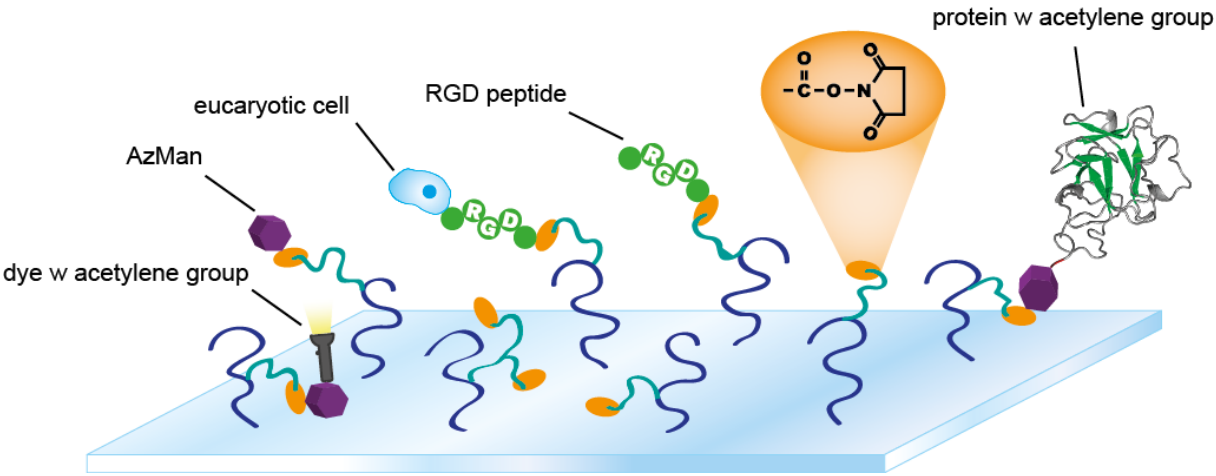

Figure 41 Schematic of Nexterion® H glass surface. Hydrophilic polymer (blue) coated to glass surface, on which long and flexible, hydrophilic spacers (green) tether reactive groups (orange) - NHS activated carboxylic groups. AzMan resp. RGD-peptide can be printed on the glass surface via EDC/NHS chemistry, allowing further decoration via CuAAC resp. cell adhesion.

The same surface decoration as outlined before was used to investigate cell adhesion of MG-63 cells to the glass slides. 10 000 MG-63 cells were seeded per well and incubated for 8 h then fixated and the cytoskeleton and nuclei were stained with Alexa 488 phalloidin and DAPI. Surfaces decorated exclusively with the GRGDS peptide (**Figure 43B**) and with a combination of GRGDS and AzMan (molar ratio 6.8/1) (**Figure 43A**) induced cell adherence and cell spreading. On surfaces lacking decoration with the integrin recognition RGD cells were unable to induce cell spreading, and adhesion as indicated in (**Figure 43C, D**).

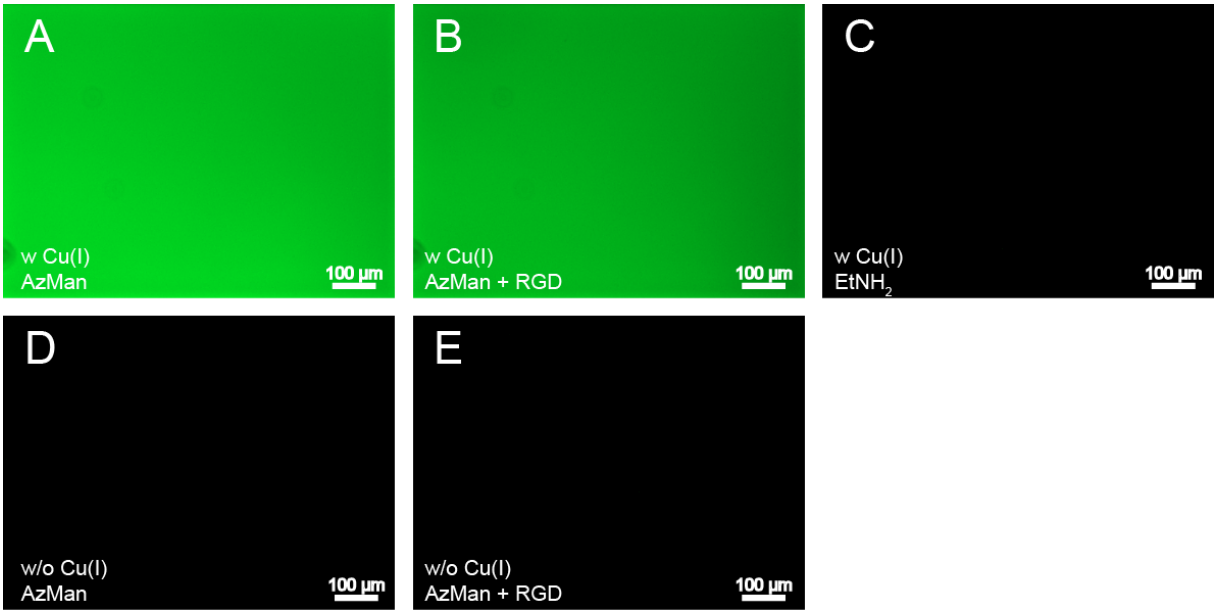

Figure 42. Decorated Nexterion® H slides were incubated with click chemistry reactions. Each well was also incubated with the click dye: Acetylene flour F 488 N3 (green). **(A)** CuAAC of dye with Cu(I) on surface decorated with 0.06 mM Azido-Mannose-sugar (AzMan). **(B)** CuAAC of dye with Cu(I) on surface decorated with 0.41 mM GRGDS-Peptide (RGD) and 0.06 mM Azido-Mannose-sugar. **(C)** CuAAC of dye with Cu(I) on undecorated surface (activated carboxylic groups were saturated with 10 % ethanolamine). **(D)** CuAAC of dye without Cu(I) on surface decorated with 0.06 mM Azido-Mannose-sugar (AzMan). **(E)** CuAAC of dye with Cu(I) on surface decorated without 0.41.mM GRGDS-Peptide and 0.06.mM Azido-Mannose-sugar.

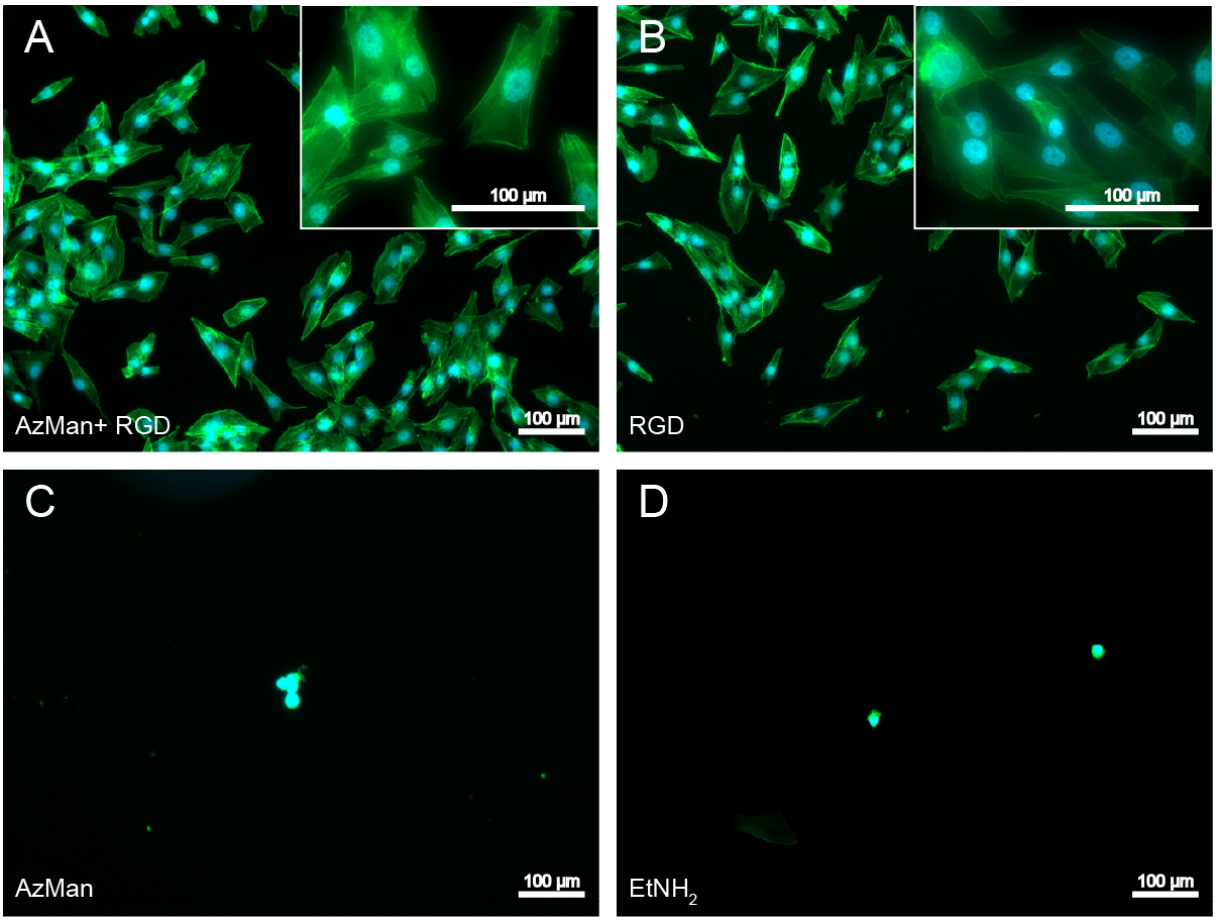

Figure 43. Decorated Nexterion® H slides with seeded MG-63 cells. Cytoskeleton of seeded MG-63 cells were stained with Alexa-488 phalloidin (green) and the cell nuclei with DAPI (blue). **(A)** Surface decorated with 0.41 mM GRGDS-Peptide and 0.06 mM Azido-Mannose-sugar. **(B)** Surface decorated with 0.41 mM GRGDS-Peptide. **(C)** Surface decorated with 0.06 mM Azido-Mannose-sugar. **(D)** Activated carboxylic groups of the surface were saturated with 10 % ethanolamine.

To quantify fluorescence intensities as read out for CuAAC based modification on the glass surface, the integrated density of the images was calculated. The fluorescence intensity after the click reaction with the florescence dye in presence of Cu(I) ions as catalyst on surfaces decorated with GRGDS and AzMan in comparison to AzMan were both significant higher than the corresponding controls, which lacked Cu(I) ions in the click reaction mixture (**Figure 44A**).

To quantify cell spreading on the surfaces decorated exclusively with GRGDS peptide and with a mixture of GRGDS peptide and the azido mannose sugar, 10 000 MG-63 cells were seeded and the cytoskeleton and cell nuclei of the adherent cells were co-stained with Alexa-488 phalloidin and with DAPI. The area of the cells as indicator for cell spreading was

individually calculated. Cell spreading on GRGDS modified surfaces was indistinguishable from cell spreading on surfaces, which were treated by a mixture of the GRGDS peptide and the azido mannose sugar (**Figure 44B**), indicating that the azide mannose functionality does not impair cell adhesion.

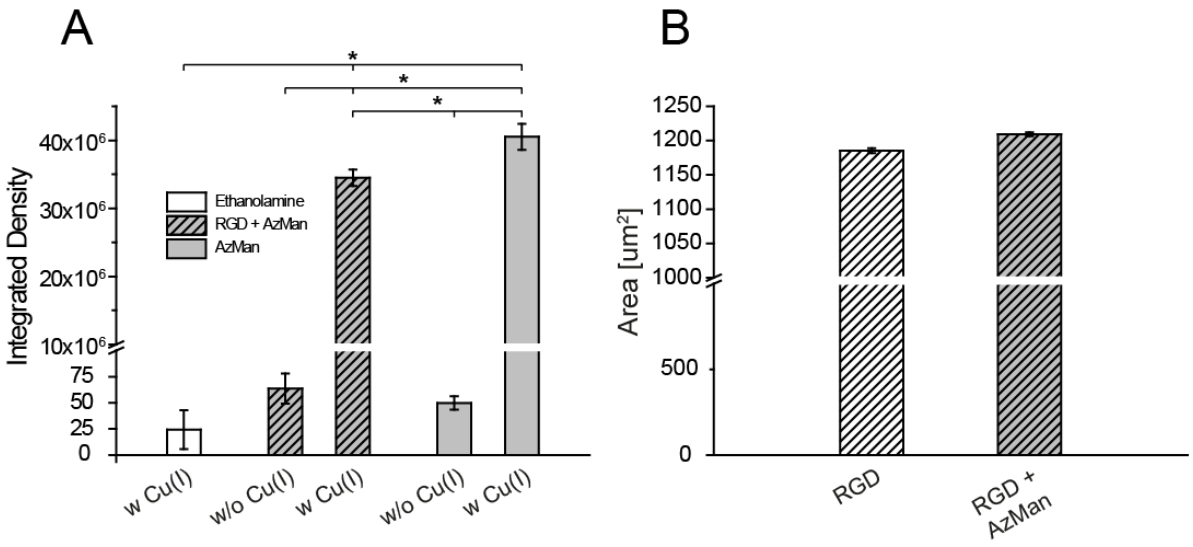

Figure 44. Decorated Nexterion H slides. (A) Measured fluorescence emission of Acetylen flour F 488 on the surface of Nexterion® H slides after click reaction dependent on various decorations. White column (n=2) activated carboxylic groups were saturated with 10 % ethanolamine, gray-streaked column (n=3) surface decoration with 0.41 mM GRGDS-Peptide and 0.06 mM AzMan, gray column surface (n=3) decoration with 0.06 mM AzMan. **(B)** Spreading of adhesive MG-63 cells on decorated Nexterion® H slides dependent on decoration after 8 h incubation and subsequent Phalloidin-DAPI staining. White-streaked column (mean ± standard error of mean, n=60) surface decoration with 0.41 mM GRGDS-Peptide, gray-streaked column (mean ± standard error of mean, n=64) surface decoration with 0.41 mM GRGDS-Peptide and 0.06 mM AzMan. The asterisk highlights significant differences ($p < 0.05$).

DISCUSSION AND OUTLOOK

We designed a fusion-protein of His6-tagged thioredoxin and the 155 amino acid variant of murine FGF-2. The expression of mFGF-2 was successfully performed by following established protocols [143]. Several N-termini variations of mFGF-2 have been so far identified [10], [12]–[15]. The gene encoding for the variant of mFGF-2 used in this thesis was chosen due to its pro-longed N-terminus that was resolved in the crystal or NMR structure (pdb file 1BLA & 1BFB) to have possibilities of further variations, such as incorporation of a non-natural amino acids (e.g. pyrrolysine analogues [115]) without restricting the binding properties of mFGF-2 to its natural binding partners (HSPG as low affinity receptors and FGFRs as high affinity receptors). Although oxidative instabilities due to the four free thiol groups of cysteines in the wild type form of mFGF-2 have been reported, we chose this variant in order to enable chemical modification such as coupling of maleimide diethylentriaminepentaacetic acid (maleimide DTPA) as a chelator via maleimide chemistry to image complexed radioactive ^{111}In via single photon emission computed tomography (SPECT) in mice [110]. Therefore the expression plasmid pHisTrx with an His6- tagged thioredoxin at the N-terminus [145] was used to circumvent inclusion body formation (intracellular aggregates of misfolded proteins [160]) and to drive mFGF-2 expression into the bacterial cytoplasm during recombinant expression.

To maximize mFGF-2 yields, the T7 promoter system was induced with IPTG (0.2 mM) for 4 h at 30 °C [161], [162]. Three sonication cycles resulted into maximal extraction of the fusion-protein from the bacterial cells (**Figure 8**). The pHisTrx-mFGF-2 fusion-protein was purified from other bacterial proteins via affinity chromatography implementing heparin columns. Cleavage of mFGF-2 from the fusion-protein was completed after 24h of incubation with thrombin. The final product mFGF-2 was purified by via heparin affinity chromatography and stored in PBS buffer supplemented with 0.5 M DTT for short-term storage. Mass spectrometric analysis revealed that mFGF-2 was fully expressed (**Figure 11**) with high purity of < 95 %, as demonstrated by RP-HPLC (**Figure 12**). Furthermore, proper folding of mFGF-2 during expression and handling during the downstream process was retained, as demonstrated by fluorescence spectroscopy (**Figure 10**) and unaltered potency (**Figure 13**). To facilitate storage and shipping mFGF-2 samples were lyophilized with 20 % w/v sucrose as cryoprotectivum. RP-HPLC analysis indicated that reconstituted samples maintained a high degree of stability with at least 88 % mFGF-2 content after 60 days with no significant degradation products (**Figure 15**).

Mammalian Suspension type HEK 293 Freestyle cells were chosen for the expression of recombinant mFGFBP1. These cells allow for rapid and efficient insertion of plasmid DNA and high expression rates due to high cell-concentrations with easy means of purifying proteins secreted into the cell supernatant [152]. Besides enabling post-translational modifications of proteins, complex chaperon systems of mammalian cells result into proper folded and therefore biologically active proteins. To facilitate protein purification a pFuse vector (Invitrogen®) encoding for tobacco etch virus protease cleavable N-terminal fusion-protein of Fc tagged murine FGFBP1 was chosen. The Fc-tag is commonly used during recombinant antibody purification [150]–[152]. The cell viability of HEK 293 Freestyle cells was monitored during the transfection with plasmid DNA – PEI complexes [149] over the period of 6 days during expression. Trypan blue staining revealed a significant drop of cell viability after 3 days of expression (**Figure 16**). Therefore the time of expression was restricted to 3 days in accordance to the expression patterns observed by Western Blot analysis, in which the highest concentration of Fc-FGFBP1 was detectable on day 3 of expression (**Figure 17**). A defined single band with approximately 80 kDa was observable, whereas the calculated molecular mass of the Fc-FGFBP1 fusion-protein is 56.6 kDa. This shift in the electrophoretic mobility is likely to occur due to the extensive glycosylation as observed by Lametsch et al, and due to the basicity of the fusion-protein (p*I* 9.02). The slower electrophoretic mobility as observed by SDS-PAGE gave first insights into glycosylation pattern as a post-translational modification.

Protein A based purification of the fusion-protein resulted in the elution of a single peak as shown in the chromatogram (**Figure 18**). Western blot analysis confirmed bands with the same electrophoretic mobility of approx. 80 kDa as observed during protein expression. However, either due to a higher protein concentration after purification or due to the duration (> 8h) of the purification process and contact to an acidic environment (pH 3) of the elution buffer we observed degradation processes as indicated by truncated forms of the fusion-protein, (multiple bands ranging from 15 to 70 kDa in size, **Figure 17**). Therefore a more rapid method to exchange the elution buffer was performed. Instead of dialyzing extensively against PBS overnight, size exclusion chromatography (SEC) was performed with prior neutralization of the elution buffer with 1 M tris buffer pH 8 (**Figure 19**). The Fc-tag removal was performed at ambient temperatures (2-8 °C) in alignment to the manufacturer's protocols of human FGFBP1 derived from NSO mouse myeloma cell line (R&D Systems). Short incubation periods with the tobacco etch virus protease did not result into complete cleavage

of the fusion-protein (**Figure 21**). Longer incubation periods exceeding 48 h were required for a better efficiency of cleavage. In SDS-PAGE analysis diffuse bands of released FGFBP1 were observed, as indication of gradual degradation during the course of cleavage of periods longer than 2h (**Figure 22**). Removing the Fc-tag in the afore-mentioned A protein based affinity chromatography resulted into the complete removal of Fc-FGFBP1 and free Fc-tag, however the FGFBP1 band remained diffuse and multiple bands ranging from 80 to 25 kDa were still present. This insufficient purity of the FGFBP1 was problematic for subsequent analytical procedures. One could possibly address this problem by increasing the concentration of AcTEV® protease during the incubation of Fc-FGFBP1, allowing shorter incubation times at low temperatures e.g. 4° C could elevate the cleavage percentage of the fusion-protein, thus adding a prolonged time frame for upstream processes, in which FGFBP1 has not yet been degraded.

The main limitation with the recombinant expression of FGFBP1 was not primary the stability of the fusion-protein but the stability of the FGFBP1 after cleavage from the Fc-tag. The fusion-protein showed good overall stability over 7 days in PBS pH 7.4 stored at 4 °C (**Figure 28**). Samples of FGFBP1 stored at 4° C and analyzed via SDS-PAGE 2 days post purification lacked bands of ~ 37 kDa corresponding to FGFBP1 (data not shown). We hypothesize that the untagged FGFBP1 is prone to proteolytic degradation. Search engines such as Peptide Cutter (Expasy) revealed multiple cleaving enzymes to cut the amino acid sequence of FGFBP1 at various sites. Pepsin, Chymotrypsin, Arg-C protease, proteinkinase K and Asp- N endopeptidase are just a few of the common protease interacting with the binding protein. Cellular originated proteases, which could not be fully removed during the purification steps could also contribute to the degradation of FGFBP1.

Truncated forms in which especially the N- or C-terminus are altered might positively influence the overall stability of the protein. According to the N-end rule different N-terminal residues influence the extent and rate of degradation, by being marked by ubiquitin ligases for degradation [163], [164]. However the lack of a crystal structure of FGFBP1 restricts the design of a stabilized FGFBP1 variant by site-specific mutation. So far two binding site to binding partners of FGFBP1 have been identified despite the lack of structural insight. A recent study based on the phage display technology identified the C-terminus (amino acid residues #193-234) to be responsible for binding of FGF-2 [74]. The binding site for heparan sulfates was identified in the middle of the protein composed of a basic amino acid cluster

(amino acid residues #110-143) [76]. All five intramolecular disulfide bonds are strongly conserved throughout all species and thus are likely to form the tertiary core structure.

Formation of covalent aggregates such as dimers or multimers of FGFBP1 has been postulated [71], [165]. Findings of Aigner et al. showed discrepancies of observed and calculated molecular weights of FGFBP1 apparently due to formation of dimers [166] or posttranslational modifications. If FGFBP1 truly has the tendency to dimerize and thus form stable aggregates it would explain the Western blot positive bands of higher molecular weights and the disappearance of monomeric FGFBP1 after short storage in aqueous environment. Altering the surface net charge of the protein could prevent the formation of stable complexes. Our recombinant expressed FGFBP1 has an isoelectric point (p*I*) of 9.41 in virtue of over 40 basic amino acids (both arginines and lysines). In this thesis, FGFBP1 was stored at a physiological pH of 7.4. Being shortly exposed to an acidic pH (pH 3; elution conditions from protein A affinity chromatography **Figure 22**) drove the eluated protein containing solution to turn turbid, which was reversed after neutralizing to a physiological pH. Therefore, in future studies storage of FGFBP1 in respect to stability could be tested and analyzed at a pH < 7.4. Covalent PEGylation of proteins has been shown to significantly reduce their micron aggregate formation by altering the attractive protein-protein interaction to a repulsive one [167]. Furthermore, PEGylation of proteins can reduce enzymatic proteolysis by masking its surface which also results into a prolonged half-life [168]. By using polysorbat 20 or polysorbat 80 in protein formulation similar effects can be achieved, surface absorption and protein agglomeration are minimized [169].

Another approach to address the instability of FGFBP1 is by changing the protein expression system. Switching to another plasmid system such as the vector pHLsec, based on the mammalian vector pLEXm (derived from the pLEX vector (Invitrogen®) only suitable for bacterial expression) [170]. Adding a C-terminal His_6-tag to the protein for a purification step not based on protein A affinity and an optimized secretion signal for the expressed protein to easily harvest the protein from the supernatant of suspension cells. Also exchanging the cell lines for expression could alter the overall stability of the protein in virtue of different chaperon systems of the cells and glycosylation pattern (**Figure 23**) more favorable in terms of stability. Implementing strategies to improve protein stability by optimizing the glycosylation site, resulted into high yields of stabilized recombinant protein [168], [171]. This can be achieved by adding defined glycosylation sites (e.g. N-G-T) via point mutation and possibly a point mutation of an amino acid more in favor of stabilizing FGFBP1 could be

a strategy in the future. Addition of external glutamine and arginine to protein formulations has shown to augment the solubility of proteins by preventing aggregation and precipitation without affecting specific protein-protein interactions which are important for our subsequent SPR and iTC measurements, and moreover protecting the protein from proteolytic degradation [172]. As FGFBP1 possess a binding site for heparan sulfate, adding LMW heparin to the protein as stabilizing agent could prevent degradation of FGFBP1.

Basic fibroblast growth factor (FGF-2, bFGF) is stored in the extra cellular matrix (ECM), where it interacts with heparin sulfate proteoglycans (HSPGs) [77]. HSPGs are essential for increasing the affinity of FGF-2 for its receptors as for facilitating dimerization and oligomerization of FGF-2 [47]. Therefore, we investigated the influence of buffer type and pH dependency on the thermodynamic interaction of heparin as a surrogate for HS with FGF-2.

We detailed the thermodynamic interaction between FGF-2 and heparin by analyzing via iTC. Incrementally titrating heparin to an excess of FGF-2 in PBS resulted in similar dissociation constant (K_D), stoichiometry (n) as previous reported at a pH of 7.4 [173]. Altering the environmental conditions (acidic: pH 5.5, physiological: pH 7.4, alkaline: pH 8.5) resulted in constant stoichiometry of ~ three molecules of FGF-2 interacting with one molecule of heparin. The calculated K_D values were indistinguishable from each other and therefore also the overall free energy change (ΔG). Whereas the binding of the two interaction partner was enthalpically dominated, the enthalpic contribution of the interaction increased with a decrease of pH (**Table 7**), whereas the entropic contribution ($T\Delta S$) decreased with elevating pH. Constant free energy levels as results by a reciprocal relationship between entropy and enthalpy are known as the enthalpy-entropy (H/S) compensating mechanism [174]. As NMR studies have shown that water molecules are bound in the cavity of FGF-2 we hypothesize that the release of these bound water molecules during complexation of heparin with FGF-2 drove the entropy change, particularly at acidic conditions.

We then switched the buffer type from PBS to tris buffer with the aim to investigate the influence of the buffer type. We aimed at studying if tris buffer was suitable for its stabilizing effect on FGF-2, since tris buffers were reported to stabilize other globular proteins such as BSA [175]. By incrementally adding heparin to an excess of FGF-2 at pH 7.4 resulted into similar findings (**Table 8**) as previously reported [176] and were in line with the results obtained with PBS as buffer system (**Table 7**). Stoichiometry (n) was unaltered with one molecule of heparin binding approximately three molecules of FGF-2 and a K_D value of ~ 200

nM. However, titrations of heparin in FGF-2 at acidic conditions (pH 5.5) resulted into a turbidity of the mixture, while conducting the experiment (6^a; **Table 5**). A possible reason could be that Tris is unsuitable as buffer at pH values below 7. Furthermore the turbidity could arise from formation of FGF-2 dimers resp. oligomers as reported by Conrad et al. with HS facilitating the self-association of FGF-2 [177].

Regulation of cell growth, differentiation and angiogenesis via FGF-2 in adult human plays a pivotal role in wound healing and tumor growth [30], [99], [178]. These pathological states exhibit low pH-values due to hypoxia (low pO2 levels) of the extracellular environment of the impacted tissue [179], [180]. Release and storage of ECM bound growth factors such as VEGF are increased at acidic pH [181]. Biomolecular pulling AFM experiments of FGF-2 and heparin resulted in stabilized complexes at acidic values generating a storage place of FGF-2 [182]. Since necrosis of human and mouse tumors releases intracellular potassium ions into the extra cellular environment to suppress T-cell effector function [183], the influence of a K^+ based buffer should be investigated, as showing that the buffer type – potentially the cation (Na^+, tris) – have an influence on the thermodynamic parameters of the binding of FGF-2 to heparin.

With the aforementioned stability issues of FGFBP1 the measurement of binding properties via iTC proved to be difficult, therefore we detailed the interaction of hFGFBP1 (purchased) and mFGF-2 in absence and presence of heparin using surface plasmon resonance (SPR). As detailed in **Figure 2B** murine and human FGFBP1 shows high homology in amino acid sequence and the same pattern of the five disulfide bonds suggesting a conserved tertiary structure [65], [69], [70], [74], [75]. SPR measurements have previously shown the possibility to thoroughly investigate the binding properties of FGF-2 with FGFR in the presence and absence of low MW heparin [184]. Biotinylated FGFBP1 was immobilized on neutravidin-decorated biosensors. We were able to investigate multiple analytes on one biosensor decorated with hFGFBP1 and to report sensograms determining the activity of full length hFGFBP1 with FGF-2 via SPR. Extremely rapid association and dissociation periods (**Figure 32**) were plotted to measure the resulting dissociation constant (K_D) of 69±12 nM in equilibrium at pH 7.4 in HBS (**Table 9**). The findings are in good agreement with a previously determined K_D of 82 nM derived from binding kinetics of mFGF-2 with the FGF-2 binding C-terminus of hFGFBP1 (amino acid residues #193-234), recombinantly expressed in *E. Coli* [74]. The addition of low MW heparin to the analyte FGF-2 prior to SPR analysis triggered complexation [46], [47], [55] and allowed us to investigate the influence of heparin

on the binding interaction between hFGFBP1 and FGF-2, as FGF-2 is stored in the ECM and hFGFBP1 is hypothesized to release the growth factor thereof. A 10-fold molecular excess and an equimolar mixture of FGF-2 to heparin resulted into dissociation constants comparable to measurements in the absence of low MW heparin (**Table 9**). However, FGF-2 did not bind to FGFBP1 in the presence of a 10-fold excess of heparin (**Figure 36A**). With increasing heparin concentration the maximal binding capacity (R_{max}) of immobilized FGFBP1 for FGF-2 decreased. We therefore hypothesized a decreased activity of the surface attached FGFBP1. Additionally, FGFBP1 and heparin did not show binding to each other (**Figure 36B**). This finding might point to the fact that there is no direct interaction of the two partners FGFBP1 and heparin as analyzed by our SPR set up. We confirmed bioactivity of FGFBP1 at this point as no changes in binding of FGF-2 to FGFBP1 after treatment of the biosensor surface with low MW heparin. K_D and R_{max} remained constant and comparable to the experiments prior to heparin treatment, assuming an aberration of the signal of 200 nM mFGF-2 as analyte (**Figure 37**) with decreased R_{max} and K_D.

We detailed for the first time the kinetic binding parameters of FGF-2 and FGFBP1 in the presence or absence of heparin. However the chosen SPR setup did not elucidate a proper release mechanism of FGF-2 bound to heparin via FGFBP1. FGF-2 is *in vivo* immobilized and stored in the ECM by interaction with HSPG. Herein, we immobilized biotinylated FGFB1 to the neutravidin-coated biosensor. Different aspects and conclusion have to be drawn in this matter: (i) possible steric hindrance of the formed FGF-2-heparin complex interfered with proper binding, as physiologically relevant FGFBP1 is soluble in extracellular fluids and not bound by the ECM. (ii) Up to date, exclusively the domain of FGFBP1 crucial for the binding of FGF-2 has been identified [74] but neither the amino acids of the C-terminus responsible for binding nor the kind of binding (e.g. electrostatic, nonionic) have been investigated. As the experiments were conducted in 0.5 M NaCl (No binding in 0.15 M NaCl, data not shown), electrostatical interaction could have been affected, rendering FGFBP1 unable to bind FGF-2 in the presence of heparin excess. The binding of FGF-2 and heparin comprises both electrostatical and nonionic binding (hydrogen bonds, van der Waals interaction and hydrophobic interaction), reflecting 30 % and 70 % of the total interaction, respectively (Thompson et al). (iii) The group of Ibrahimi et al. studied the order of the ternary complex formation between FGFR, FGF-2 and HSPG, in which the kinetics of protein-protein interaction played a crucial role and was furthermore influenced by thermodynamic mediated interaction [184]. (iv) By binding FGF-2 *in vivo* HSPG limits the

space in which soluble FGF-2 diffuses and thus concentrates FGF-2 at the cell surface/ ECM facilitating encounters of FGF-2 with FGFBP1 whereas dissociation constant in equilibrium might be negligible due to sheer abundance of FGF-2 [184]. (v) Every sensogram, indicating binding of FGF-2 with FGFBP1, featured extremely high k_{on} and k_{off} as kinetic characteristics. This finding points to short interaction periods of FGF-2 with FGFBP1, which could be compensated, by sheer numbers of FGF-2 stored to the cell surface / ECM.

To establish a set up for investigating surface decoration on planar non-adhesive surfaces (Nexterion® H slides) MG-63 cells were used due to their dose dependent response to growth factors such as IGFI [139], [156] and FGF-2 (**Figure 13**). To ensure enhanced cell adhesion in spite of the hydrophilic polymers and spacers coated to the surface an adhesive ligand and integrin recognition molecule (RGD-motif) was synthetized. The amino acid sequence GRGDS for the short peptide was chosen because of previous reports of enhancement of cell adhesion to silk scaffolds [158]. Via solid phase peptide synthesis the correct peptide was synthesized and confirmed by MALDI-MS (**Figure 39A**). RP-FPLC purification removed impurities, possible hindering cell based assays (**Figure 38B** and **Figure 39B**). Azido Mannose (AzMan) was kindly supplied (Elisabeth Memmel, Institute of Organic Chemistry Würzburg). Previous findings showed the ability of azide-functionalized sugars as viable agents for chemical decoration strategies such as CuAAC [185]–[187]. To the surface of Nexterion ® H slides AzMan and GRGDS-peptide were decorated via EDC /NHS chemistry, both essential in their purpose for further cell assays. Surfaces lacking decoration of GRGDS did not support adhesion of MG-63 cells (**Figure 43C,D**). Decoration with the RGD-motif in presence or absence of AzMan resulted into cell attachment (**Figure 43A,B**). We assume that cell spreading in respect of area occupied by the cells is only slightly reduced on surfaces decorated with both AzMan and GRGDS in comparison to surfaces exclusively decorated with the GRGDS peptide. (**Figure 44B**). On the other hand we showed that the CuAAC chemistry was specific for the reaction between AzMan and the fluorescence dye Acetylene flour F 488. Undecorated surfaces did not show an immobilization of the fluorophor (**Figure 42C**), furthermore surfaces decorated exclusively with AzMan and a mixture of AzMan and the RGD peptide (molar ratio 1/6.8) but lacking the catalyst Cu(I) during the click reaction did not result into immobilization of the fluorescence dye (**Figure 42D,E**). Fluorescence was demonstrated on decorated surfaces as mentioned above with subsequent click reaction in the presence of Cu(I) (**Figure 42A,B**). Quantified fluorescence intensities as read out for CuAAC based modification on the glass surface, revealed that the fluorescence intensity after the click

reaction with the florescence dye in presence of Cu(I) ions as catalyst on surfaces decorated with GRGDS and AzMan in comparison to AzMan were both significant higher than the corresponding controls, which lacked Cu(I) ions in the click reaction mixture (**Figure 44A**).

These preliminary pilot data revealed that covalent and specific immobilization on non-adhesive surfaces implementing CuAAC is feasible. Furthermore, our conditions (temperature, duration, reagents and concentration of reagents) during the click reaction are biocompatible for mammalian cells such as NIH 3T3 and HEK 293-F cells [114]. Combining results of our findings, as mentioned above, and the findings of an site specific decoration via CuAAC of particles with plk-FGF-2 (incorporation of the non-canonical amino acid propargyl-L-lysine to the N-terminus of FGF-2) to spatially stimulate proliferation of MG-63 cells [115] opens future avenues for the design of a cell based assay, in which biologics are site specifically immobilized onto Nexterion H ® slides and cell stimulation mediated by the immobilized biologic can be assessed. With the necessity of spatial controlled immobilizing in a specific and site directed manner of growth factors and cytokines for tissue regeneration and differentiation of cells [96] this test system might entail numerous advantages for cell based assays to elucidate the roles of concentration gradients of growth factors and the bioactivity of immobilized pharmaceutical proteins. (i) Nexterion H® slides are compatible for microscopic imaging and observation of cells (**Figure 43**). (ii) “Clickable” sugars are biocompatible [114] . (iii) Compared to peptides sugars are far less degraded by enzymes and pose a lower immunogenic threat. (iv) The surface of Nexterion H® slides with its hydrophilic polymers and spacers (**Figure 41**) form a virtually 3-D structure that can be modified to simulate the ECM and investigate properties of bound growth factors, while maintain cell adhesion mediated by the immobilized RGD-peptide.

REFERENCES

[1] D. Gospodarowicz, “Purification of a fibroblast growth factor from bovine pituitary.,” *J. Biol. Chem.*, vol. 250, no. 7, pp. 2515–20, Apr. 1975.

[2] A. Seida, J. Wada, M. Kunitomi, Y. Tsuchiyama, N. Miyatake, M. Fujii, S. Kira, K. Takahashi, K. Shikata, and H. Makino, “Serum bFGF levels are reduced in Japanese overweight men and restored by a 6-month exercise education.,” *Int. J. Obes.*, vol. 27, no. 11, pp. 1325–1331, 2003.

[3] M. Allouche and A. Bikfalvi, “The role of fibroblast growth factor-2 (FGF-2) in hematopoiesis.,” *Prog. Growth Factor Res.*, vol. 6, no. 1, pp. 35–48, 1995.

[4] R. S. Morrison, A. Sharma, J. de Vellis, and R. A. Bradshaw, “Basic fibroblast growth factor supports the survival of cerebral cortical neurons in primary culture.,” *Proc. Natl. Acad. Sci. U. S. A.*, vol. 83, no. 19, pp. 7537–41, 1986.

[5] A. Bikfalvi, S. Klein, G. Pintucci, and D. B. Rifkin, “Biological Roles of Fibroblast Growth Factor-2 1,” *Endocr. Rev.*, vol. 18, no. 1, pp. 26–45, Feb. 1997.

[6] M. A. Nugent and R. V Iozzo, “Fibroblast growth factor-2.,” *Int. J. Biochem. Cell Biol.*, vol. 32, pp. 115–120, 2000.

[7] D. Gospodarowicz and J. Cheng, “Heparin protects basic and acidic FGF from inactivation,” *J. Cell. Physiol.*, vol. 128, no. 3, pp. 475–484, Sep. 1986.

[8] A. Sommer and D. B. Rifkin, “Interaction of heparin with human basic fibroblast growth factor: Protection of the angiogenic protein from proteolytic degradation by a glycosaminoglycan,” *J. Cell. Physiol.*, vol. 138, no. 1, pp. 215–220, Jan. 1989.

[9] O. Saksela, D. Moscatelli, A. Sommer, and D. B. Rifkin, “Endothelial cell-derived heparan sulfate binds basic fibroblast growth factor and protects it from proteolytic degradation.,” *J. Cell Biol.*, vol. 107, no. 2, pp. 743–51, 1988.

[10] H. Prats, M. Kaghad, a C. Prats, M. Klagsbrun, J. M. Lélias, P. Liauzun, P. Chalon, J. P. Tauber, F. Amalric, and J. a Smith, “High molecular mass forms of basic fibroblast growth factor are initiated by alternative CUG codons.,” *Proc. Natl. Acad. Sci. U. S. A.*, vol. 86, no. 6, pp. 1836–1840, 1989.

[11] R. Z. Florkiewicz and A. Sommer, “Human basic fibroblast growth factor gene encodes four polypeptides: three initiate translation from non-AUG codons.,” *Proc. Natl. Acad. Sci. U. S. A.*, vol. 86, no. 11, pp. 3978–3981, 1989.

[12] Q. Natalina, P. F. Fern, and B. R. Daniel, “The NH2-terminal extension of high molecular weight bFGF is a nuclear targeting signal,” *J. Cell. Physiol.*, vol. 147, no. 2, pp. 311–318, 1991.

[13] M. Renko, N. Quarto, T. Morimoto, and D. B. Rifkin, “Nuclear and cytoplasmic localization of different basic fibroblast growth factor species,” *J. Cell. Physiol.*, vol. 144, no. 1, pp. 108–114, Jul. 1990.

[14] B. Bugler, F. Amalric, and H. Prats, “Alternative initiation of translation determines cytoplasmic or nuclear localization of basic fibroblast growth factor.,” *Mol. Cell. Biol.*, vol. 11, no. 1, pp. 573–7, Jan. 1991.

[15] R. Z. Florkiewicz, A. Baird, and A.-M. Gonzalez, “Multiple Forms of bFGF: Differential Nuclear and Cell Surface Localization,” *Growth Factors*, vol. 4, no. 4, pp. 265–275, Jan. 1991.

[16] J. A. Abraham, J. L. Whang, A. Tumolo, A. Mergia, J. Friedman, D. Gospodarowicz, and J. C. Fiddes, “Human basic fibroblast growth factor: nucleotide sequence and genomic organization.,” *EMBO J.*, vol. 5, no. 10, pp. 2523–8, 1986.

[17] A. E. Eriksson, B. W. Matthews, and L. S. Cousens, “Refinement of the structure of human basic fibroblast growth factor at 1.6 Å resolution and analysis of presumed heparin binding sites by selenate substitution,” *Protein Sci.*, vol. 2, no. 8, pp. 1274–1284, Aug. 1993.

[18] X. Zhu, H. Komiya, A. Chirino, S. Faham, G. M. Fox, T. Arakawa, B. T. Hsu, and D. C. Rees, “Three-dimensional structures of acidic and basic fibroblast growth factors.,” *Science*, vol. 251, no. 4989, pp. 90–3, Jan. 1991.

[19] a E. Eriksson, L. S. Cousens, L. H. Weaver, and B. W. Matthews, “Three-dimensional structure of human basic fibroblast growth factor.,” *Proc. Natl. Acad. Sci. U. S. A.*, vol. 88, no. 8, pp. 3441–5, 1991.

[20] D. Estapé, J. van den Heuvel, and U. Rinas, “Susceptibility towards intramolecular disulphide-bond formation affects conformational stability and folding of human basic fibroblast growth factor.,” *Biochem. J.*, vol. 335 (Pt 2, pp. 343–9, Oct. 1998.

[21] P. CACCIA, G. NITTI, O. CLETINI, P. PUCCI, M. RUOPPOLO, F. BERTOLERO, B. VALSASINA, F. ROLETTO, C. CRISTIANI, G. CAUET, P. SARMIENTOS, A. MALORNI, and G. MARINO, “Stabilization of recombinant human basic fibroblast growth factor by chemical modifications of cysteine residues,” *Eur. J. Biochem.*, vol. 204, no. 2, pp. 649–655, Mar. 1992.

[22] J. Zhang, L. S. Cousenst, and P. J. Barrt, “Three-dimensional structure of human basic fibroblast growth factor , a structural homolog of interleukin 1 , 8,” vol. 88, no. April, pp. 3446–3450, 1991.

[23] H. Ago, Y. Kitagawa, A. Fujishima, Y. Matsuura, and Y. Katsube, “Crystal structure of basic fibroblast growth factor at 1.6 A resolution.,” *J. Biochem.*, vol. 110, no. 3, pp. 360–363, 1991.

[24] S. A. Thompson, “The disulfide structure of bovine pituitary basic fibroblast growth factor.,” *J. Biol. Chem.*, vol. 267, no. 4, pp. 2269–73, Feb. 1992.

[25] S. A. Thompson and J. C. Fiddes, “Chemical characterization of the cysteines of basic fibroblast growth factor.,” *Ann. N. Y. Acad. Sci.*, vol. 638, pp. 78–88, 1991.

[26] J. J. Feige and a Baird, “Basic fibroblast growth factor is a substrate for protein phosphorylation and is phosphorylated by capillary endothelial cells in culture.,” *Proc. Natl. Acad. Sci. U. S. A.*, vol. 86, no. 9, pp. 3174–3178, 1989.

[27] D. Gospodarowicz, N. Ferrara, L. Schweigerer, and G. Neufeld, “Structural

characterization and biological functions of fibroblast growth factor.," *Endocr. Rev.*, vol. 8, no. 2, pp. 95–114, May 1987.

[28] G. Neufeld and D. Gospodarowicz, "Basic and acidic fibroblast growth factors interact with the same cell surface receptors.," *J. Biol. Chem.*, vol. 261, no. 12, pp. 5631–5637, 1986.

[29] G. Neufeld and D. Gospodarowicz, "The identification and partial characterization of the fibroblast growth factor receptor of baby hamster kidney cells.," *J. Biol. Chem.*, vol. 260, no. 25, pp. 13860–13868, Nov. 1985.

[30] C. Basilico and D. Moscatelli, "The Fgf Family of Growth Factors and Oncogenes," in *Advances in Cancer Research*, vol. 59, 1992, pp. 115–165.

[31] M. Jaye, J. Schlessinger, and C. a Dionne, "Fibroblast growth factor receptor tyrosine kinases: molecular analysis and signal transduction.," *Biochim. Biophys. Acta*, vol. 1135, pp. 185–199, 1992.

[32] W. L. McKeehan, J. Hou, P. Adams, F. Wang, G. C. Yan, and M. Kan, "Heparin-binding fibroblast growth factors and prostate cancer.," *Adv. Exp. Med. Biol.*, vol. 330, pp. 203–13, 1993.

[33] J. Z. Hou, M. K. Kan, K. McKeehan, G. McBride, P. Adams, and W. L. McKeehan, "Fibroblast growth factor receptors from liver vary in three structural domains," *Science (80-.).*, vol. 251, no. 4994, pp. 665–668, 1991.

[34] J. Schlessinger, A. N. Plotnikov, O. A. Ibrahimi, A. V Eliseenkova, B. K. Yeh, A. Yayon, R. J. Linhardt, and M. Mohammadi, "Crystal Structure of a Ternary FGF-FGFR-Heparin Complex Reveals a Dual Role for Heparin in FGFR Binding and Dimerization," *Mol. Cell*, vol. 6, no. 3, pp. 743–750, 2000.

[35] P. L. Lee, D. E. Johnson, L. S. Cousens, V. A. Fried, and L. T. Williams, "Purification and complementary DNA cloning of a receptor for basic fibroblast growth factor.," *Science (80-.).*, vol. 245, no. 4913, pp. 57–60, 1989.

[36] D. E. Johnson, P. L. Lee, J. Lu, and L. T. Williams, "Diverse forms of a receptor for acidic and basic fibroblast growth factors.," *Mol. Cell. Biol.*, vol. 10, no. 9, pp. 4728–36, 1990.

[37] a Yayon, Y. Zimmer, G. H. Shen, a Avivi, Y. Yarden, and D. Givol, "A confined variable region confers ligand specificity on fibroblast growth factor receptors: implications for the origin of the immunoglobulin fold.," *EMBO J.*, vol. 11, no. 5, pp. 1885–1890, 1992.

[38] T. Miki, D. P. Bottaro, T. P. Fleming, C. L. Smith, W. H. Burgess, a M. Chan, and S. a Aaronson, "Determination of ligand-binding specificity by alternative splicing: two distinct growth factor receptors encoded by a single gene.," *Proc. Natl. Acad. Sci. U. S. A.*, vol. 89, no. January, pp. 246–250, 1992.

[39] E. T. Alarid, J. S. Rubin, P. Young, M. Chedid, D. Ron, S. A. Aaronson, and G. R. Cunha, "Keratinocyte growth factor functions in epithelial induction during seminal vesicle development," *Proc Natl Acad Sci USA*, vol. 91, no. 3, pp. 1074–1078, 1994.

[40] A. Avivi, A. Yayon, and D. Givol, "A novel form of FGF receptor-3 using an

alternative exon in the immunoglobulin domain III," *FEBS Lett.*, vol. 330, no. 3, pp. 249–252, 1993.

[41] A. Orr-Urtreger, M. T. Bedford, T. Burakova, E. Arman, Y. Zimmer, A. Yayon, D. Givol, and P. Lonai, "Developmental localization of the splicing alternatives of fibroblast growth factor receptor-2 (FGFR2).," *Developmental biology*, vol. 158, no. 2. pp. 475–86, 1993.

[42] G. Yan, Y. Fukabori, G. McBride, S. Nikolaropolous, and W. L. McKeehan, "Exon switching and activation of stromal and embryonic fibroblast growth factor (FGF)-FGF receptor genes in prostate epithelial cells accompany stromal independence and malignancy.," *Mol. Cell. Biol.*, vol. 13, no. 8, pp. 4513–4522, 1993.

[43] E. Gilbert, F. Delgatto, P. Championarnaud, M. C. Gesnel, and R. Breathnach, "Control of BEK and K-SAM Splice Sites in Alternative Splicing of the Fibroblast Growth Factor Receptor-2 Pre-Messenger RNA," *Mol Cell Biol*, vol. 13, no. 9, pp. 5461–5468, 1993.

[44] J. Xu, Z. Liu, and D. M. Ornitz, "Temporal and spatial gradients of Fgf8 and Fgf17 regulate proliferation and differentiation of midline cerebellar structures," *Development*, vol. 127, no. 9, pp. 1833–1843, 2000.

[45] V. P. Eswarakumar, I. Lax, and J. Schlessinger, "Cellular signaling by fibroblast growth factor receptors," *Cytokine Growth Factor Rev.*, vol. 16, pp. 139–149, 2005.

[46] D. Moscatelli, "High and low affinity binding sites for basic fibroblast growth factor on cultured cells: Absence of a role for low affinity binding in the stimulation of plasminogen activator production by bovine capillary endothelial cells," *J. Cell. Physiol.*, vol. 131, no. 1, pp. 123–130, Apr. 1987.

[47] A. Yayon, M. Klagsbrun, J. D. Esko, P. Leder, and D. M. Ornitz, "Cell-surface, heparin-like molecules are required for binding of basic fibroblast growth-factor to its high-affinity receptor," *Cell*, vol. 64, no. 4, pp. 841–848, 1991.

[48] A. C. Rapraeger, S. Guimond, A. Krufka, and B. B. Olwin, "[11] Regulation by heparan sulfate in fibroblast growth factor signaling," in *Cell*, vol. 67, 1994, pp. 219–240.

[49] D. M. Ornitz and P. Leder, "Ligand specificity and heparin dependence of fibroblast growth factor receptors 1 and 3.," *J. Biol. Chem.*, vol. 267, no. 23, pp. 16305–16311, 1992.

[50] D. M. Ornitz, A. Yayon, J. G. Flanagan, C. M. Svahn, E. Levi, and P. Leder, "Heparin is required for cell-free binding of basic fibroblast growth factor to a soluble receptor and for mitogenesis in whole cells.," *Mol. Cell. Biol.*, vol. 12, no. 1, pp. 240–7, 1992.

[51] A. C. Rapraeger, A. Krufka, and B. B. Olwin, "Requirement of heparan sulfate for bFGF-mediated fibroblast growth and myoblast differentiation.," *Science*, vol. 252, no. 5013, pp. 1705–8, 1991.

[52] T. Spivak-Kroizman, M. A. Lemmon, I. Dikic, J. E. Ladbury, D. Pinchasi, J. Huang, M. Jaye, G. Crumley, J. Schlessinger, and I. Lax, "Heparin-induced oligomerization of FGF molecules is responsible for FGF receptor dimerization, activation, and cell proliferation," *Cell*, vol. 79, no. 6, pp. 1015–1024, 1994.

[53] M. Rusnati, C. Urbinati, and M. Presta, “Internalization of basic fibroblast growth factor (bFGF) in cultured endothelial cells: Role of the low affinity heparin-like bFGF receptors,” *J. Cell. Physiol.*, vol. 154, no. 1, pp. 152–161, Jan. 1993.

[54] D. M. Ornitz, A. B. Herr, M. Nilsson, J. Westman, C. M. Svahn, and G. Waksman, “FGF binding and FGF receptor activation by synthetic heparan-derived di- and trisaccharides.,” *Science*, vol. 268, no. April, pp. 432–6, 1995.

[55] J. Schlessinger, I. Lax, and M. Lemmon, “Regulation of growth factor activation by proteoglycans: What is the role of the low affinity receptors?,” *Cell*, vol. 83, no. 3, pp. 357–360, Nov. 1995.

[56] G. Venkataraman, V. Sasisekharan, A. B. Herr, D. M. Ornitz, G. Waksman, C. L. Cooney, R. Langer, and R. Sasisekharan, “Preferential self-association of basic fibroblast growth factor is stabilized by heparin during receptor dimerization and activation.,” *Proc. Natl. Acad. Sci. U. S. A.*, vol. 93, no. 2, pp. 845–850, 1996.

[57] M. Roghani and D. Moscatelli, “Basic fibroblast growth factor is internalized through both receptor-mediated and heparan sulfate-mediated mechanisms.,” *J. Biol. Chem.*, vol. 267, no. 31, pp. 22156–22162, 1992.

[58] E. P. Murono, A. L. Washburn, D. P. Goforth, and N. Wu, “Evidence that both receptor- and heparan sulfatee proteoglycan- bound basic fibroblast growth factor are internalized by cultured immature leydig cells,” *Mol. Cell. Endocrinol.*, vol. 98, pp. 81–90, 1993.

[59] D. F. Lazarous, M. Scheinowitz, M. Shou, E. Hodge, M. A. S. Rajanayagam, S. Hunsberger, W. G. Robison, J. A. Stiber, R. Correa, S. E. Epstein, and E. F. Unger, “Effects of Chronic Systemic Administration of Basic Fibroblast Growth Factor on Collateral Development in the Canine Heart,” *Circulation*, vol. 91, no. 1, pp. 145–153, 1995.

[60] D. F. Lazarous, M. Shou, J. A. Stiber, D. M. Dadhania, V. Thirumurti, E. Hodge, and E. F. Unger, “Pharmacodynamics of basic fibroblast growth factor: Route of administration determines myocardial and systemic distribution,” *Cardiovasc. Res.*, vol. 36, no. 1, pp. 78–85, 1997.

[61] T. Tokunaga, C. Shukunami, N. Okamoto, T. Taniwaki, K. Oka, H. Sakamoto, J. Ide, H. Mizuta, and Y. Hiraki, “FGF-2 Stimulates the Growth of Tenogenic Progenitor Cells to Facilitate the Generation of Tenomodulin-Positive Tenocytes in a Rat Rotator Cuff Healing Model,” *Am. J. Sports Med.*, pp. 2411–2422, 2015.

[62] M. Ruel, R. J. Laham, J. A. Parker, M. J. Post, J. A. Ware, M. Simons, and F. W. Sellke, “Long-term effects of surgical angiogenic therapy with fibroblast growth factor 2 protein.,” *J. Thorac. Cardiovasc. Surg.*, vol. 124, no. 1, pp. 28–34, 2002.

[63] M. A. Eisenberger, L. M. Reyno, D. I. Jodrell, V. J. Sinibaldi, K. H. Tkaczuk, R. Sridhara, E. G. Zuhowski, M. H. Lowitt, S. C. Jacobs, and M. J. Egorin, “Suramin, an Active Drug for Prostate Cancer: Interim Observations in a Phase I Trial,” *JNCI J. Natl. Cancer Inst.*, vol. 85, no. 8, pp. 611–621, Apr. 1993.

[64] M. M. Walther, W. D. Figg, and W. M. Linehan, “Intravesical suramin: a novel agent for the treatment of superficial transitional-cell carcinoma of the bladder,” *World J. Urol.*, vol. 14, no. 1, pp. S8–S11, 1996.

[65] D. Q. Wu, M. K. Kan, G. H. Sato, T. Okamoto, and J. D. Sato, “Characterization and molecular cloning of a putative binding protein for heparin-binding growth factors.,” *J. Biol. Chem.*, vol. 266, no. 25, pp. 16778–85, Sep. 1991.

[66] H.-D. Beer, M. Bittner, G. Niklaus, C. Munding, N. Max, A. Goppelt, and S. Werner, “The fibroblast growth factor binding protein is a novel interaction partner of FGF-7, FGF-10 and FGF-22 and regulates FGF activity: implications for epithelial repair.,” *Oncogene*, vol. 24, no. 34, pp. 5269–77, Aug. 2005.

[67] F. Czubayko, R. V Smith, H. C. Chung, and A. Wellstein, “Tumor growth and angiogenesis induced by a secreted binding protein for fibroblast growth factors,” *J. Biol. Chem.*, vol. 269, no. 45, pp. 28243–28248, 1994.

[68] M. Mongiat, J. Otto, R. Oldershaw, F. Ferrer, J. D. Sato, and R. V Iozzo, “Fibroblast growth factor-binding protein is a novel partner for perlecan protein core.,” *J. Biol. Chem.*, vol. 276, no. 13, pp. 10263–71, Mar. 2001.

[69] R. Lametsch, J. T. Rasmussen, L. B. Johnsen, S. Purup, K. Sejrsen, T. E. Petersen, and C. W. Heegaard, “Structural characterization of the fibroblast growth factor-binding protein purified from bovine prepartum mammary gland secretion.,” *J. Biol. Chem.*, vol. 275, no. 26, pp. 19469–74, Jun. 2000.

[70] a Kurtz, H. L. Wang, N. Darwiche, V. Harris, and A. Wellstein, “Expression of a binding protein for FGF is associated with epithelial development and skin carcinogenesis.,” *Oncogene*, vol. 14, no. 22, pp. 2671–81, 1997.

[71] J. Rak and R. S. Kerbel, “bFGF and tumor angiogenesis--back in the limelight?,” *Nat Med*, vol. 3, no. 10, pp. 1083–1084, 1997.

[72] F. Czubayko, E. D. Liaudet-Coopman, A. Aigner, A. T. Tuveson, G. J. Berchem, and A. Wellstein, “A secreted FGF-binding protein can serve as the angiogenic switch in human cancer.,” *Nat. Med.*, vol. 3, no. 10, pp. 1137–1140, 1997.

[73] H. Stöppler, C. Malerczyk, K. Block, A. Aigner, and F. Czubayko, “The human papillomavirus (HPV) 16 E6 oncoprotein leads to an increase in gene expression of the angiogenic switch molecule FGF-BP in non-immortalized human keratinocytes.,” *Oncogene*, vol. 20, no. 50, pp. 7430–6, 2001.

[74] B. Xie, E. Tassi, M. R. Swift, K. McDonnell, E. T. Bowden, S. Wang, Y. Ueda, Y. Tomita, A. T. Riegel, and A. Wellstein, “Identification of the fibroblast growth factor (FGF)-interacting domain in a secreted FGF-binding protein by phage display.,” *J. Biol. Chem.*, vol. 281, no. 2, pp. 1137–44, Jan. 2006.

[75] A. Aigner, C. Malerczyk, R. Houghtling, and A. Wellstein, “Tissue distribution and retinoid-mediated downregulation of an FGF-binding protein (FGF-BP) in the rat.,” *Growth Factors*, vol. 18, no. 1, pp. 51–62, 2000.

[76] X. C. Wang, J. H. Chen, J. W. Crab, and J. D. Sato, “Purification of heparin-binding protein HBp17 and identification of HBp17 heparin binding site.,” *Biochem. Mol. Biol. Int.*, vol. 46, no. 1, pp. 81–7, Sep. 1998.

[77] J. Folkman and M. Klagsbrun, “Angiogenic factors.,” *Science*, vol. 235, no. 4787, pp. 442–7, Jan. 1987.

[78] I. J. Mason, “The ins and outs of fibroblast growth factors.,” *Cell*, vol. 78, no. 4, pp. 547–52, Aug. 1994.

[79] E. R. Sauter, M. Nesbit, D. Tichansky, Z. J. Liu, T. Shirakawa, J. Palazzo, and M. Herlyn, “Fibroblast growth factor-binding protein expression changes with disease progression in clinical and experimental human squamous epithelium.,” *Int. J. Cancer*, vol. 92, no. 3, pp. 374–81, May 2001.

[80] A. Beenken and M. Mohammadi, “The FGF family: biology, pathophysiology and therapy.,” *Nat. Rev. Drug Discov.*, vol. 8, no. 3, pp. 235–53, Mar. 2009.

[81] N. Turner and R. Grose, “Fibroblast growth factor signalling: from development to cancer.,” *Nat. Rev. Cancer*, vol. 10, no. FebRuARy, pp. 116–129, 2010.

[82] A. Wellstein and F. Czubayko, “Inhibition of fibroblast growth factors,” *Breast Cancer Res. Treat.*, vol. 38, no. 1, pp. 109–119, Feb. 1996.

[83] I. Vlodavsky, P. Bashkin, R. Ishai-Michaeli, T. Chajek-Shaul, R. Bar-Shavit, A. Haimovitz-Friedman, M. Klagsbrun, and Z. Fuks, “Sequestration and release of basic fibroblast growth factor.,” *Ann. N. Y. Acad. Sci.*, vol. 638, pp. 207–20, 1991.

[84] D. Moscatelli, “Basic fibroblast growth factor (bFGF) dissociates rapidly from heparan sulfates but slowly from receptors. Implications for mechanisms of bFGF release from pericellular matrix,” *J. Biol. Chem.*, vol. 267, no. 36, pp. 25803–25809, 1992.

[85] P. Bashkin, S. Doctrow, M. Klagsbrun, C. M. Svahn, J. Folkman, and I. Vlodavsky, “Basic fibroblast growth factor binds to subendothelial extracellular matrix and is released by heparitinase and heparin-like molecules.,” *Biochemistry*, vol. 28, pp. 1737–1743, 1989.

[86] C. J. Powers, S. W. McLeskey, and a Wellstein, “Fibroblast growth factors, their receptors and signaling.,” *Endocr. Relat. Cancer*, vol. 7, no. 3, pp. 165–97, Sep. 2000.

[87] E. D. Liaudet-Coopman, A. M. Schulte, M. Cardillo, and A. Wellstein, “A tetracycline-responsive promoter system reveals the role of a secreted binding protein for FGFs during the early phase of tumor growth,” *Biochem.Biophys.Res.Commun.*, vol. 229, no. 3, pp. 930–937, 1996.

[88] E. D. Liaudet-Coopman and A. Wellstein, “Regulation of gene expression of a binding protein for fibroblast growth factors by retinoic acid,” *J. Biol. Chem.*, vol. 271, no. 35, pp. 21303–21308, 1996.

[89] E. D. Liaudet-Coopman, G. J. Berchem, and A. Wellstein, “In vivo inhibition of angiogenesis and induction of apoptosis by retinoic acid in squamous cell carcinoma.,” *Clin. Cancer Res.*, vol. 3, no. 2, pp. 179–84, Feb. 1997.

[90] G. C. Gurtner, S. Werner, Y. Barrando, and M. T. Longaker, “Wound repair and regeneration,” *Eur. Surg. Res.*, vol. 49, no. 1, pp. 35–43, 2012.

[91] S. Barrientos, O. Stojadinovic, M. S. Golinko, H. Brem, and M. Tomic-Canic, “Growth factors and cytokines in wound healing,” *Wound Repair Regen.*, vol. 16, no. 5, pp. 585–601, 2008.

[92] S. Braun, U. auf dem Keller, H. Steiling, and S. Werner, “Fibroblast growth factors in

epithelial repair and cytoprotection.," *Philos. Trans. R. Soc. Lond. B. Biol. Sci.*, vol. 359, no. 1445, pp. 753–7, 2004.

[93] D. L. Miller, S. Ortega, O. Bashayan, R. Basch, and C. Basilico, "Compensation by fibroblast growth factor 1 (FGF1) does not account for the mild phenotypic defects observed in FGF2 null mice.," *Mol. Cell. Biol.*, vol. 20, no. 6, pp. 2260–2268, 2000.

[94] L. Guo, L. Degenstein, and E. Fuchs, "Keratinocyte growth factor is required for hair development but not for wound healing," *Genes Dev*, vol. 10, no. 2, pp. 165–175, 1996.

[95] K. N. Broadley, A. M. Aquino, S. C. Woodward, A. Buckley-Sturrock, Y. Sato, D. B. Rifkin, and J. M. Davidson, "Monospecific antibodies implicate basic fibroblast growth factor in normal wound repair," *Lab. Invest.*, vol. 61, no. 5, pp. 571–575, 1989.

[96] F.-M. Chen, M. Zhang, and Z.-F. Wu, "Toward delivery of multiple growth factors in tissue engineering," *Biomaterials*, vol. 31, no. 24, pp. 6279–6308, Aug. 2010.

[97] E. Vögelin, N. F. Jones, J. I. Huang, J. H. Brekke, and J. M. Toth, "Practical Illustrations in Tissue Engineering: Surgical Considerations Relevant to the Implantation of Osteoinductive Devices," *Tissue Eng.*, vol. 6, no. 4, pp. 449–460, Aug. 2000.

[98] N. Papanas and E. Maltezos, "Benefit-risk assessment of becaplermin in the treatment of diabetic foot ulcers," *Drug Saf*, vol. 33, no. 6, pp. 455–461, 2010.

[99] L. Uebersax, H. P. Merkle, and L. Meinel, "Biopolymer-based growth factor delivery for tissue repair: from natural concepts to engineered systems," *Tissue Eng Part B Rev*, vol. 15, no. 3, pp. 263–289, 2009.

[100] C. S. McKay and M. G. Finn, "Click Chemistry in Complex Mixtures: Bioorthogonal Bioconjugation," *Chem. Biol.*, vol. 21, no. 9, pp. 1075–1101, 2014.

[101] M.-H. Seo, J. Han, Z. Jin, D.-W. Lee, H.-S. Park, and H.-S. Kim, "Controlled and Oriented Immobilization of Protein by Site-Specific Incorporation of Unnatural Amino Acid," *Anal. Chem.*, vol. 83, no. 8, pp. 2841–2845, Apr. 2011.

[102] L. Nebhani and C. Barner-Kowollik, "Orthogonal Transformations on Solid Substrates: Efficient Avenues to Surface Modification," *Adv. Mater.*, vol. 21, no. 34, pp. 3442–3468, Sep. 2009.

[103] E. Steen Redeker, D. T. Ta, D. Cortens, B. Billen, W. Guedens, and P. Adriaensens, "Protein engineering for directed immobilization," *Bioconjug. Chem.*, vol. 24, no. 11, pp. 1761–1777, 2013.

[104] D. Brady and J. Jordaan, "Advances in enzyme immobilisation," *Biotechnol. Lett.*, vol. 31, no. 11, pp. 1639–1650, Nov. 2009.

[105] C. Mateo, O. Abian, M. Bernedo, E. Cuenca, M. Fuentes, G. Fernandez-Lorente, J. M. Palomo, V. Grazu, B. C. C. Pessela, C. Giacomini, G. Irazoqui, A. Villarino, K. Ovsejevi, F. Batista-Viera, R. Fernandez-Lafuente, and J. M. Guisán, "Some special features of glyoxyl supports to immobilize proteins," *Enzyme Microb. Technol.*, vol. 37, no. 4, pp. 456–462, Sep. 2005.

[106] S. V. Rao, K. W. Anderson, and L. G. Bachas, “Oriented immobilization of proteins,” *Mikrochim. Acta*, vol. 128, no. 3–4, pp. 127–143, Sep. 1998.

[107] M. A. Gauthier and H.-A. Klok, “Peptide/protein–polymer conjugates: synthetic strategies and design concepts,” *Chem. Commun.*, vol. 32, no. 23, p. 2591, 2008.

[108] P. Jonkheijm, D. Weinrich, H. Schröder, C. M. Niemeyer, and H. Waldmann, “Chemical Strategies for Generating Protein Biochips,” *Angew. Chemie Int. Ed.*, vol. 47, no. 50, pp. 9618–9647, Dec. 2008.

[109] Z. Pei, H. Anderson, A. Myrskog, G. Dunér, B. Ingemarsson, and T. Aastrup, “Optimizing immobilization on two-dimensional carboxyl surface: pH dependence of antibody orientation and antigen binding capacity,” *Anal. Biochem.*, vol. 398, no. 2, pp. 161–168, Mar. 2010.

[110] A. Moscaroli, G. Jones, T. Lühmann, L. Meinel, S. Wälti, A. Blanc, E. Fischer, M. Hilbert, R. Schibli, and M. Béhé, “Radiolabeled ^{111} In-FGF-2 Is Suitable for *In Vitro* / *Ex Vivo* Evaluations and *In Vivo* Imaging,” *Mol. Pharm.*, p. acs.molpharmaceut.6b00913, 2017.

[111] W. Huang, J. Wang, D. Bhattacharyya, and L. G. Bachas, “Improving the Activity of Immobilized Subtilisin by Site-Specific Attachment to Surfaces,” *Anal. Chem.*, vol. 69, no. 22, pp. 4601–4607, 1997.

[112] J. E. Butler, “Solid supports in enzyme-linked immunosorbent assay and other solid-phase immunoassays.,” *Methods*, vol. 22, no. 1, pp. 4–23, Sep. 2000.

[113] T. Cha, A. Guo, and X.-Y. Zhu, “Enzymatic activity on a chip: The critical role of protein orientation,” *Proteomics*, vol. 5, no. 2, pp. 416–419, Feb. 2005.

[114] M. Gutmann, E. Memmel, A. C. Braun, J. Seibel, L. Meinel, and T. Lühmann, “Biocompatible Azide–Alkyne ‘Click’ Reactions for Surface Decoration of Glyco-Engineered Cells,” *ChemBioChem*, vol. 17, no. 9, pp. 866–875, 2016.

[115] T. Lühmann, G. Jones, M. Gutmann, J.-C. Rybak, J. Nickel, M. Rubini, and L. Meinel, “Bio-orthogonal Immobilization of Fibroblast Growth Factor 2 for Spatial Controlled Cell Proliferation,” *ACS Biomater. Sci. Eng.*, vol. 1, pp. 740–746, 2015.

[116] T. Lühmann, V. Spieler, V. Werner, M.-G. Ludwig, J. Fiebig, T. D. Mueller, and L. Meinel, “Interleukin-4-Clicked Surfaces Drive M2 Macrophage Polarization,” *ChemBioChem*, vol. 17, no. 22, pp. 2123–2128, Nov. 2016.

[117] H. Zhao, E. Heusler, G. Jones, L. Li, V. Werner, O. Germershaus, J. Ritzer, T. Luehmann, and L. Meinel, “Decoration of silk fibroin by click chemistry for biomedical application,” *J. Struct. Biol.*, vol. 186, no. 3, pp. 420–430, 2014.

[118] V. V. Rostovtsev, L. G. Green, V. V. Fokin, and K. B. Sharpless, “A Stepwise Huisgen Cycloaddition Process: Copper(I)-Catalyzed Regioselective ‘Ligation’ of Azides and Terminal Alkynes,” *Angew. Chemie Int. Ed.*, vol. 41, no. 14, pp. 2596–2599, Jul. 2002.

[119] E. Saxon and C. R. Bertozzi, “Cell Surface Engineering by a Modified Staudinger Reaction,” *Science (80-.).*, vol. 287, no. 5460, pp. 2007–2010, 2000.

[120] H. Staudinger and E. Hauser, “Über neue organische Phosphorverbindungen IV

Phosphinimine," *Helv. Chim. Acta*, vol. 4, no. 1, pp. 861–886, 1921.

[121] J. E. Moses and A. D. Moorhouse, "The growing applications of click chemistry," *Chem. Soc. Rev.*, vol. 36, no. 8, pp. 1249–1262, 2007.

[122] A. Michael, "Ueber die Einwirkung von Diazobenzolimid auf Acetylendicarbonsäuremethylester," *J. für Prakt. Chemie*, vol. 48, no. 1, pp. 94–95, Jun. 1893.

[123] R. Huisgen, "1,3-Dipolar Cycloadditions. Past and Future," *Angew. Chemie Int. Ed. English*, vol. 2, no. 10, pp. 565–598, Oct. 1963.

[124] R. Huisgen, "Centenary Lecture - 1,3-Dipolar Cycloadditions," *Proc. Chem. Soc.*, no. October, pp. 357–396, 1961.

[125] R. Huisgen, "Kinetics and Mechanism of 1,3-Dipolr Cycloadditions," *Angew. Chemie Int. Ed. English*, vol. 2, no. 11, pp. 633–645, Nov. 1963.

[126] H. C. Kolb, M. G. Finn, and K. B. Sharpless, "Click Chemistry: Diverse Chemical Function from a Few Good Reactions," *Angew. Chemie Int. Ed.*, vol. 40, no. 11, pp. 2004–2021, 2001.

[127] T. R. Chan, R. Hilgraf, K. B. Sharpless, and V. V Fokin, "Polytriazoles as Copper(I)-Stabilizing Ligands in Catalysis," *Org. Lett.*, vol. 6, no. 17, pp. 2853–2855, Aug. 2004.

[128] V. O. Rodionov, S. I. Presolski, S. Gardinier, Y.-H. Lim, and M. G. Finn, "Benzimidazole and related ligands for Cu-catalyzed azide-alkyne cycloaddition.," *J. Am. Chem. Soc.*, vol. 129, no. 42, pp. 12696–704, Oct. 2007.

[129] J. Kalia and R. T. Raines, "Advances in Bioconjugation," *Curr. Org. Chem.*, vol. 14, no. 2, pp. 138–147, Jan. 2010.

[130] J. C. M. van Hest and F. L. van Delft, "Protein Modification by Strain-Promoted Alkyne-Azide Cycloaddition," *ChemBioChem*, vol. 12, no. 9, pp. 1309–1312, Jun. 2011.

[131] J. M. Baskin, J. A. Prescher, S. T. Laughlin, N. J. Agard, P. V. Chang, I. A. Miller, A. Lo, J. A. Codelli, and C. R. Bertozzi, "Copper-free click chemistry for dynamic in vivo imaging," *Proc. Natl. Acad. Sci.*, vol. 104, no. 43, pp. 16793–16797, Oct. 2007.

[132] N. J. Agard, J. A. Prescher, and C. R. Bertozzi, "A Strain-Promoted [3 + 2] Azide−Alkyne Cycloaddition for Covalent Modification of Biomolecules in Living Systems," *J. Am. Chem. Soc.*, vol. 126, no. 46, pp. 15046–15047, 2004.

[133] M. Amblard, J.-A. Fehrentz, J. Martinez, and G. Subra, "Methods and protocols of modern solid phase Peptide synthesis.," *Mol. Biotechnol.*, vol. 33, no. 3, pp. 239–54, Jul. 2006.

[134] J. C. M. Van Hest, K. L. Kiick, D. A. Tirrell, and R. V August, "Efficient Incorporation of Unsaturated Methionine Analogues into Proteins in Vivo," no. 4, pp. 1282–1288, 2000.

[135] S. Eger, M. Scheffner, A. Marx, and M. Rubini, "Synthesis of defined ubiquitin dimers," *J. Am. Chem. Soc.*, vol. 132, no. 46, pp. 16337–16339, 2010.

[136] J. Tominaga, N. Kamiya, S. Doi, H. Ichinose, and M. Goto, "An enzymatic strategy for site-specific immobilization of functional proteins using microbial transglutaminase," *Enzyme Microb. Technol.*, vol. 35, no. 6–7, pp. 613–618, Dec. 2004.

[137] J. Tominaga, N. Kamiya, S. Doi, H. Ichinose, and T. Maruyama, "Design of a Specific Peptide Tag that Affords Covalent and Site-Specific Enzyme Immobilization Catalyzed by Microbial Transglutaminase," pp. 2299–2304, 2005.

[138] X. Mu, N. Kong, W. Chen, T. Zhang, M. Shen, and W. Yan, "High-level expression, purification, and characterization of recombinant human basic fibroblast growth factor in Pichia pastoris.," *Protein Expr. Purif.*, vol. 59, no. 2, pp. 282–8, Jun. 2008.

[139] O. Germershaus, I. Schultz, T. Lühmann, M. Beck-Broichsitter, P. Högger, and L. Meinel, "Insulin-like growth factor-I aerosol formulations for pulmonary delivery," *Eur. J. Pharm. Biopharm.*, vol. 85, no. 1, pp. 61–68, 2013.

[140] U. K. Laemmli, "Cleavage of structural proteins during the assembly of the head of bacteriophage T4.," *Nature*, vol. 227, no. 5259, pp. 680–5, Aug. 1970.

[141] M. W. Pantoliano, R. A. Horlick, B. A. Springer, D. E. Van Dyk, T. Tobery, D. R. Wetmore, J. D. Lear, A. T. Nahapetian, J. D. Bradley, and W. P. Sisk, "Multivalent ligand-receptor binding interactions in the fibroblast growth factor system produce a cooperative growth factor and heparin mechanism for receptor dimerization.," *Biochemistry*, vol. 33, no. 34, pp. 10229–48, Aug. 1994.

[142] C. H. Squires, J. Childs, S. P. Eisenberg, P. J. Polverini, and A. Sommer, "Production and characterization of human basic fibroblast growth factor from Escherichia coli.," *J. Biol. Chem.*, vol. 263, no. 31, pp. 16297–302, Nov. 1988.

[143] R. Chen, J. John, A. Lavrentieva, S. Müller, M. Tomala, Y. Zhao, R. Zweigerdt, S. Beutel, B. Hitzmann, C. Kasper, U. Martin, U. Rinas, F. Stahl, and T. Scheper, "Cytokine production using membrane adsorbers: Human basic fibroblast growth factor produced by Escherichia coli," *Eng. Life Sci.*, vol. 12, no. 1, pp. 29–38, Feb. 2012.

[144] D. C. Mikles, V. Bhat, B. J. Schuchardt, B. J. Deegan, K. L. Seldeen, C. B. McDonald, and A. Farooq, "pH modulates the binding of early growth response protein 1 transcription factor to DNA," *FEBS J.*, vol. 280, no. 15, pp. 3669–3684, Aug. 2013.

[145] R. A. Kammerer, T. Schulthess, R. Landwehr, A. Lustig, D. Fischer, and J. Engel, "Tenascin-C hexabrachion assembly is a sequential two-step process initiated by coiled-coil α-helices," *J. Biol. Chem.*, vol. 273, no. 17, pp. 10602–10608, 1998.

[146] E. R. LaVallie, E. a DiBlasio, S. Kovacic, K. L. Grant, P. F. Schendel, and J. M. McCoy, "A thioredoxin gene fusion expression system that circumvents inclusion body formation in the E. coli cytoplasm.," *Biotechnology. (N. Y).*, vol. 11, no. 2, pp. 187–193, 1993.

[147] J. Wang, A. Hong, J. S. Ren, F. Y. Sun, Y. J. Shi, K. Liu, Q. L. Xie, Y. Dai, Z. Y. Li, and Y. Chen, "Biochemical properties of C78SC96S rhFGF-2: A double point-mutated rhFGF-2 increases obviously its activity," *J. Biotechnol.*, vol. 121, no. 4, pp. 442–447, 2006.

[148] V. Sluzky, Z. Shahrokh, P. Stratton, G. Eberlein, and Y. J. Wang, "Chromatographic

methods for qantitative analysis of native, denaturated and aggregated basic fibroblast grownt factor in solution formulaions," *Pharm. Res.*, vol. 1, no. 4, pp. 485–491, 1994.

[149] (Moremen Lab), "Transient Transfection of HEK-293F Suspension Cultures using PEI." [Online]. Available: http://glycoenzymes.ccrc.uga.edu/MammalianExpression/MammalianTransfectionPEI.pdf. [Accessed: 11-Nov-2015].

[150] G. Kronvall, "A Surface Component in Group A, C, and G Streptococci with Non-Immune Reactivity for Immunoglobulin G," *J. Immunol.*, vol. 111, no. 5, pp. 1401–1406, 1973.

[151] H. Hjelm, K. Hjelm, and J. Sjöquist, "Protein a from Staphylococcus aureus. Its isolation by affinity chromatography and its use as an immunosorbent for isolation of immunoglobulins," *FEBS Lett.*, vol. 28, no. 1, pp. 73–76, 1972.

[152] A. A. Shukla, B. Hubbard, T. Tressel, S. Guhan, and D. Low, "Downstream processing of monoclonal antibodies-Application of platform approaches," *J. Chromatogr. B Anal. Technol. Biomed. Life Sci.*, vol. 848, no. 1, pp. 28–39, 2007.

[153] S. M. Moghimi, P. Symonds, J. C. Murray, A. C. Hunter, G. Debska, and A. Szewczyk, "A two-stage poly(ethylenimine)-mediated cytotoxicity: Implications for gene transfer/therapy," *Mol. Ther.*, vol. 11, no. 6, pp. 990–995, 2005.

[154] A. T. Marttila, O. H. Laitinen, K. J. Airenne, T. Kulik, E. A. Bayer, M. Wilchek, and M. S. Kulomaa, "Recombinant NeutraLite Avidin: A non-glycosylated, acidic mutant of chicken avidin that exhibits high affinity for biotin and low non-specific binding properties," *FEBS Lett.*, vol. 467, no. 1, pp. 31–36, 2000.

[155] L. Chaiet and F. J. Wolf, "The properties of streptavidin, a biotin-binding protein produced by Streptomycetes," *Arch. Biochem. Biophys.*, vol. 106, pp. 1–5, 1964.

[156] M. N. Pollak, C. Polychronakos, and M. Richard, "Insulinlike growth factor I: a potent mitogen for human osteogenic sarcoma.," *J. Natl. Cancer Inst.*, vol. 82, no. 4, pp. 301–5, Feb. 1990.

[157] S. P. Massia and J. a Hubbell, "An RGD spacing of 440 nm is sufficient for integrin alpha V beta 3-mediated fibroblast spreading and 140 nm for focal contact and stress fiber formation.," *J. Cell Biol.*, vol. 114, no. 5, pp. 1089–100, Sep. 1991.

[158] S. Hofmann, M. Hilbe, R. J. Fajardo, H. Hagenmüller, K. Nuss, M. Arras, R. Müller, B. von Rechenberg, D. L. Kaplan, H. P. Merkle, and L. Meinel, "Remodeling of tissue-engineered bone structures in vivo.," *Eur. J. Pharm. Biopharm.*, vol. 85, no. 1, pp. 119–29, Sep. 2013.

[159] J. Cornish, K. E. Callon, C. Q. Lin, C. L. Xiao, T. B. Mulvey, G. J. Cooper, and I. R. Reid, "Trifluoroacetate, a contaminant in purified proteins, inhibits proliferation of osteoblasts and chondrocytes.," *Am. J. Physiol.*, vol. 277, no. 5 Pt 1, pp. E779–E783, 1999.

[160] F. Baneyx and M. Mujacic, "Recombinant protein folding and misfolding in Escherichia coli," *Nat. Biotechnol.*, vol. 22, no. 11, pp. 1399–1408, Nov. 2004.

[161] C. H. Schein, "Production of soluble recombinant proteins in bacteria," *Nat.*

Biotechnol., vol. 7, pp. 1141–1149, 1989.

[162] T. H. Al-Samarrai, "Effect of 4% glycerol and low aeration on result of expression in Escherichia coli of Cin3 and three Venturia inaequalis EST's recombinant proteins," *Am. J. Mol. Biol.*, vol. 3, no. 1, pp. 1–9, 2013.

[163] A. Varshavsky, "The N-end rule pathway and regulation by proteolysis," *Protein Sci.*, vol. 20, no. 8, pp. 1298–1345, 2011.

[164] T. Tasaki, S. M. Sriram, K. S. Park, and Y. T. Kwon, "The N-end rule pathway.," *Annu. Rev. Biochem.*, vol. 81, pp. 261–89, 2012.

[165] R. S. Kerbel, A. Viloria-Petit, F. Okada, and J. Rak, "Establishing a link between oncogenes and tumor angiogenesis," *Mol Med*, vol. 4, no. 5, pp. 286–295, 1998.

[166] a Aigner, M. Butscheid, P. Kunkel, E. Krause, K. Lamszus, A. Wellstein, and F. Czubayko, "An FGF-binding protein (FGF-BP) exerts its biological function by parallel paracrine stimulation of tumor cell and endothelial cell proliferation through FGF-2 release.," *Int. J. Cancer*, vol. 92, no. 4, pp. 510–7, May 2001.

[167] L. S. Holm, A. Mcumber, J. E. Rasmussen, M. Obiols-Rabasa, P. W. Thulstrup, M. R. Kasimova, T. W. Randolph, and M. Van De Weert, "The effect of protein PEGylation on physical stability in liquid formulation," *J. Pharm. Sci.*, vol. 103, no. 10, pp. 3043–3054, 2014.

[168] M. W. Popp, S. K. Dougan, T.-Y. Chuang, E. Spooner, and H. L. Ploegh, "Sortase-catalyzed transformations that improve the properties of cytokines," *Proc. Natl. Acad. Sci.*, vol. 108, no. 8, pp. 3169–3174, Feb. 2011.

[169] B. A. Kerwin, "Polysorbates 20 and 80 Used in the Formulation of Protein Biotherapeutics: Structure and Degradation Pathways," *J. Pharm. Sci.*, vol. 97, no. 8, pp. 2924–2935, Aug. 2008.

[170] A. R. Aricescu, W. Lu, and E. Y. Jones, "A time- and cost-efficient system for high-level protein production in mammalian cells," *Acta Crystallogr. Sect. D Biol. Crystallogr.*, vol. 62, no. 10, pp. 1243–1250, 2006.

[171] E. K. Culyba, J. L. Price, S. R. Hanson, A. Dhar, C.-H. Wong, M. Gruebele, E. T. Powers, and J. W. Kelly, "Protein Native-State Stabilization by Placing Aromatic Side Chains in N-Glycosylated Reverse Turns," *Science (80-.).*, vol. 331, no. 6017, pp. 571–575, Feb. 2011.

[172] A. P. Golovanov, G. M. Hautbergue, S. A. Wilson, and L.-Y. Lian, "A Simple Method for Improving Protein Solubility and Long-Term Stability," *J. Am. Chem. Soc.*, vol. 126, no. 14, pp. 8933–8939, 2004.

[173] L. D. Thompson, M. W. Pantoliano, and B. a Springer, "Energetic characterization of the basic fibroblast growth factor-heparin interaction: identification of the heparin binding domain.," *Biochemistry*, vol. 33, no. 13, pp. 3831–40, Apr. 1994.

[174] B. Breiten, M. R. Lockett, W. Sherman, S. Fujita, M. Al-Sayah, H. Lange, C. M. Bowers, A. Heroux, G. Krilov, and G. M. Whitesides, "Water networks contribute to enthalpy/entropy compensation in protein-ligand binding," *J. Am. Chem. Soc.*, vol. 135, no. 41, pp. 15579–15584, 2013.

[175] M. Taha and M.-J. Lee, “Interactions of TRIS [tris(hydroxymethyl)aminomethane] and related buffers with peptide backbone: Thermodynamic characterization,” *Phys. Chem. Chem. Phys.*, vol. 12, no. 39, p. 12840, 2010.

[176] B. A. Springer, M. W. Pantoliano, F. A. Barbera, P. L. Gunyuzlu, L. D. Thompson, W. F. Herblin, S. A. Rosenfeld, and G. W. Book, “Identification and concerted function of 2 receptor-binding surfaces on basic fibroblast growth-factor required for mitogenesis,” *J. Biol. Chem.*, vol. 269, no. 43, pp. 26879–26884, 1994.

[177] H. Edward Conrad, “Fibroblast Growth Factors,” in *Heparin-Binding Proteins*, Elsevier, 1998, p. 301–III.

[178] R. J. Tomanek, H. K. Hansen, and L. P. Christensen, “Temporally expressed PDGF and FGF-2 regulate embryonic coronary artery formation and growth,” *Arterioscler. Thromb. Vasc. Biol.*, vol. 28, no. 7, pp. 1237–1243, 2008.

[179] J. Chiche, M. C. Brahimi-Horn, and J. Pouysségur, “Tumour hypoxia induces a metabolic shift causing acidosis: A common feature in cancer,” *J. Cell. Mol. Med.*, vol. 14, no. 4, pp. 771–794, 2010.

[180] R. S. Schwartz, H. K. Eltzschig, and P. Carmeliet, “Hypoxia and Inflammation,” *N. Engl. J. Med.*, vol. 364, no. 7, pp. 656–665, Feb. 2011.

[181] A. L. Goerges and M. A. Nugent, “pH regulates vascular endothelial growth factor binding to fibronectin: A mechanism for control of extracellular matrix storage and release,” *J. Biol. Chem.*, vol. 279, no. 3, pp. 2307–2315, 2004.

[182] S. Sevim, S. Ozer, G. Jones, J. Wurzel, L. Feng, A. Fakhraee, N. Shamsudhin, O. Ergeneman, E. Pellicer, J. Sort, S. Pané, B. J. Nelson, H. Torun, and T. Lühmann, “Nanomechanics on FGF-2 and Heparin Reveal Slip Bond Characteristics with pH Dependency,” *ACS Biomater. Sci. Eng.*, p. acsbiomaterials.6b00723, Apr. 2017.

[183] R. Eil, S. K. Vodnala, D. Clever, C. A. Klebanoff, M. Sukumar, J. H. Pan, D. C. Palmer, A. Gros, T. N. Yamamoto, S. J. Patel, G. C. Guittard, Z. Yu, V. Carbonaro, K. Okkenhaug, D. S. Schrump, W. M. Linehan, R. Roychoudhuri, and N. P. Restifo, “Ionic immune suppression within the tumour microenvironment limits T cell effector function,” *Nature*, vol. 537, no. 7621, pp. 539–543, Sep. 2016.

[184] O. a Ibrahimi, F. Zhang, S. C. L. Hrstka, M. Mohammadi, and R. J. Linhardt, “Kinetic model for FGF, FGFR, and proteoglycan signal transduction complex assembly.,” *Biochemistry*, vol. 43, no. 16, pp. 4724–30, Apr. 2004.

[185] S. Letschert, A. Göhler, C. Franke, N. Bertleff-Zieschang, E. Memmel, S. Doose, J. Seibel, and M. Sauer, “Super-Resolution Imaging of Plasma Membrane Glycans,” *Angew. Chemie Int. Ed.*, vol. 53, no. 41, pp. 10921–10924, Oct. 2014.

[186] A. Homann, R. U. Qamar, S. Serim, P. Dersch, and J. Seibel, “Bioorthogonal metabolic glycoengineering of human larynx carcinoma (HEp-2) cells targeting sialic acid,” *Beilstein J. Org. Chem.*, vol. 6, pp. 2–8, 2010.

[187] E. Memmel, A. Homann, T. A. Oelschlaeger, and J. Seibel, “Metabolic glycoengineering of Staphylococcus aureus reduces its adherence to human T24 bladder carcinoma cells,” *Chem. Commun.*, vol. 49, no. 66, pp. 7301–7303, 2013.

ABBREVIATIONS

Å	Angström
aa	amino acids
AB	antibody
ACN	acetonitrile
APS	ammonium persulfate
Az	azido
Boc	tert-Butoxycarbonyl
BSA	bovine serum albumin
CuAAC	copper(I)-catalyzed-azide-alkyne cycloaddition
Da	Dalton
DAD	diode array detector
DMEM	Dulbecco's modified Eagle's medium
DNA	desoxy ribonucleic acid
DTT	dithiothreitol
EC_{50}	half maximal effective concentration
ECM	extracellular matrix
EDC	1-ethyl-3-(3-dimethyl-aminopropyl) carbodiimide
EDTA	ethylenediaminetetraacetic acid
$EtNH_2$	ethanolamine
EtOAc	ethylacetate
FCS	fetal calf serum
FGF	fibroblast growth factor
FGFBP	fibroblast growth factor binding protein
FGFR receptor	fibroblast growth factor
Fmoc	fluorenylmethyloxy-carbonyl chloride
GAG	glycosaminoglycan
GdmCL	guanidine hydrochloride
HCD	higher-energy C-trap dissociation
HPLC	high performance liquid chromatography
HS	heparansulfate
HSPG	heparansulfat proteoglycans
Ig	immunoglobulin
IPTG	isopropyl β-D-1-thiogalactopyranoside
iTC	isothermal titration calorimetry
iv	intravenous
LB	lysogeny broth
LC	liquid chromatography
MALDI	matrix-assisted laser desorption/ionization
Man	mannose
MEM	minimum essential medium
MeOH	methanol
MS	mass spectrometry
MTG	microbial transglutaminase
MTT	3-(4,5-dimethylthiazol-2yl)-2,5-diphenyl-tetrazolium bromide

NEA	non essential aminoacids
NHS	N-hydroxysuccinimide
OD	optical density
PAGE	polyacrylamide gel electrophoresis
PBS	phosphate buffered saline
PEI	polyethylenimine
PG	proteoglycans
p*I*	isoelectric point
plk	pyrrolysine analogue
PMSF	phenylmethylsulfonyl fluoride
ppm	parts per million
RNA	ribonucleic acid
rpm	rotation per minute
sc	subcutaneous
SDS	sodium dodecyl sulfate
SPPS	solidphase peptide synthesis
SPR	surface plasmon resonance
TB	terrific broth
TBTA	Tris(benzyltriazolylmethyl) amine
TEMED	tetramethylethylenediamine
TFA	trifluoroacetic acid
THF	tetrahydrofuran
THPTA	tris(3-hydroxypropyl-triazolylmethyl)amine
tris	tris(hydroxymethyl) aminomethane
UV	ultraviolet
v/v	volume concentration
w/v	mass concentration
w/w	mass fraction
WST-1	2-(4-Iodophenyl)-3-(4-nitrophenyl)-5-(2,4-disulfophenyl)-2H-tetrazolium

Published portions of this dissertation

Publications

Zhao, H., Heusler, E., Jones, G., Li, L., Werner, V., Germershaus, O., Ritzer, J., Lühmann, T. and Meinel, L. (2014). "Decoration of silk fibroin by click chemistry for biomedical application." J Struct Biol, 186(3): 420-430. www.ncbi.nlm.nih.gov/pubmed/24576682

Lühmann, T., Jones, G., Gutmann, M., Rybak, J.-C., Nickel, J., Rubini, M. and Meinel, L. (2015). "Bio-orthogonal Immobilization of Fibroblast Growth Factor 2 for Spatial Controlled Cell Proliferation." ACS Biomater Sci Eng 2015, 1(9), pp. 740-746. pubs.acs.org/doi/abs/10.1021/acsbiomaterials.5b00236

Moscaroli, A., Jones, G., Lühmann. T., Meinel, L., Wälti, S., Blanc, A., Fischer, E., Hilbert, M., Schibli, R. and Béhé M. (2017). „Radiolabeled ^{111}In-FGF-2 Is Suitable for In Vitro/Ex Vivo Evaluations and *In Vivo* Imaging.“ Molecular Pharmaceutics 2017, 14(3), 639-648. http://pubs.acs.org/doi/full/10.1021/acs.molpharmaceut.6b00913

Sevim, S., Özer, S., Jones, G., Wurzel, J., Feng, L., Fakhraee, A., Shamsudhin, N., Ergeneman, O., Pellicer, E., Sort, J., Pané, S., Nelson, B., Torun, H. and Lühmann, T. (2017). "Nanomechanics on FGF-2 and heparin reveal slip bond characteristics with pH dependency." ACS Biomater Sci Eng. 2017 Mar 28, doi: 10.1021/acsbiomaterials.6b00723, [Epub ahead of print]. http://pubs.acs.org/doi/abs/10.1021/acsbiomaterials.6b00723

Poster presentations

Jones, G, Memmel, E., Seibel, J., Lühmann, T., Meinel. L., Site-directed immobilization of a FGF-2 analogue via click chemistry, 10th CRS German Local Chapter Meeting, February 17-28, 2014, Kiel, Germany.

Jones, G., Lühmann, T., Meinel, L., Expression and purification of fibroblast growth factor-binding protein 1, 5th NBBA seminar, June 12, 2013, Würzburg, Germany.

Jones, G., Lühmann, T., Meinel, L., Expression and purification of fibroblast growth factor-binding protein 1, 9th CRS German Local Chapter Meeting, March 21-22, 2013, Ludwigshafen, Germany.

CURRICULIM VITAE

ACKNOWLEDGMENTS

My sincerest thanks go to Prof. Dr. Dr. Lorenz Meinel for giving me the opportunity to do my PhD in his research group. Throughout my doctorate, I was attended by his valuable and wide scientific skills, his encouragement, helpful guidance and constructive feedback. Furthermore he enabled outstanding equipment conditions at his chair facilitating experimental procedures.

I deeply thank Dr. Tessa Lühmann for her dedicated guidance of my work, her constant support throughout all steps of my PhD especially while writing my thesis. I am very grateful for her most valuable and honest scientific advice.

Many thanks go to Dr. Martin Béhé from the Paul Scherrer Institute for the harmonic cooperation concerning radioactive coupling of proteins. This thanks is extended to Alessandra Moscaroli for her constant feedback on scientific matter and great hospitality during my visits at the PSI.

Additionally, I want to acknowledge the essential help, long fruitful discussions and scientific and personal advice of Prof. Dr. Thomas Müller and Dr. Juliane Fiebig from the Department for Molecular Plant-Physiology and Biophysics – Botany I.

Furthermore, I am very grateful to Dr. Clemens Grimm, Jann-Patrick Pelz and Jyotischman Veepaschnit from the Department of Biochemistry in Würzburg for inviting me into their labs to conduct multiple protein purifications. I am also very grateful for Dr. Elisabeth Memmel and Prof. Dr. Jürgen Seibel of the Institute of Organic Chemistry Würzburg for the supply of azido-sugars and productive discussions concerning surface decoration. Many thanks to Dr. Joachim Nickel of the Fraunhofer Institute (IGB) Würzburg for inviting me to his lab where I could experience a very pleasant and productive time.

I also want to thank all my PhD colleagues and other members of the team for the atmosphere in our group and the truly memorable time in Würzburg. Christine Schneider, Doris Moret and Dr. Sascha Zügner gave me a lot of support regarding organization and student supervision. Thank you Alexandra Braun, Marcus Gutmann and Joel Wurzel for your help while writing my thesis. Special thanks to Eva Heusler, Marika Kutscher, Doris Moret, Sasche Zügner and Isabel Schultz for making new friends and having relaxed, personal and work related conversations in and off campus.

I would like to thank Georg Walter, Matthias Völker and Karl Vollmuth for their help regarding technical problems of all kind and their time to socialize early in the morning in the workshop.

Thank you Valentin Zanner for your magnificent creative input on figures and being a great tutor for illustration programs.

I want to thank Marika Kutscher, Rebecca Fiederling, Philipp Wöhrle and Isabel Schultz for proof-reading this thesis.

Finally, I want to thank my family close friends and of course Isabel Schultz for their infinite support and encouragement during this scientific journey.